

# Sodium-Ion Battery Materials and Electrochemical Properties Reviewed

*Kudakwashe Chayambuka, Grietus Mulder, Dmitri L. Danilov, and Peter H. L. Notten\**

The demand for electrochemical energy storage technologies is rapidly increasing due to the proliferation of renewable energy sources and the emerging markets of grid-scale battery applications. The properties of batteries are ideal for most electrical energy storage (EES) needs, yet, faced with resource constraints, the ability of current lithium-ion batteries (LIBs) to match this overwhelming demand is uncertain. Sodium-ion batteries (SIBs) are a novel class of batteries with similar performance characteristics to LIBs. Since they are composed of earth-abundant elements, cheaper and utility scale battery modules can be assembled. As a result of the learning curve in the LIB technology, a phenomenal progression in material development has been realized in the SIB technology. In this review, innovative strategies used in SIB material development, and the electrochemical properties of anode, cathode, and electrolyte combinations are elucidated. Attractive performance characteristics are herein evidenced, based on comparative gravimetric and volumetric energy densities to state-of-the-art LIBs. In addition, opportunities and challenges toward commercialization are herein discussed based on patent data trend analysis. With extensive industrial adaptations expected, the commercial prospects of SIBs look promising and this once discarded technology is set to play a major role in EES applications.

## 1. Introduction

Following the successful commercialization of lithium-ion batteries (LIBs) by the Sony corporation in 1991,<sup>[1]</sup> LIB have

become the electricity storage system of choice over the past 26 years, combining superb energy density, compact and lightweight designs, and outstanding cycle life compared to other rechargeable battery technologies.<sup>[2]</sup>

Despite the commercial success and proliferation of LIB in consumer electronics and recently in battery electric vehicles, LIBs are believed to be too expensive for stationary, large-scale, electrical energy storage (EES) and, in addition, there are concerns on the resource availability of LIB components.<sup>[3,4]</sup> Historically, the technology of choice for EES applications is pumped-hydro which continues to dominate due to very large unit sizes, accounting for over 95% of the total rated power globally (data derived from the US DOE, global energy storage database).<sup>[5,6]</sup> However, the number of new pumped-hydro installations is dwindling as a result of its specific geographic and geological requirements.<sup>[7]</sup> A technological incentive is therefore to find alternative EES options that are installation flexible, cost effective,

energy efficient, and environmentally benign in order to match the rapid growth in intermittent renewable energy sources.

The properties of electrochemical energy storage technologies are, in general, ideal for a grid scale EES. LIBs in particular have the ability to respond rapidly to load changes, have a high energy density combined with an excellent Coulombic efficiency, exhibit low standby losses, and have modular designs that facilitate upscaling.<sup>[7,8]</sup> Yet, faced with the aforementioned resource constraints and adverse ecological hazards upon disposal (due to toxic elements), the ability of LIBs to meet large-scale EES demands, remains uncertain.<sup>[7]</sup> The needs and challenges outlined above have motivated the research for an alternative, scalable battery technology, composed of cheap, abundant, and environmentally benign materials to match the performance and economical success of LIBs.

Given the relative abundance of elemental sodium (compared to lithium in the Earth's crust, see Figure 1) and the low electrochemical potential of Na (-2.71 V vs the standard hydrogen electrode, SHE), which is only 330 mV above that of Li, rechargeable batteries based on sodium hold great promise to meet large-scale EES demands. For example, high-temperature ZEBRA cells<sup>[9]</sup> based on the Na/NiCl<sub>2</sub> system and sodium sulfur cells<sup>[10]</sup> have already demonstrated the potential of sodium-based electrochemical energy storage. These batteries

K. Chayambuka, G. Mulder  
VITO  
Boeretang 200, 2400 Mol, Belgium  
K. Chayambuka, G. Mulder  
EnergyVille  
Thor Park 8310, 3600 Genk, Belgium  
K. Chayambuka, Dr. D. L. Danilov, Prof. P. H. L. Notten  
Eindhoven University of Technology  
Postbus 513, 5600 MB, Eindhoven, The Netherlands  
E-mail: p.h.l.notten@tue.nl  
Dr. D. L. Danilov, Prof. P. H. L. Notten  
Forschungszentrum Jülich  
Fundamental Electrochemistry (IEK-9)  
D-52425 Jülich, Germany  
Prof. P. H. L. Notten  
University of Technology Sydney  
Broadway, Sydney, NSW 2007, Australia

 The ORCID identification number(s) for the author(s) of this article can be found under <https://doi.org/10.1002/aenm.201800079>.

DOI: 10.1002/aenm.201800079

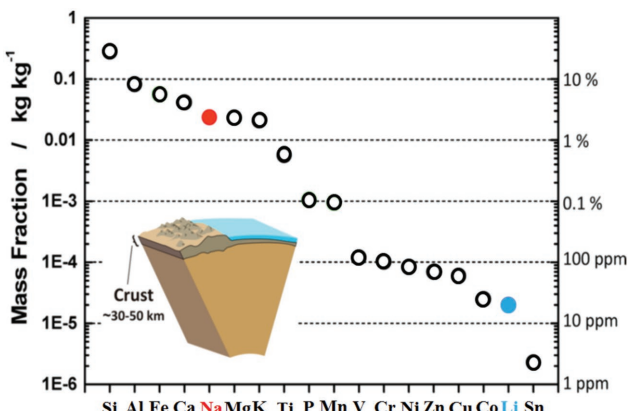


**Figure 1.** Abundance of elements in the Earth's crust. The energy carrying elements for comparison are highlighted in red for Na and blue for Li. Adapted with permission.<sup>[17]</sup> Copyright 2014, American Chemical Society.

have already been commercialized for stationary and automotive applications.<sup>[11–14]</sup> Their major disadvantage, however, is a high operating temperature of  $\approx 300\text{ }^{\circ}\text{C}$ , which conjures safety hazards and reduces the round trip energy efficiency of the cells.<sup>[12,14]</sup> A room temperature battery therefore remains the only viable option to match the performance and characteristics of state-of-the-art LIBs.

The *revival* of room temperature sodium-ion batteries (SIBs), based on intercalation materials analogous to the current LIB technology, has thus emerged as a promising strategy. Revival because up until the late 1980s, SIBs were fervently researched alongside LIBs.<sup>[15,16]</sup> The discovery of graphite as a cheap, electrochemically active and high-capacity anode in LIB, and the failure of sodium insertion in graphite, resulted in the near abandonment of the research in Na intercalation materials for SIB application.<sup>[17]</sup> A decade later, in the year 2000, Stevens and Dahn<sup>[18]</sup> reported the successful electrochemical insertion of sodium in hard carbon (HC), at a specific capacity close to that of lithium in graphite ( $\approx 372\text{ mAh g}^{-1}$ ). This discovery, coupled with a growing need of a complementary technology to the LIB became a major turning point in the rejuvenated interest in the SIB concept.

Since this discovery, the SIBs have increasingly gained traction, buoyed by further discoveries in anodic and cathodic materials. Much of this rapid progress in material development is attributed to the similarities between SIBs and LIBs. Fundamentally, the voltage range and operating principles of the SIBs and LIBs are identical. This similarity has allowed the years of conceptual understanding and development in LIBs to be directly transferred, thereby allowing a rapid growth in the SIB technology. Besides borrowing from material synthesis routes, the same production lines used to manufacture LIB cells can be used to make SIB cells without any modification.<sup>[19]</sup> Several companies such as Faradion (UK)<sup>[20]</sup> and Sumitomo<sup>[21]</sup> (Japan) have thus announced plans to commercialize SIBs, the latter having initially disclosed plans to start mass production as early as 2016.<sup>[22]</sup>

Although SIBs are not projected to compete with LIBs for volumetric and gravimetric energy density, they are expected to leverage their resource abundance to be price competitive and



**Kudakwashe Chayambuka** is a researcher at Energy Technology unit (ETE) of the Flemish Institute for Technological Research (VITO) and is Ph.D. candidate at the Technical University of Eindhoven (TU/e) Faculty of Electrical Engineering. He focuses on the electrochemical modeling of sodium-ion batteries and other energy storage systems such as Li-ion and NiMH batteries using MATLAB and COMSOL *Multiphysics*.



**Grietus Mulder** is researcher at the Flemish Technological Institute VITO in the unit Energy Technology with a background in applied physics. He specializes in the field of electrical energy storage for automotive and renewable energy applications. He developed battery testing methods and software marketed as "BATAL," used for automotive applications like plugin hybrid vehicles and also for the integration of photovoltaic energy in a smart grid network. He also works on electrochemical modeling of batteries with the help of the COMSOL *Multiphysics* software.



**Peter H. L. Notten** joined Philips Research Laboratories (Eindhoven, The Netherlands) from 1975 to 2010. He received his Ph.D. degree from Eindhoven University in 1989. Since then he focused on energy storage research, including hydrogen and lithium storage materials, new battery technologies, modeling electrochemical systems, and design of battery-management algorithms. In 2000 he was appointed as professor at TU/e where he now heads the group Energy Materials and Devices. In 2014 he has been appointed as International Adjunct Faculty at Amrita University, Coimbatore (India), as group leader at Forschungszentrum Jülich (Germany), and in 2018 as honorary professor at University of Technology Sydney.

therefore complement LIBs in stationary and large-scale applications. This is further expected to stabilize the costs of lithium-based batteries as they enter the mass market of electric vehicles by suppressing Li, Co, and Cu resource constraints. In this

regard, the SIB technology is neither behind nor beyond, but rather beside that of LIB. Success of the SIB concept will now depend on more industrial players adapting this promising technology and investing in large-scale production facilities, following the example set by the Tesla/Panasonic gigafactory.<sup>[23]</sup> It is henceforth critical to rapidly close the chasm between the chains of production of the two battery technologies since the proliferation of SIBs in large-scale EES will eventually rely on the ability to match the economies of scale in LIBs.

In this review, we discuss the electrochemical and material properties among anode, cathode, and electrolyte components, as well as full-cell SIB characteristics. Several “complete-set” reviews have also appeared in recent years. Yabuuchi et al.<sup>[17]</sup> made a comprehensive review of SIBs, on the back of a series of research efforts. This review in particular focuses on anode and cathode material properties. Kundu et al.<sup>[12]</sup> further discussed the challenges in the emerging chemistry of SIBs. While these studies remain relevant and important literature today, the SIB technology has rapidly progressed since then. Nayak et al.<sup>[24]</sup> recently reviewed the different electrochemical properties between LIB and SIB chemistries while, discussions on full-cell SIB have only started to appear in reviews, in the publication by Hwang et al.<sup>[25]</sup>

Herein, we expand on recent advances in full-cells through a benchmarking study of five possible SIB combinations. In addition, we focus on the electrochemical properties of the most studied active materials and electrolytes for use in SIBs, including redox potentials, gravimetric capacities, and capacity losses during cycling. Therefore, recent advances in SIB research are highlighted and comparative volumetric and gravimetric capacities at cell level are provided. The main goal is to provide the reader a perspective on some of the practical challenges toward the commercialization of SIBs. For this purpose, a technological trend analysis for SIBs is performed for the first time, which provides an overview of groundbreaking progress in this emerging EES technology.

## 2. Comparison between Sodium and Lithium

Developing the SIB technology is mainly driven by the success of LIBs and the similarities in chemical properties between the two alkali metals: Na and Li. This has allowed the years of understanding and development of the LIB technology to be directly transferred to the SIB, resulting in a rapid growth. While contemporary concerns regarding the cost and resource availability of lithium to meet the ever-increasing demands of EES have led researchers to revive this once discarded technology, an inspection into the physical properties of sodium and lithium reveals why these two charge carriers for energy storage were once equally regarded.

Lithium and sodium are two members of the group 1 elements of the periodic table. They are trivially named alkali metals and they possess one loosely held electron in their valence shell. Alkali metals are therefore very reactive and their melting point, hardness, conductivity, and first ionization energy decrease down the group.<sup>[26]</sup> Table 1 lists some of the physical properties that are of interest in developing SIBs and LIBs.

**Table 1.** Physical properties of lithium and sodium.

Property <sup>a)</sup>	Li	Na
Atomic mass [g mol <sup>-1</sup> ]	6.94	22.99
Electron configuration <sup>b)</sup>	[He] 2s <sup>1</sup>	[Ne] 3s <sup>1</sup>
Cationic radius [Å]	0.76	1.02
Standard electrode potential [V]	-3.04	-2.71
Melting point [°C]	180.5	97.7
Density [g cm <sup>-3</sup> ]	0.971	0.534
First ionization energy [kJ mol <sup>-1</sup> ]	520.2	495.8
Theoretical gravimetric capacity [mAh g <sup>-1</sup> ]	3861	1165
Theoretical volumetric capacity [mAh cm <sup>-3</sup> ]	2062	1131

<sup>a)</sup>Data derived from refs. [17,27]; <sup>b)</sup>The abbreviated notation is used for the electron configuration.

One of the most important figures of merit for comparison is the redox potentials of the two alkali elements. The standard reduction potential of Na<sup>+</sup>/Na of -2.71 V versus SHE is about 330 mV above that of Li<sup>+</sup>/Li, -3.04 V. Since this potential forms the thermodynamic minimum limit for the anode, in most cases, the anodic electrode potentials for SIBs will always be higher than those of LIB.

Another important physical property to compare is the melting point of both metals. Na is a soft metal with a low melting point of 97.7 °C compared to that of Li at 180.5 °C. This low melting point is a drawback for developing solid-state SIBs, considering the high temperatures necessary to have functional solid-state electrolyte conductivity.

## 3. Charge Insertion Mechanisms in Electrode Materials

The charge insertion mechanisms for the insertion of sodium into the matrix of the host active materials used in SIB electrodes can be classified as intercalation, alloying, and conversion. Palacín made a clear illustrative figure (see Figure 2), outlining these three charge insertion mechanisms and their relative, concomitant structural changes.<sup>[28]</sup> Although this illustration is based on host materials for LIBs, it remains relevant for understanding insertion mechanisms in SIB materials.

The use of the terms insertion and intercalation in electrode materials can be somewhat confusing, in Figure 2 for example, the term insertion was replaced with intercalation according to the standard adopted in this review. Poinsignon and Armand defined an insertion electrode material as an electrode that intrinsically possesses the three functions of electronic and ionic conductivity, i.e., mixed conductivity, and a source of chemical potential.<sup>[29]</sup> The term “insertion” has also been used to generally describe reactions involving the transfer of a guest species (atom, ion, or molecule) into a host crystal lattice.<sup>[30]</sup> This obviously covers a wide range of electrode materials. The IUPAC recommendations of 1994 define “intercalation” as a term strictly reserved for the case of topotactic insertion of a guest into a 2D host.<sup>[30]</sup> Nevertheless, the term is occasionally used in reference to insertion in 1D as well as 3D host

## Mechanisms in charge insertion

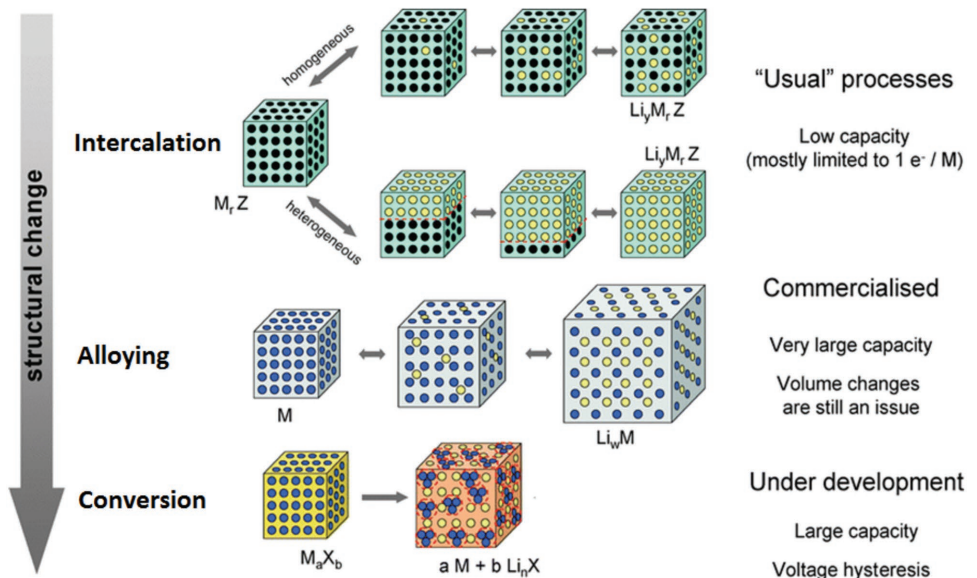


**Figure 2.** A schematic representation of the different mechanisms in charge insertion observed in electrode materials for lithium-ion batteries. Black circles: voids in the crystal structure; blue circles: metal; yellow circles: lithium. Similar classifications are also used in sodium-ion batteries. Adapted with permission.<sup>[28]</sup> Copyright 2009, The Royal Society of Chemistry.

structures.<sup>[31]</sup> Evidently, no strict differentiation exists in literature between insertion and intercalation and in some cases both terms are used synonymously.

In this review, the term intercalation is reserved to the restricting condition that the host matrix largely retains its structural integrity during the charge insertion/disinsertion process. This is mostly true for interlayer insertion of sodium guest ions in crystalline compounds and not, for example, the insertion of sodium into a metallic matrix during alloying since such processes are associated with major structural changes. Compared to other insertion mechanisms, volume changes associated with intercalation reactions are generally negligible. The larger size of  $\text{Na}^+$  can however be expected to impose a greater strain on the volume and structure of the host compared to analogous, lithium-based mechanisms. Volume changes in composite electrodes are particularly undesirable and best avoided; besides the ingenious electrode designs needed to support the volume changes, they also result in sluggish electrode kinetics due to the extra activation energy needed to move phase boundaries.

Beyond the intercalation-based electrodes in current SIB applications and in parallel to recent developments in LIBs, alloy-based elements or compounds are likewise investigated as promising electrodes for next-generation, high-capacity anode materials. During alloying and similar to the mechanism and nomenclature shown in Figure 2, the  $\text{Na}^+$  ions are added to the electrode active material in the following reaction mechanism



where M is the electrode active material, usually a group 14 or 15 element or compound. In a topotactic insertion of Na in M,

the alloying reaction is classified as a solid-solution reaction.<sup>[32]</sup> Here, no phase transformations take place. Conversely, if the insertion of Na is concomitant with phase changes, the alloying reaction is classified as an addition reaction.

Based on the gravimetric capacity, alloy electrodes are an order of magnitude higher than intercalation-based compounds. In addition, a low operating voltage of  $\approx 0.5$  V versus  $\text{Na}^+/\text{Na}$  makes them safer anode materials with high energy density.<sup>[33]</sup> The critical challenge, however, is controlling the huge volume changes observed during cycling, up to 300% v/v in some cases. This results in pulverizations, particle disconnections, and eventual isolation of the active materials.<sup>[33]</sup> Evidently, the achievable cycleability in composite electrodes is unimpressive due to the mechanical stress and loss of electrical contact.<sup>[34,35]</sup> Ingenious strategies in electrode architecture are thus required for their successful usage, yet several have been implemented.<sup>[36–38]</sup>

Besides intercalation and alloying reactions, conversion reactions are the other class of insertion mechanisms. In this relatively new insertion process, very little has been agreed on the underlying mechanism. However, several reports on Li-based conversion reactions have emerged, enabling some degree of appreciation.<sup>[39,40]</sup> Similar to alloy reactions, conversion mechanisms offer another avenue to achieve higher gravimetric capacity; however, similar challenges related to large volume expansions persist. Another disadvantage is the typical voltage hysteresis during (dis)charging cycles which further reduces their energy efficiency.<sup>[41]</sup> Contrary to other insertion mechanisms, conversion reactions are not limited to only one electron exchange per equivalent mole of the host compound.<sup>[41,42]</sup> This enables them to achieve a phenomenally high gravimetric capacity.

## 4. Anode Materials

The negative electrode constitutes the electrode with the lowest potential. In SIBs where the solvated  $\text{Na}^+$  is the principal charge carrier, the thermodynamically lowest electrode potential is given by the reduction potential of sodium ( $-2.71\text{ V}$  vs SHE). To increase the energy density of the cell, it is therefore desirable to have a negative electrode with theoretically the lowest potential and highest specific capacity.

The most suitable negative material, from a thermodynamic viewpoint, is therefore metallic sodium with the lowest possible cell potential and a high theoretical capacity of  $1165\text{ mAh g}^{-1}$ . For safety concerns, the use of metallic electrodes in room temperature secondary batteries has not been achieved to an appreciable extent. This is because an unstable surface passivation layer or solid electrolyte interphase (SEI) forms on the electrodeposited sodium surface. The continual reaction of newly formed surfaces with the electrolyte during plating thus constrains the cycleability. Further challenges relate to dendritic growth during (dis)charge cycles. If unconstrained, these lead to internal short-circuiting and thermal runaway. It is here worth mentioning that the use of metallic anodes in rechargeable room temperature lithium-based or sodium-based battery systems has been an unresolved challenge for nearly half a century.<sup>[43]</sup> The hope is finding a suitable electrolyte or protective surface layers that remain stable at these highly reducing potentials.<sup>[44]</sup>

Having hit a brick wall with metallic Na, the research for an alternative anode then turned to active material hosts capable of charge insertion at potentials slightly above  $0\text{ V}$  versus  $\text{Na}^+/\text{Na}$ . This avoids safety challenges arising from metallic plating. In LIBs, the electrolytic decomposition of ethylene carbonate for example coincidentally leads to a particularly favorable SEI which is electrically nonconductive and prevents further electrolyte decomposition.<sup>[31,45]</sup> As previously highlighted, it was the discovery of graphite as a high specific capacity and robust anode material for LIB and the lack of a comparatively cheap, low potential anodic material for SIB applications which bottlenecked the progress in SIB research. It is therefore only prudent to begin with a review of the current progress in negative electrode materials for SIBs.

### 4.1. Intercalation-Based Negative Electrode Materials

#### 4.1.1. Carbon-Based Intercalation Materials

Graphite, the anode of choice in LIBs with a high theoretical specific capacity of  $372\text{ mAh g}^{-1}$ , operates at a flat and low potential of  $\approx 0.15\text{ V}$  versus  $\text{Li}^+/\text{Li}$  and is stable over many cycles. When applied to the SIB system, the electrochemical insertion of sodium into graphite results in  $\text{NaC}_{64}$ , corresponding to very low theoretical capacity of only  $35\text{ mAh g}^{-1}$ .<sup>[46,47]</sup> It was initially proposed that the larger  $\text{Na}^+$  ion mismatches the graphite interlayer distance of  $3.35\text{ \AA}$  and results in a less favorable formation energy for sodium binary graphite intercalation compounds (b-GIC).<sup>[27,45,48,49]</sup> Yet, this could not explain the fact that other b-GIC such as  $\text{MC}_6$  and  $\text{MC}_8$  (where M is the alkali metal) are readily formed with heavier alkali metals such as K,

Rb, and Cs.<sup>[50,51]</sup> It is therefore evident from the above that the ionic radii of the alkali metals are, at least, not the only inhibiting factor.

Nobuhara et al.<sup>[52]</sup> using a first-principles approach and Liu et al.<sup>[50]</sup> using quantum mechanical methods independently applied density functional theory (DFT) calculations in the Vienna ab initio simulation package and discovered that the energy of formation ( $E_f$ ) of b-GIC is of the order  $\text{Na} > \text{Li} > \text{K} > \text{Rb} > \text{Cs}$ . Figure 3a illustrates a Hess law diagram for the formation of b-GIC. Figure 3b,c confirms that Na has the weakest binding energy to a given substrate and Figure 3d,e compares the bond lengths in various alkali metal carbons (AMC).<sup>[50,52]</sup> The low Na uptake in graphite therefore can be explained from the thermodynamics of the competition between the first ionization of sodium and the enthalpy of ion–substrate bonding.<sup>[50]</sup>

To further illustrate that indeed it is not the size of the alkali metal, high-capacity sodium intercalation in graphite has been demonstrated, using the  $\text{Na}^+$ -solvent cointercalation phenomena, wherein the solvent molecules act as a “nonstick” shell.<sup>[45]</sup> This cointercalation mechanism can be expressed as



where  $\text{C}_n$  represents the carbon atoms in the graphite lattice, S the solvent molecule, and  $\text{Na}^+ \text{S}_y \text{C}_n^-$  is the ternary graphite intercalation compound (t-GIC). Here, graphite is reduced to form t-GIC and this electrochemical pathway had already been demonstrated as far back as 1965 by Golé and co-workers.<sup>[47,53]</sup> Figure 4a–c illustrates the reversible gravimetric capacity and voltage profiles obtained during the  $\text{Na}^+$ -solvent cointercalation process.<sup>[45,54,55]</sup>

Using ether-based electrolytes, Jache and Adelhelm<sup>[45]</sup> obtained storage capacities of about  $100\text{ mAh g}^{-1}$  while Cohn et al.<sup>[55]</sup> explored cointercalation in graphene, obtaining capacities above  $150\text{ mAh g}^{-1}$  with only a negligible capacity fade over 8000 cycles (see Figure 4b). Another interesting characteristic of cycling is the small voltage polarization between (dis)charging cycles, indicative of a highly reversible and energy efficient redox process. Promising performances of SIB full cells based on  $\text{Na}^+$ -solvent cointercalation such as the graphite// $\text{Na}_{1.5}\text{VPO}_{4.8}\text{F}_{0.7}$  are illustrated in Figure 4d.<sup>[54]</sup> Yet, as further explained in Section 5.2.3, ether-based solvents have a narrow electrochemical stability window that limits possible cell configurations. Further electrolyte optimizations are therefore necessary for the practical use of the solvent cointercalation phenomenon.

Expanded graphite (EG) is yet another carbonaceous anode material that has been proposed for SIB application.<sup>[48]</sup> The charge insertion mechanism in EG is illustrated in Figure 5a, where pure intercalation is therein assumed. Further explorations in the role of the oxygen-containing surface groups in the insertion mechanism are however needed. A comparison between the voltage profiles obtained in EG and the typically observed voltage profiles in hard carbon-based electrodes (see Figure 5b,c) reveals that the voltage profiles reported in EG only show a sloping profile and do not manifest a plateau region. This fundamental difference could be a result of the modification of the distribution of intercalation sites due to the presence of heteroatoms, such as the oxygen-containing surface groups.

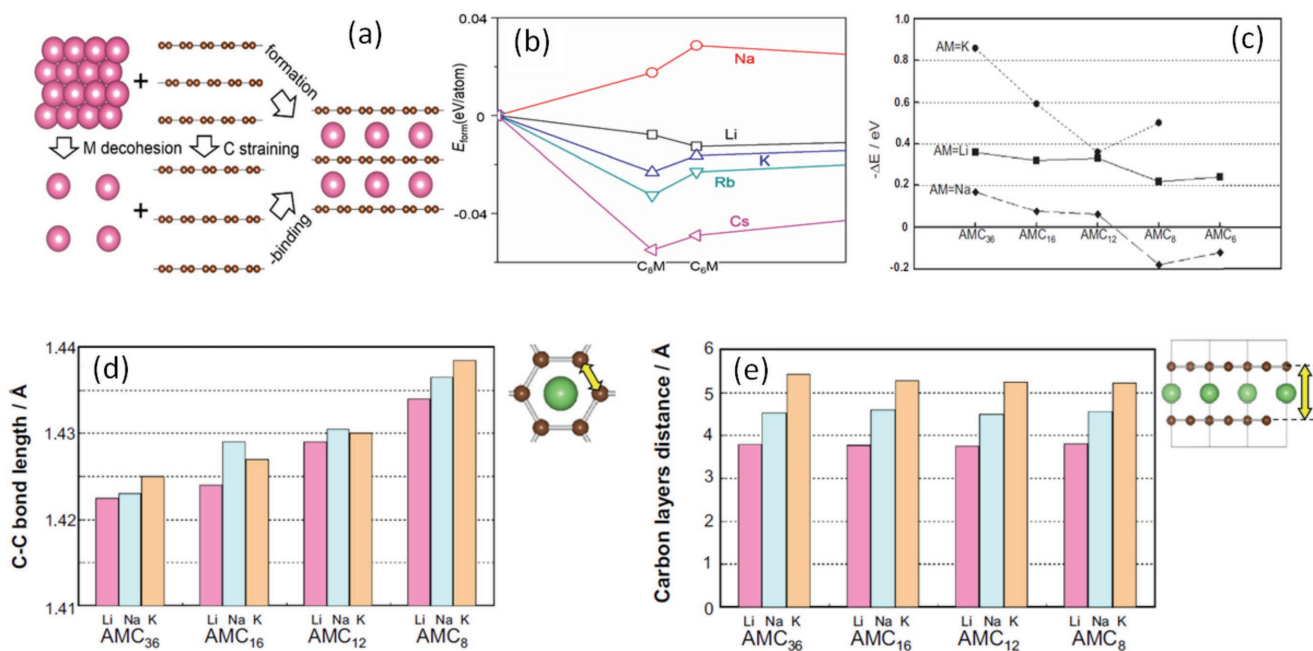


**Figure 3.** a) The formation mechanism of alkaline metal GIC. b) DFT calculated formation energies of alkaline metal GIC. c) First-principles calculated formation energies of alkaline metal GIC. d) The bond lengths between the carbon atoms in the carbon layers intercalated with alkali metals (AMC) and e) the lengths between the carbon layers intercalated with alkali metals. a,b) Reproduced with permission.<sup>[50]</sup> Copyright 2016, National Academy of Sciences/Proceedings. c-e) Reproduced with permission.<sup>[52]</sup> Copyright 2013, Elsevier.

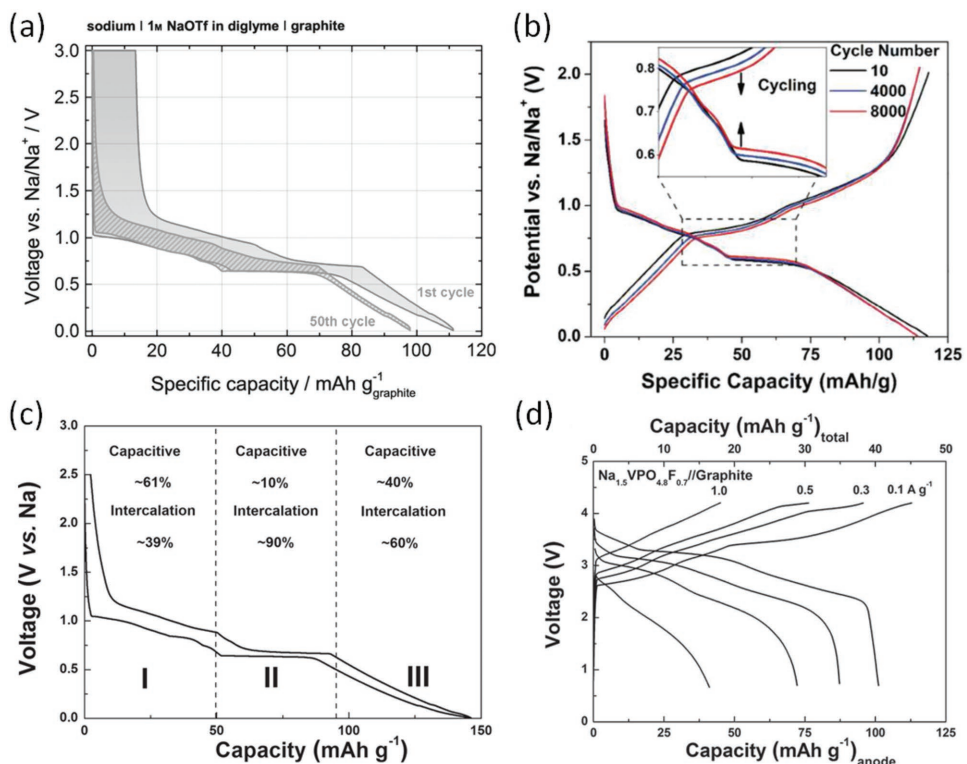


**Figure 4.** Exploring the solvent cointercalation phenomena. a) Charge and discharge characteristics of a  $\text{Na}/\text{Graphite}$  half-cell. b) Charge and discharge profile of  $\text{Na}/\text{Graphene}$  half-cell. c) The proposed mechanism in the  $\text{Na}^+$ -solvent cointercalation processes in graphite. d) A SIB full cell based on solvent cointercalation graphite anode at various C-rates.  $\text{Na}_{1.5}\text{VPO}_{4.8}\text{F}_{0.7}$  is used as the cathode while  $\text{NaPF}_6$  dissolved in diethylene glycol dimethyl ether is used as the electrolyte. a) Reproduced with permission.<sup>[45]</sup> Copyright 2014, Wiley-VCH. b) Reproduced with permission.<sup>[55]</sup> Copyright 2015, American Chemical Society. c,d) Reproduced with permission.<sup>[54]</sup> Copyright 2014, Wiley-VCH.

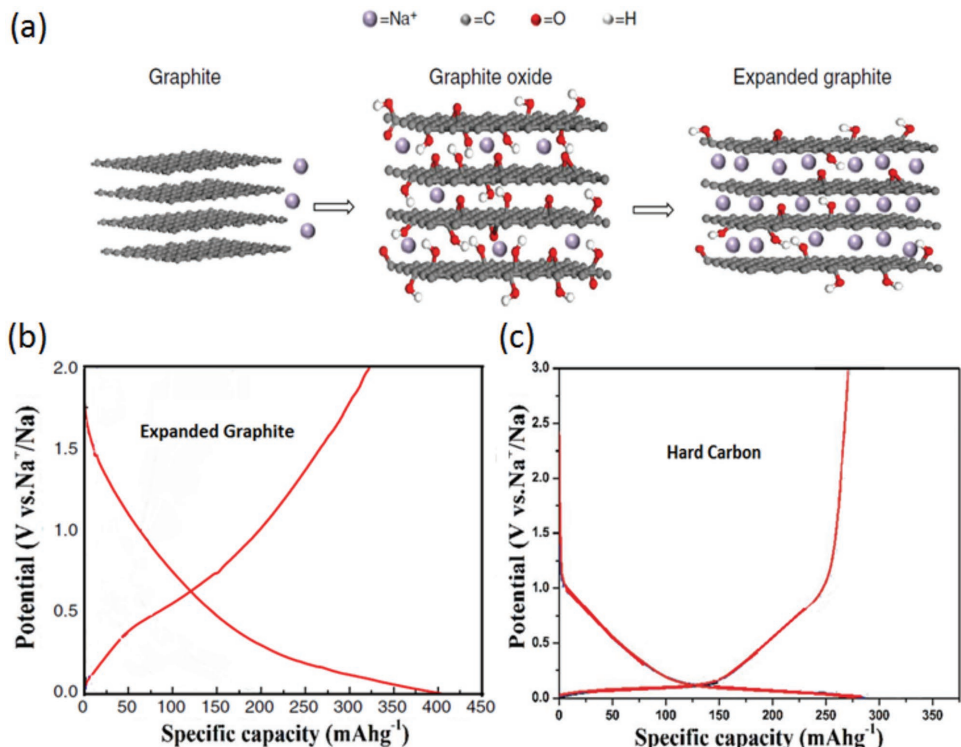


**Figure 5.** Overview of sodium storage in hard carbon and expanded graphite. a) Illustrative figure showing sodium intercalation in graphite, graphite oxide, and expanded graphite. b) Voltage profile in expanded graphite showing a sloping potential. c) Typical voltage profile in hard carbon. a,b) Adapted with permission.<sup>[48]</sup> Copyright 2014, Macmillan Publishers Limited. c) Adapted with permission.<sup>[56]</sup> Copyright 2015, The Royal Society of Chemistry.

The state-of-the-art anode material for SIBs is hard carbon, prominent since its inception in the year 2000.<sup>[27]</sup> Hard carbons are usually prepared by high-temperature carbonization of solid phase organic and polymer precursors such as cellulose,<sup>[57]</sup> glucose,<sup>[18]</sup> sugar,<sup>[58]</sup> and polypyrrole.<sup>[59]</sup> The complex microstructure of HC is composed of graphene-like parallel layers embedded in a microporous amorphous phase. This structure is frequently exemplified by the “house of cards” model, which is here shown in **Figure 6c**. The charge and discharge voltage profile of HC is also shown in **Figure 6d,e**. From these results, two characteristic features are evident: i) a sloping region from  $\approx 1$  V and ii) a long plateau region commencing from about 0.1 V until reaching 0 V (vs  $\text{Na}^+/\text{Na}$ ). From an electrochemical point of view, regions (i) and (ii) can be understood as successive solid solution and two-phase charge insertion mechanisms, respectively.

Although HC has an impressive specific capacity of close to 300  $\text{mAh g}^{-1}$ , which approximates to that of graphite in LIB, much of this capacity occurs at a very low potential, close to sodium plating. Due to safety concerns, this characteristic limits the rate capability of HC since overpotentials from electrode kinetics would result in the undesired metallic plating (at high charging rates). The most critically unresolved issue however is the first cycle irreversible capacity loss in HC anodes.<sup>[60]</sup> Following the first cycle, a significant amount of sodium ions are either trapped in the microstructure or consumed in the SEI formation. This brings a conundrum in cell balancing since the cathode material is the source of the cations and the safety objective of avoiding metallic Na plating demands the capacity

in the anode to be higher than that of the cathode. This anodic capacity loss cannot therefore be compensated by allowing an excess capacity in the cathode and translates to an enormous loss in energy density of HC-based SIBs.

The microstructural properties of HC, in particular its microporosity and degree of graphitization, are known to bear a huge influence on electrochemical performance.<sup>[60]</sup> **Figure 6a,b** shows X-ray powder diffraction and Raman spectra of HC, respectively, which have resulted in the “house of cards” model. The relative intensity ratio,  $I_D/I_G$ , between different HC samples is used as an indicator of the degree of graphitization. Scanning electron microscope (SEM) images of HC are shown in **Figure 6f** while the effect of the degree of graphitization on the cycling performance of three HC samples is illustrated in **Figure 6g**. The optimization of the electrode performance of HC with the intent to reduce the first cycle irreversible capacity loss, enhance electrical conductivity, and improve cycleability thus requires a mastering of the synthesis methods and their impact on the microstructure.<sup>[60–62]</sup>

Controversy in correlating the microstructural properties of HC to the observed voltage profile has led to spirited systematic studies to elucidate the sodium storage mechanism in HC as illustrated in **Figure 7**.<sup>[63,64]</sup> Early studies by Stevens and Dahn hypothesized an intercalation mechanism between parallel graphene sheets for the sloping voltage region, i.e., region (i), on account of an observed interlayer expansion during Na insertion, while nanopore filling in a process analogous to adsorption was ascribed to the plateau voltage profile, i.e., region (ii).<sup>[46]</sup> This mechanism, termed “intercalation–adsorption” and

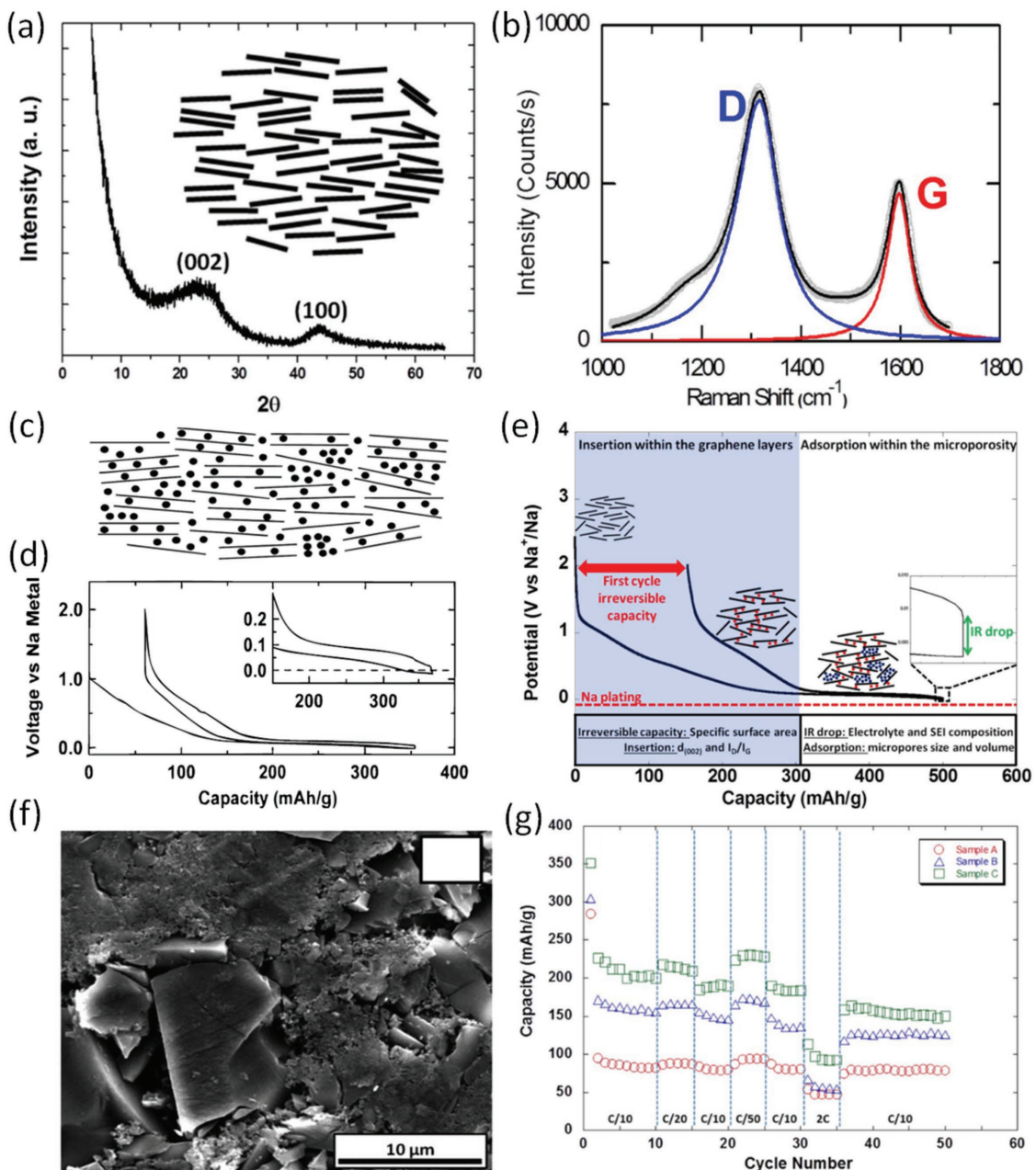


**Figure 6.** Microstructure and electrochemical properties of hard carbon. a) Typical X-ray powder diffraction pattern ( $\text{Cu K}\alpha$ ), and the inset shows a remodeled structure. b) Raman spectrum for hard carbon showing two characteristic bands: D-band, with intensity  $I_D$  and G-band with intensity  $I_G$ , and the ratio  $I_D/I_G$  indicates the degree of graphitization. c) The house of cards model showing intercalation in hard carbon.<sup>[18]</sup> d) Typical charge and discharge voltage profile for hard carbon, sodium insertion shown in red dots and adsorption within the micropores shown in the blue dots, and the inset zooms into the low-potential region. e) Classification of the different steps in the mechanism of Na insertion in hard carbon. f) SEM microscope image of tape-casted carbon-coated hard carbon. g) Cycleability and rate capability tests for three different samples of hard carbon electrodes prepared at 1100 °C under different Ar flow rates. a,b,e-g) Reproduced under the terms of the CC-BY Licence 4.0.<sup>[60]</sup> Copyright 2015, The Authors. c,d) Reproduced by permission.<sup>[18]</sup> Copyright 2000, The Electrochemical Society.

shown in Figure 7a was further corroborated by the subsequent works of Komaba et al.,<sup>[62]</sup> wherein ex situ small-angle X-ray scattering measurements were used to probe the nanopore structure of the HC and confirmed nanopore filling in the low-voltage plateau.

Contradictory findings however emerged as Cao et al.<sup>[49]</sup> revealed the Na ions are incapable of intercalating when the

graphene interlayer spacing is less than 3.7 Å. Tsai et al.<sup>[65]</sup> sought to clarify the effect of the graphene interlayer distance and the presence of copious point defects in HC using DFT calculations. It was therein concluded that a large initial interlayer distance of 3.8 Å as well as vacancy defects could greatly enhance sodium storage due to the strong ionic bond between Na<sup>+</sup> ions and the defects. An “adsorption–intercalation”

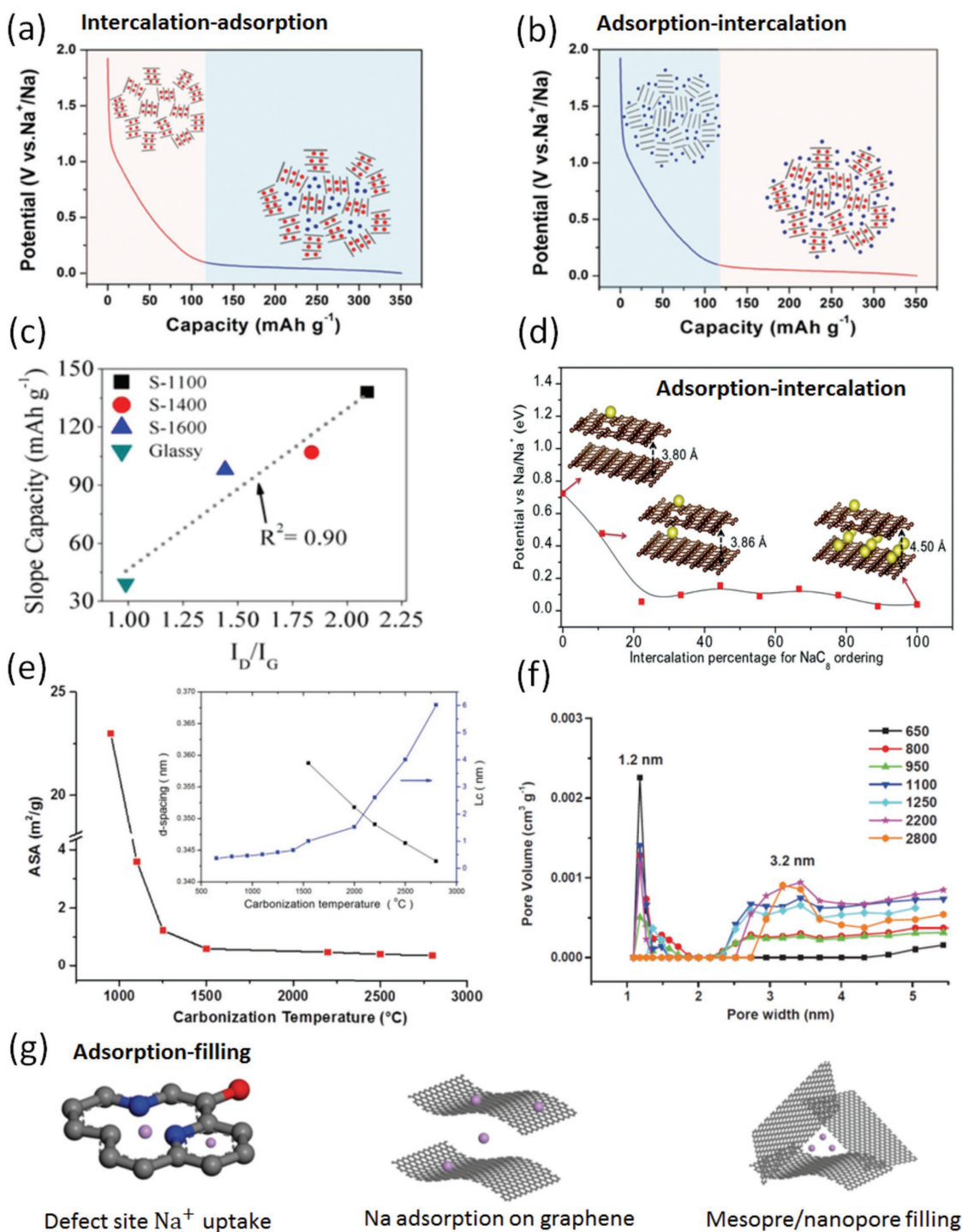


**Figure 7.** Controversy in correlating the microstructural properties of HC. a) The intercalation–adsorption mechanism. b) The adsorption–intercalation mechanism. c) Slope capacity as a function of defect concentration ( $I_D/I_G$ ). d) The adsorption–intercalation mechanism determined by DFT calculations. e) The active surface area in hard carbon as a function of the carbonization temperature, inset showing the  $d$ -spacing evolution as a function of carbonization temperature. f) Evolution of pore size distribution as a function of the carbonization temperature in hard carbon. g) Proposed mechanisms in Na insertion in hard carbon based SIB anodes. a,b) Reproduced with permission.<sup>[63]</sup> Copyright 2017, Wiley-VCH. c,d) Reproduced with permission.<sup>[64]</sup> Copyright 2015, American Chemical Society. e–g) Reproduced with permission.<sup>[64]</sup> Copyright 2015, Wiley-VCH.

mechanism, here illustrated in Figure 7b,d, was thus premised. The sloping region was correlated with the simultaneous occurrence of adsorption on defect sites and intercalation in

graphene layers, while the plateau region was assigned an intercalation mechanism on sites around the defects. Experimental studies by Bommier et al.<sup>[66]</sup> on “defect-free” glassy carbon and

samples of sucrose-derived HC, carbonized in the temperature range of 1100–1600 °C, further corroborated this mechanism. Raman spectra deduced intensity ratio:  $I_D/I_G$  was therein used as an indication of defect concentration and a linear correlation versus “slope capacity,” i.e., the region (i) capacity, is reported (Figure 7c). Glassy carbon, with the least of such defects, showed the least slope capacity as expected. The voltage profile was further analyzed using the galvanostatic intermittent titration technique (GITT), wherein a sharp decline in the diffusion coefficient was observed in the low-voltage plateau region. This phenomena, a common occurrence in Li intercalation compounds, led to the conclusion that the region (ii) plateau voltage profile was indeed an intercalation mechanism of Na in graphene layers. Yet, an anomalous increase of the GITT-deduced diffusion coefficient at the very end of the discharge process posed questions.

Later, Zhang et al.<sup>[64]</sup> prepared carbon nanofibers (CNFs) with tailored graphitization degrees by varying the pyrolysis temperature between 650 and 2800 °C and obtained a spectrum of CNFs with different pore size distribution, degree of graphitization, and amount of N and O heteroatoms. As the carbonization temperature increased, a rise in the degree of graphitization, a decrease in the active surface area (ASA), and a gradual disappearance of heteroatom surface groups are reported. An interesting observation herein illustrated in Figure 7e,f is the evolution in the ASA, *d*-spacing, and pore size distribution with temperature. The pore width migrates from an average of 1.2 nm for low-temperature synthesized CNFs to 3.2 nm (small mesopores) for CNFs synthesized at temperatures above 950 °C. Based on systematic experimental results, the Na storage mechanism in the sloping voltage region is described as two processes of  $\text{Na}^+$  bonding on the defect sites induced by heteroatoms and Na adsorption onto the surfaces of randomly oriented graphene layers. The low-voltage plateau was therein correlated to “small mesopore” filling and this marked a partial return to Dahn and Stevens’s initial nanopore filling model. Figure 7g illustrates these three proposed processes in the “adsorption-filling” mechanism. Although *in situ* X-ray diffraction experimental evidence could not conclusively exclude the possibility of intercalation in the sloping region, the consistency of the obtained *d*-spacing, however, discarded possibilities of either intercalation or Na plating in the low-voltage plateau region.

However, recent systematic experimental and simulation studies by Qiu et al.<sup>[63]</sup> rejuvenated the adsorption–intercalation mechanism. Therein, cellulose-derived HC samples, carbonized in the 900–1500 °C range, were analyzed. In addition to similar results as reported by Bommier et al.,<sup>[66]</sup> wherein the slope capacity is correlated to the defect concentration, the plateau capacity was further correlated to the pyrolysis temperature. A maximum plateau capacity of 220 mAh g<sup>-1</sup> is thus reported for HC synthesized at 1300 °C. On account of these findings, the sloping potential is described as Na adsorption on surface defect sites while the plateau region was correlated to Na insertion into graphene layers. In response to the question of the increase in the diffusion coefficient at the end of discharge, a novel theory was therein proffered, wherein highly attractive interactions within intercalated Na are thought to give rise to this phenomenon.

These contradictory hypotheses, while being supported by meticulous experimental evidence, could also be rooted to the different materials and methods in the original studies. Regardless of this clear lack of a universally agreed mechanistic model, several significant steps toward optimization of HC anode materials in SIB have been realized recently.<sup>[67–69]</sup> For example, HC prepared in the 1000–2000 °C temperature range shows the best electrochemical performance with regard to a minimum slope capacity and a prominent plateau voltage without significant Na plating. In addition, the decrease in the ASA as a function of the increase in carbonization temperature advantageously results in an increase in Coulombic efficiency due to reduced SEI formation. On the other hand, nitrogen-doped and defective HC nanoshells do not exhibit any voltage plateau.<sup>[69]</sup> These findings have led to improved HC performances for SIB application.

#### 4.1.2. Titanium-Based Compounds

Several titanium-based compounds are extensively studied as possible intercalation hosts in SIBs, and this is partly due to their promising applications in LIBs.<sup>[70–74]</sup> Prior to discovery of HC electrodes, only two titanium-based anode materials were known:  $\text{TiS}_2$ <sup>[75,76]</sup> and NASICON-type  $\text{NaTi}_2(\text{PO}_4)_3$ .<sup>[77,78]</sup> NASICON is an acronym for NAtrium SuperIonic CONductor. In recent times, several titanium-based compounds such as titanium oxides, titanates, and titanium phosphates have emerged as potential anodes for LIBs and SIBs.

Titanium dioxide ( $\text{TiO}_2$ ), a naturally occurring oxide of titanium, exists in several polymorphs such as rutile, anatase, and brookite.<sup>[79]</sup> Because  $\text{TiO}_2$  is abundant, environmentally friendly, and inexpensive, it has emerged as the most attractive noncarbonaceous anode material.<sup>[17,27]</sup> Among its polymorphs, anatase-type  $\text{TiO}_2$ , with an open 3D framework, has achieved a relatively high reversible capacity in LIBs. Figure 8a shows the configuration of  $\text{TiO}_2$  octahedra in anatase. Although microsized anatase is electrochemically active in LIBs, accommodating about 0.5 moles of Li ions per formula unit (168 mAh g<sup>-1</sup>),<sup>[80]</sup> the same material is puzzlingly inactive in SIBs and this finding initially leads to the belief that the larger sized sodium ions could not diffuse into the 3D framework.<sup>[81]</sup> Nevertheless, quantum chemical theory ab initio calculations suggested that, in spite of a larger ionic radius, sodium insertion in anatase is feasible.<sup>[82]</sup> It was therein shown that sodium diffusion barrier in anatase is not significantly larger in comparison to that of lithium.

The first successful sodium intercalation in anatase-type  $\text{TiO}_2$  occurred in its nanocrystal forms.<sup>[83]</sup> Nanocrystalline  $\text{TiO}_2$  has an impressive rate capability at a moderate gravimetric capacity of about 150 mAh g<sup>-1</sup> and exhibits stable cycleability up to 1000 cycles.<sup>[83,84]</sup> Furthermore, an outstanding rate capability of 11 C-rate is reported in carbon-coating free samples, the highest among either carbonaceous or Ti-based SIB anodes.<sup>[84]</sup> This is a phenomenal achievement, given the fact that  $\text{TiO}_2$  has intrinsically a low electric conductivity. Figure 8a illustrates the crystal configuration in  $\text{TiO}_2$ . Figure 8b shows a high-resolution SEM image of pristine  $\text{TiO}_2$  nanoparticles. The electrochemical properties of  $\text{TiO}_2$  are illustrated in Figure 8c–f, where a large first cycle irreversible capacity loss is highlighted, and based on

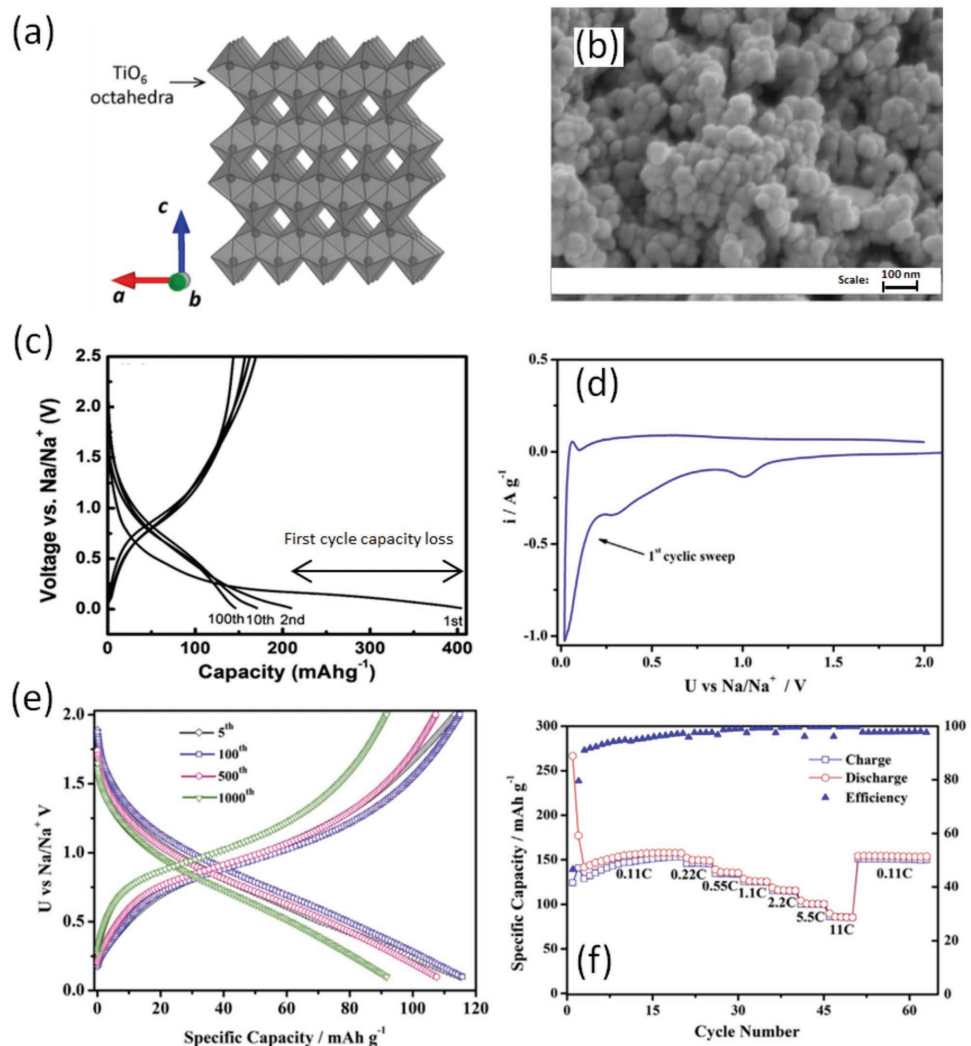


**Figure 8.** Properties of anatase-type  $\text{TiO}_2$ . a) Schematic illustration of the configuration of  $\text{TiO}_2$  octahedra and b) SEM image of pristine  $\text{TiO}_2$  nanoparticles.<sup>[84]</sup> c) First 100 charge and discharge voltage profiles of  $\text{TiO}_2$  showing the first cycle irreversible capacity loss and d) cyclic voltammogram of  $\text{TiO}_2$  illustrating the first cycle sweep. e) Extended cycling voltage profiles of  $\text{TiO}_2$  showing 1000 cycles. f) Rate capability tests of  $\text{TiO}_2$ , and a high rate of 11C is evidenced while a return to 0.11C recovers the initial capacity. a) Reproduced with permission.<sup>[17]</sup> Copyright 2014, American Chemical Society. b,d-f) Reproduced with permission.<sup>[84]</sup> Copyright 2013, Elsevier B.V. c) Reproduced with permission<sup>[83]</sup> Copyright 2013, The Royal Society of Chemistry.

the cyclic voltammetry analysis, the redox reaction appears to be kinetically limited. However, the cycleability and rate performance are clearly outstanding.

Several disadvantages however persist in anatase  $\text{TiO}_2$ , some of which are illustrated in Figure 8c. The most evident being a sloping voltage profile that undermines the available energy density. Furthermore, a first cycle Coulombic efficiency of only 42% is rather unimpressive. In general, nanosized active materials come at a penalty of increased SEI formation and side reactions at the surface of the active material and this results in the large irreversible capacity loss therein evidenced. Yet, in spite of these challenges, nanocrystalline  $\text{TiO}_2$  remains a promising candidate anode material for high-power SIB applications.

Sodium titanates, the compounds composed of  $\text{Na}_2\text{O}$  and  $\text{TiO}_2$  with a general composition series of  $\text{Na}_2\text{O} \cdot n\text{TiO}_2$ , have also been used as anode materials in SIBs.<sup>[17]</sup> In 2011, Senguttuvan et al.<sup>[85]</sup> in a quest for low-voltage transition metal

oxides investigated the electrochemical insertion of sodium in  $\text{Na}_2\text{Ti}_3\text{O}_7$  ( $n = 3$ ), a compound which hitherto had been utilized for divers proposes such as photocatalysis and heavy metal removal from waste water.<sup>[86,87]</sup> Surprisingly,  $\text{Na}_2\text{Ti}_3\text{O}_7$  can reversibly insert up to 2 moles of  $\text{Na}^+$  ions per formula equivalent, corresponding to  $\approx 200 \text{ mAh g}^{-1}$ , while  $\text{Li}_2\text{Ti}_3\text{O}_7$  can only intercalate 1.4 moles of  $\text{Li}^+$  ions.<sup>[88]</sup> An impressively low and plateau (flat) discharge potential of 0.3 V versus  $\text{Na}^+/\text{Na}$  was also evidenced, culminating to the lowest intercalation potential recorded in oxide electrodes of either LIBs or SIBs. Figure 9a–c illustrates the structure and electrochemical properties of  $\text{Na}_2\text{Ti}_3\text{O}_7$ .

While microsized  $\text{Na}_2\text{Ti}_3\text{O}_7$  is electrochemically active, it suffers from a low cycle life. On the other hand, nanosized samples of  $\text{Na}_2\text{Ti}_3\text{O}_7$  have a significantly improved cycleability, but due to the increase in surface area, the first cycle Coulombic efficiency is unimpressive. Several optimization challenges to

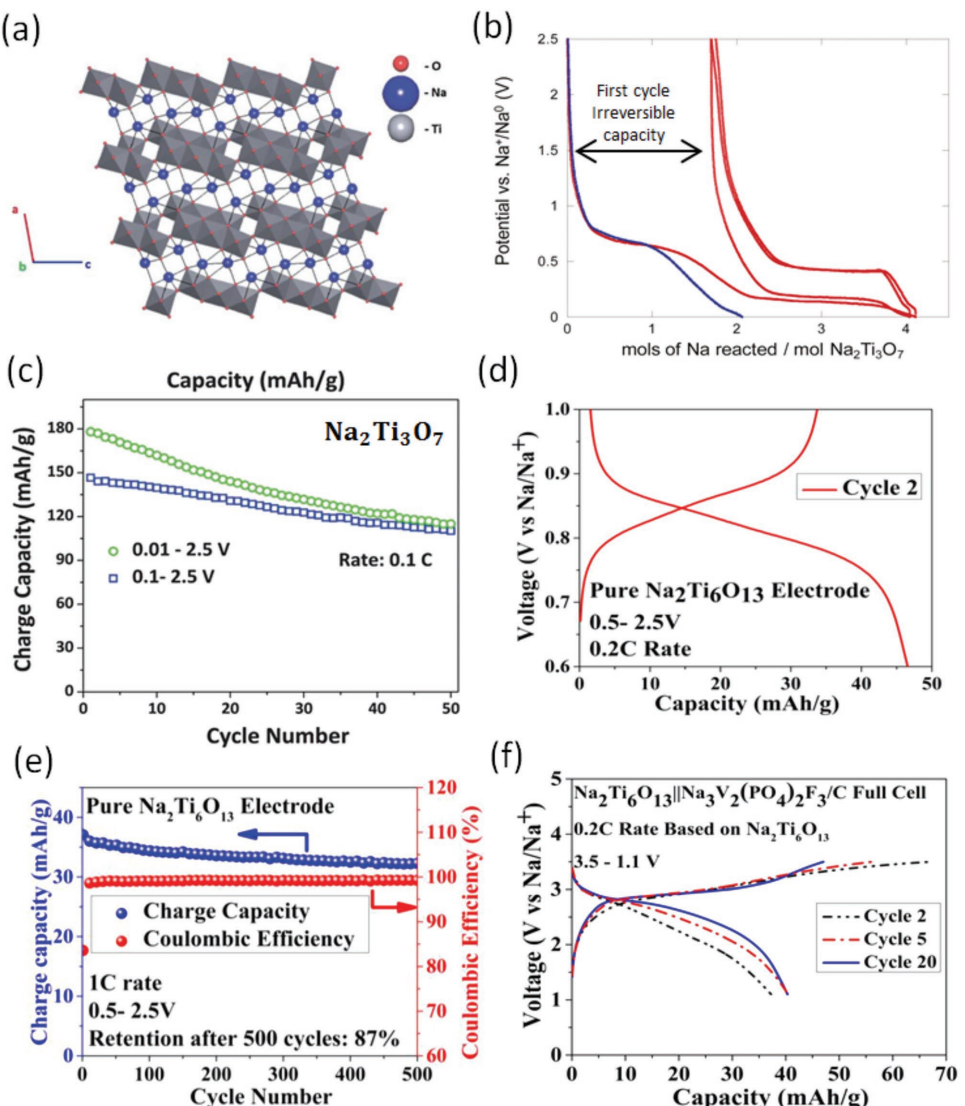


**Figure 9.** Structure and electrode performance of sodium titanates. a) Structure of  $\text{Na}_2\text{Ti}_3\text{O}_7$  viewed along the  $b$ -axis. b) Charge and discharge cycles of microsized  $\text{Na}_2\text{Ti}_3\text{O}_7$ . c) Charge capacity versus cycle number of carbon-coated, nanosized  $\text{Na}_2\text{Ti}_3\text{O}_7/\text{C}$ . d) Second cycle voltage profile of  $\text{Na}_2\text{Ti}_6\text{O}_{13}$ . e) Capacity versus cycle number for  $\text{Na}_2\text{Ti}_6\text{O}_{13}$  at 1 C-rate. f) A pure  $\text{Na}_2\text{Ti}_6\text{O}_{13}\parallel\text{Na}_3\text{V}_2(\text{PO}_4)_2\text{F}_3/\text{C}$  full cell cycled at C/5 rate. a,c) Reproduced with permission.<sup>[89]</sup> Copyright 2013, The Royal Society of Chemistry. b) Reproduced with permission.<sup>[85]</sup> Copyright 2011, American Chemical Society. d-f) Reproduced with permission.<sup>[92]</sup> Copyright 2013, The Royal Society of Chemistry.

simultaneously reduce the first cycle irreversible capacity and increase the cycleability still remain in  $\text{Na}_2\text{Ti}_3\text{O}_7$ . Interestingly, however, nanosized and carbon coated  $\text{Na}_2\text{Ti}_3\text{O}_7$  samples, as shown in Figure 9c, exhibit longer cycle life. Carbon coating has thus proved to be a highly beneficial strategy to enhance the electronic conductivity and simultaneously reduce the SEI formation in such electrode materials.<sup>[89,90]</sup>

Sodium nanotitanate  $\text{NaTi}_3\text{O}_6(\text{OH}) \cdot 2\text{H}_2\text{O}$  and its dehydrated form is another titanium-based anode material that was first reported by Shirpour et al.<sup>[91]</sup> in 2013. Although an attractively low voltage of 0.3 V versus  $\text{Na}^+/\text{Na}$  is therein reported, the voltage curve exhibits a sloping profile, an attribute of the solid-solution charge insertion mechanism. Furthermore, a severe loss in capacity in the first cycles points to the need for electrode optimization.

Nanorods of  $\text{Na}_2\text{Ti}_6\text{O}_{13}$  ( $n = 6$ ), prepared by a soft-template method, have also been studied as intercalation material for SIBs.<sup>[92]</sup> The electrochemical reaction for charge storage is written as



where  $x$  is the mole fraction of  $\text{Na}^+$  intercalated per formula unit of  $\text{Na}_2\text{Ti}_6\text{O}_{13}$ . The insertion process is also described as a solid-solution mechanism, with a very low volume expansion of only 1%, while 0.85 moles of  $\text{Na}^+$  can be accommodated in the structure ( $x = 0.85$ ), corresponding to  $42 \text{ mAh g}^{-1}$ . Additionally, an impressive cycle life of about 500 cycles with 87% capacity retention in conductive additive-free  $\text{Na}_2\text{Ti}_6\text{O}_{13}$  nanorods (see Figure 9e) and 85% capacity retention after 5000 cycles in

graphite containing composite electrodes is reported.<sup>[92]</sup> This makes  $\text{Na}_2\text{Ti}_6\text{O}_{13}$  a prospective anode material for low-cost SIB applications.

Even though a relatively flat voltage profile is observed in the (dis)charge profile, as illustrated in Figure 9d, the average voltage thereof is too high (0.8 V vs  $\text{Na}^+/\text{Na}$ ). This limits the energy density of SIB cells fabricated with a  $\text{Na}_2\text{Ti}_6\text{O}_{13}$  anode material, also considering the low gravimetric capacity of the samples. Indeed, Rudola et al.<sup>[92]</sup> prepared such a cell using a  $\text{Na}_3\text{V}_2(\text{PO}_4)_2\text{F}_3/\text{C}$  composite electrode in EC:PC and 1 M  $\text{NaClO}_4$  electrolyte. As expected, the resulting average cell voltage of 2.5 V and capacity with respect to weight of the anode of 41 mAh g<sup>-1</sup> after 20 cycles was rather low. In this study, they used an excess cathode in the balanced full cell, most likely as a strategy to overcome the anodic first cycle irreversible capacity loss.

Spinel  $\text{Li}_4\text{Ti}_5\text{O}_{12}$  (LTO), a known “zero-strain” anode material for LIBs,<sup>[93]</sup> was first reported as a sodium host in 2012 by Liang et al.<sup>[94]</sup> As a SIB anode, LTO has an attractively long plateau voltage between 0.5 and 0.8 V versus  $\text{Na}^+/\text{Na}$  and achieves a reversible capacity of 145 mAh g<sup>-1</sup>. Three-phase structural evolutions upon Na insertion are also reported, wherein pristine  $\text{Li}_4\text{Ti}_5\text{O}_{12}$  evolves to  $\text{LiNa}_6\text{Ti}_5\text{O}_{12}$  and  $\text{Li}_7\text{Ti}_5\text{O}_{12}$  upon Na insertion.<sup>[94]</sup> Early optimizations of LTO composite electrodes focused on binders.<sup>[95]</sup> Compared to conventional polyvinylidene difluoride binders, sodium alginate and carboxymethyl-cellulose sodium binders resulted in better cycleability and Coulombic efficiency. Recently, Na-doped LTO has been reported to have an improved electrode capacity of 150 mAh g<sup>-1</sup> and an enhanced cycleability of 800 cycles,<sup>[96]</sup> while a superior rate capability of 10 C-rate and 15 C-rate has been reported in carbon-coated nanosheets and LTO nanorods, respectively.<sup>[97,98]</sup> Although these electrochemical properties are desirable for a safe SIB, a general drawback for LTO is a relatively high operating electrode potential for application in high energy density cells.<sup>[27]</sup>

#### 4.2. Alloy-Based Anode Materials

The so-called “p-block” elements (Sn, Ge, P, and Sb) have been proposed as alloy-based anode materials for SIBs. These materials can form sodium-rich phases and achieve a much higher capacity than intercalation-based materials.

Conspicuous by its absence on that list is silicon, the workhorse alloy anode for LIBs with a high theoretical capacity of 4199 mAh g<sup>-1</sup>. In the SIB case, crystalline Si is electrochemically inactive at room temperature due to a large diffusion barrier.<sup>[99,100]</sup> Arrieta et al.,<sup>[101]</sup> using DFT calculations, recently reported orthorhombic  $\text{Si}_{24}$ , an open-framework silicon allotrope whose average electrode potential and theoretical capacity were deduced to be 0.3 V and 160 mAh g<sup>-1</sup>, respectively. Figure 10 shows the DFT-derived structural and electrochemical properties of  $\text{Na}_x\text{Si}_{24}$  ( $0 \leq x \leq 4$ ). Although an impressively low volume expansion of 2.3% is therein reported and attributed to geometrical flexibility in the crystalline structure, the kinetics of the solid solution reaction were still found to be sluggish because of a high sodium diffusion barrier.

Other p-block elements, Sn, Ge, P, and Sb, have nevertheless shown excellent electrochemical performances with sodium,

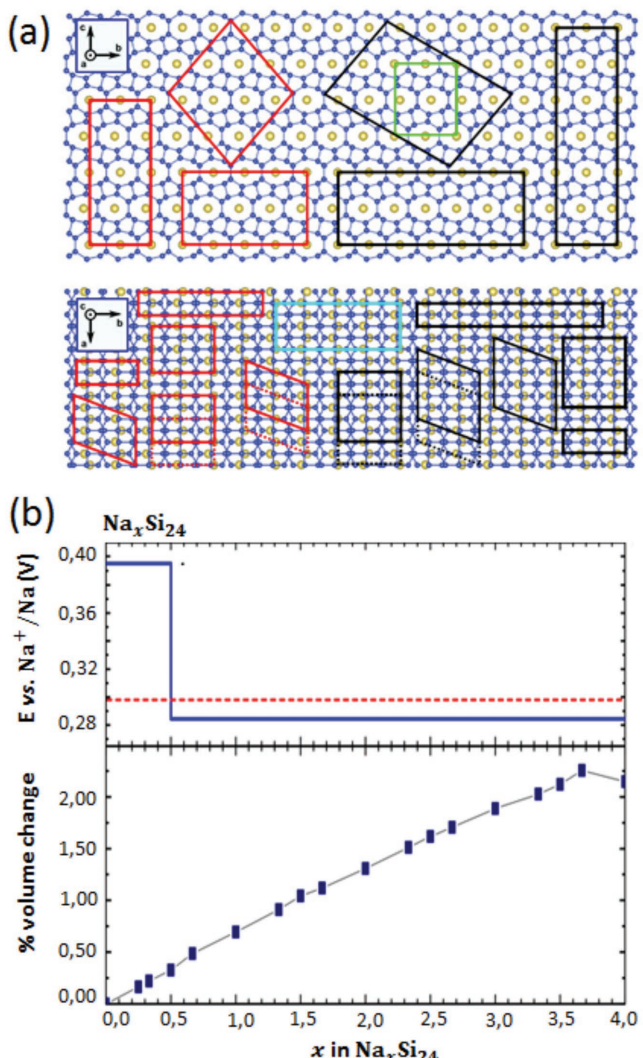


**Figure 10.** DFT-calculated properties of electrochemically sodiated Si. a) Structure of  $\text{Na}_x\text{Si}_{24}$  projected in the  $b-c$  and  $a-b$  planes. Si atoms (blue circles) and Na atoms (gold circles) are represented. The parallelograms represent various supercells used to generate  $\text{Na}_x\text{Si}_{24}$  configurations, wherein red, black, and turquoise parallelograms correspond to supercells containing 8, 12, and 16 formula units, respectively, and the green rectangle exemplifies the unit cell of four formula units equivalent. b) First-principles derived voltage curve (solid blue line) and average cell voltage (dashed red line). a,b) Reproduced under the terms of the CC-BY 4.0 Licence.<sup>[101]</sup> Copyright 2017, The Authors.

with respect to their gravimetric capacities. Figure 11 shows the comparative voltage profiles of Sn-, Ge-, P-, and Sb-based electrodes in Na cells. High first cycle electrode capacities (>500 mAh g<sup>-1</sup>) and desirably low average electrode potentials are herein evidenced. Phosphorous, for example, exhibits a first cycle capacity of 2500 mAh g<sup>-1</sup>, which is close to its theoretical specific capacity of 2597 mAh g<sup>-1</sup> (in  $\text{Na}_3\text{P}$ ). Although Sn electrodes show a sloping voltage profile, a characteristic of a solid-solution topotactic insertion (see Figure 11a), Ge, P, and Sb electrodes have well-defined plateau voltage profiles, indicative of a two-phase addition reaction that is corroborated by the differential capacity inset in Figure 11b.

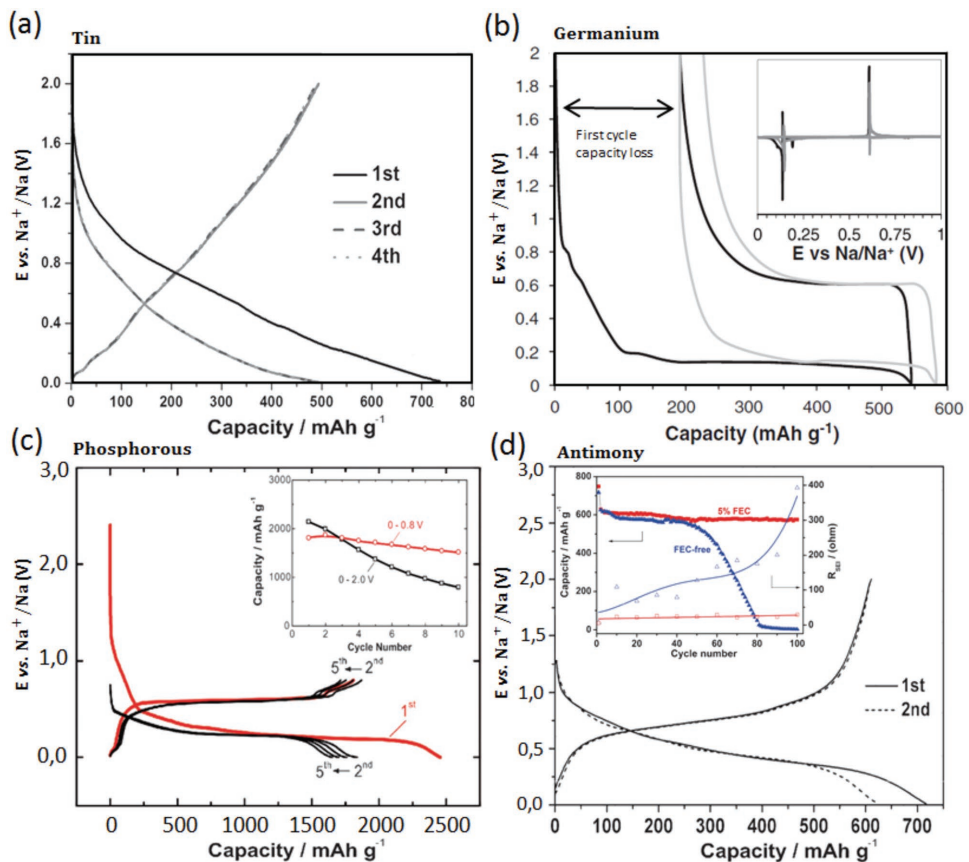


**Figure 11.** Electrochemical properties of alloy-based anode materials for sodium-ion batteries. a) Constant current charge and discharge in nanometer-sized, mesoporous carbon-embedded Sn electrodes. b) Voltage profiles in the first two charge and discharge cycles in Ge thin film electrodes. The inset shows differential capacity  $dQ/dV$  plot of the same. c) Charge and discharge voltage profiles in phosphorous composite electrodes. The inset shows the effect of the cutoff voltage on the cycleability. d) Voltage profiles of the charge and discharge cycles of nanocrystalline Sb-embedded in carbon matrix Sb@C electrodes. Inset showing the effect of fluoroethylene carbonate (FEC) additive on the cycleability of the electrodes. a) Adapted with permission.<sup>[103]</sup> Copyright 2014, Wiley-VCH. b) Adapted with permission.<sup>[104]</sup> Copyright 2013, Elsevier B.V. c) Adapted with permission.<sup>[105]</sup> Copyright 2014, Wiley-VCH. d) Adapted with permission.<sup>[106]</sup> Copyright 2012, The Royal Society of Chemistry.

Several unimpressive features are however evidenced in Figure 11b,c, these include a high overpotential between (dis)charge cycles (hysteresis) and a significantly large first cycle capacity loss in Ge and P electrodes. A further critical challenge related to the alloy insertion mechanism in either SIBs or LIBs is the large volume expansion upon charge insertion.<sup>[102]</sup> Volume expansions by sodiation of 520%, 126%, 300%, and 390% are reported of Sn, Ge, P, and Sb electrodes, respectively.<sup>[103–106]</sup> This results in mechanical bond failures which lead to a loss of electrical contact in the short term and pulverization of the host material in extended cycles. The applicability, therefore, of alloy-based electrodes in practical batteries is greatly impeded.

To enhance the cycle life, several ingenious composite electrode designs have since been put forward in order to restrict the destructive effects of the volume changes.<sup>[36–38]</sup> The first critical strategy is to make nanostructures that cannot be pulverized. This approach has the advantage of improving the structural stability of the host material and the electrochemical rate capability by reducing diffusive transport pathways. Regrettably, this also amplifies side reactions and increasing the mass loading of nanosized host materials has been found to be challenging in composite electrodes. The choice, therefore,

of binders, electrolyte, and SEI stabilizing additives becomes critical. The second strategy is carbon coating that comes with numerous beneficial effects. Besides enhancing the electrical conductivity, amorphous carbon acts as a cage to suppress pulverization and further reduces electrolyte decomposition reactions in the composite electrode.<sup>[107]</sup>

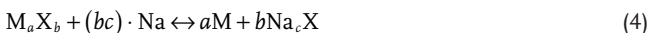
The p-block elements are environmentally friendly and available at low cost and thus fulfill the major criteria for large-scale EES applications. Although they show outstanding properties with regard to their superior specific capacities, their use requires clever strategies and further breakthroughs in material science. Current use is thus restricted by the available electrolytes and binders. The success in the commercialization of Si-based anodes in LIBs is a proof of concept that should help to steer similar technological deployments in SIB, which at this stage lags behind that of intercalation-based materials.<sup>[108]</sup>

#### 4.3. Conversion-Based Anode Materials

Several metal oxides ( $MO_x$ ) and metalsulfides (MS), in particular layered metal disulfides ( $MS_2$ , M = Mo, Sn, W, and Ti)

are reported as conversion reaction-based anode materials. The conversion reaction is however rarely exclusive and is accompanied in most cases by intercalation and/or alloying reactions during sodium insertion. We consider herein materials in which the conversion reaction is an inclusive part of the insertion mechanism.

The generalized formula for Na-based conversion reaction can thus be written as<sup>[39]</sup>



where  $X$  represents either oxygen or sulfur in the host compound, and  $a$ ,  $b$ , and  $c$  are the stoichiometric composition of the starting material and the formed Na-containing compound, respectively. Figure 12a illustrates the differences between conversion mechanism and intercalation mechanism while Figure 12b compares DFT-calculated relative cell voltage differences from either Li-based or Na-based conversion mechanisms. Figure 12c,d shows the voltage range and the associated volume expansions in Na-based conversion reactions, respectively.

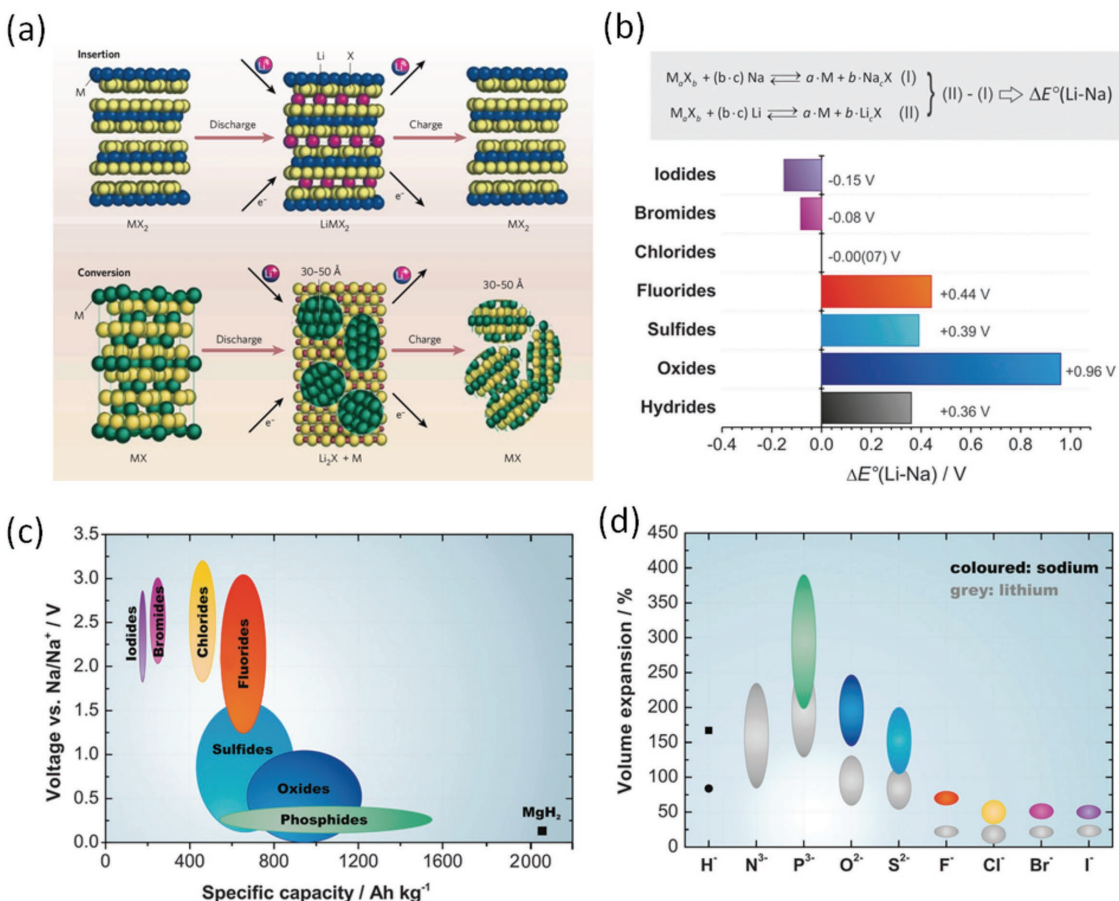
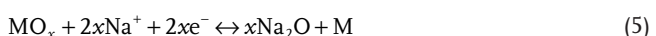


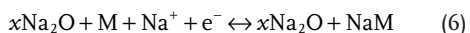
**Figure 12.** a) Schematic representation showing the contrasting reaction mechanisms occurring during discharge for insertion (top) and conversion reactions (bottom). The insertion reaction demonstrates a maximum of 1 electron transfer per transition metal (here designated as M), whereas the conversion reaction can transfer 2–6 electrons. b) Calculated differences in cell potentials between conversion reactions of  $M_aX_b$  with sodium or lithium, respectively. Positive values mean that replacing lithium by sodium in a conversion reaction will result in a lower cell voltage and vice versa. c) Specific capacities and cell potentials versus  $Na^+/Na$  for conversion reactions of different classes of materials with sodium. d) Calculated volume expansions for lithium- and sodium-based conversion reactions. a) Reproduced with permission.<sup>[41]</sup> Copyright 2008, Nature Publishing Group. b–d) Reproduced with permission.<sup>[39]</sup> Copyright 2013, the Royal Society of Chemistry.

In metalsulfides, sodium intercalates to form  $Na_xMS_\alpha$  which upon further sodium insertion decomposes into  $Na_2S$  and M via a conversion reaction. Because the conversion reactions are associated with slow kinetics and large volume expansion, one approach is to avoid the conversion step altogether by voltage control. For example, Kim et al.<sup>[109]</sup> initially investigated the electrochemical performance of natural ore pyrite ( $FeS_2$ ) in an SIB by exploiting the intercalation and conversion reactions and obtained a flat plateau voltage at 1.3 V versus  $Na^+/Na$ , a capacity of 630 mAh g<sup>-1</sup>, and a short cycle life of only 50 cycles. However, by limiting the lower cutoff voltage to 0.8 V versus  $Na^+/Na$ , to effectively avoid the conversion reaction that takes place at lower potentials, Hu et al.<sup>[110]</sup> obtained more than 20 000 cycles at a lower specific capacity of 170 mAh g<sup>-1</sup>.

The reaction pathway in metal oxide-based conversion reactions however depends on whether or not the metal M is electrochemically active for alloying. For electrochemically inactive M, for example, Fe, Co, Ni, Mn, Cu, and Mo, the metal oxide reacts with  $Na^+$  is a one-step conversion reaction, according to



and for an electrochemically active M, such as Sb, an alloying reaction further ensues



Because of multiple charge transfer reactions, such a reaction mechanism has a high specific capacity.  $\text{Sb}_2\text{O}_4$ , for example, has a specific capacity of 896 mAh g<sup>-1</sup>.<sup>[111]</sup> However, due to the deconstruction and reconstruction of the framework structures, conversion reactions are characterized by considerable voltage hysteresis in the charge and discharge cycles. Polarizations ranging from 0.7 to 1.0 V (dependent on the charge/discharge rate) are very common. Such effects are detrimental to the energy efficiency of batteries. In addition, the rate permanence and cycleability are not that impressive either, likely due to the large volume changes.

The highest cycle life of  $\approx 500$  cycles achieved in SIB anode materials that store sodium via a conversion reaction was reported for  $\text{MoO}_3$  with a moderate specific capacity of 200 mAh g<sup>-1</sup>.<sup>[112]</sup> This material however exhibits a sloping electrode voltage, reaching a high potential of 2.5 V versus  $\text{Na}^+/\text{Na}$ , which essentially undermines its utility as anode material.

#### 4.4. Anode Materials Comparison

The electrode performance of the different anode materials in Na cells is reviewed in this section, focusing on the reaction mechanisms, the electrode potentials, and the relative cycleability of the different anodic materials. While it is desirable to have a low anodic potential, there is a huge risk of electrolyte decomposition at such potentials. In general, most organic electrolytes are reduced at potentials below 0.5 V versus  $\text{Na}^+/\text{Na}$  and this question of the electrolyte will be further addressed in Section 5. Another challenge at low potentials is the risk of metallic plating, a likelihood which occurs at high charge rates. It is important therefore to bear in mind these challenges as low-voltage anodes are being pursued, whose unfavorable effects on the cycle life and safety of rechargeable batteries are well documented.

##### 4.4.1. Comparing the Average Voltage and Gravimetric Capacity of Anode Materials

Figure 13 illustrates voltage and gravimetric capacity comparison of SIB anode materials. The blue circles represent intercalation-based materials, the red squares represent conversion materials, while cyan diamonds represent alloy-based materials. A generally agreed voltage limit for anodes is 2 V versus  $\text{Na}^+/\text{Na}$ , for reasonable energy density values. It should be noted that anodic materials with higher potentials, in the range of 2–3 V

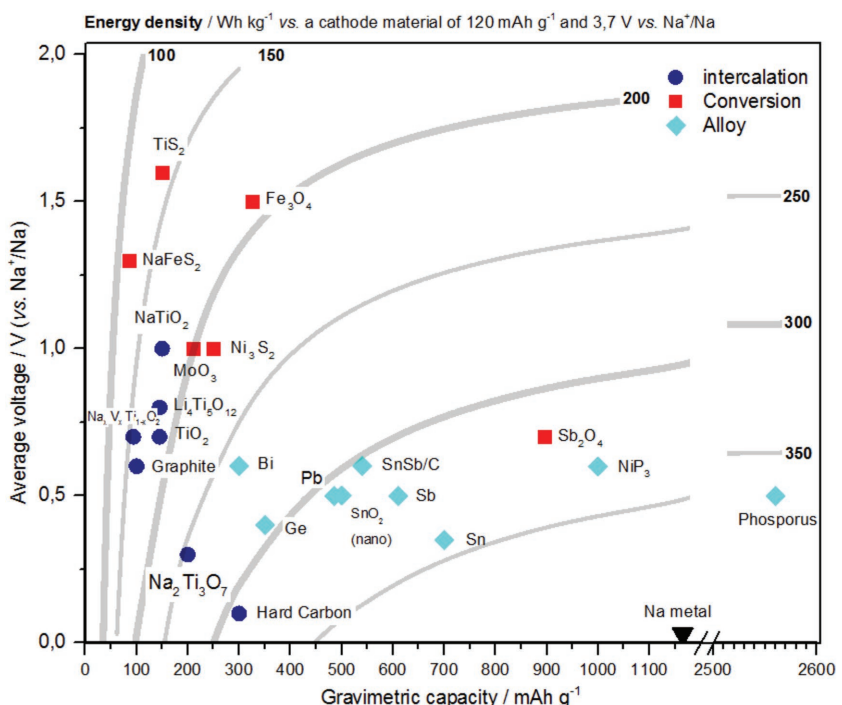


**Figure 13.** Average voltage versus the discharge capacity of various sodium-based anode materials. Intercalation materials (blue circles), conversion materials (red squares), and alloy materials (cyan diamonds). The energy density calculations are shown in the four contour lines (200, 250, 300, and 350 Wh kg<sup>-1</sup>), are based on the weight of the active material, using a theoretical cathode material with 120 mAh g<sup>-1</sup> and 3.7 V versus  $\text{Na}^+/\text{Na}$ . Data derived from refs. [45,48,55,58,75,83,84,89,92,96,100,103–106,109,111–123].

versus  $\text{Na}^+/\text{Na}$ , such as  $\text{NaTi}_2(\text{PO}_4)_3$ <sup>[124]</sup> and  $\text{Na}_{0.44}(\text{Mn}_{1-x}\text{Ti}_x)\text{O}_2$ <sup>[120]</sup> are useful in aqueous electrolyte-based systems. In this figure, contour lines of energy density at 100, 150, 200, 300, and 350 Wh kg<sup>-1</sup> are shown. A hypothetical cathode material of 120 mAh g<sup>-1</sup> and 3.7 V versus  $\text{Na}^+/\text{Na}$  is assumed for these calculations.

While the intercalation-based materials apparently have desirably low electrode potentials, they generally suffer from the low gravimetric capacity. Alloy-based materials on the other hand appear to overcome this low capacity problem and, furthermore, compared to carbonaceous materials, they have higher densities that aid their volumetric energy densities. The perils, however, of this phenomenally high capacity is a large volume expansion upon charge insertion, which brings about destructive structural deformations. Newcomer, conversion-based anode materials in contrast tend to have moderate to high voltages and are characterized by relatively low gravimetric capacities. Here,  $\text{Sb}_2\text{O}_4$  is a standout performer, yet challenges with regard to energy efficiency in a full cell further explains the subdued interest in these materials.

Metallic sodium with a desirably low working potential and a high gravimetric capacity of 1165 mAh g<sup>-1</sup> is also shown. While this gives the impression of an obvious choice, practical issues such as dendrite growth and unstable SEI formation in liquid and polymer electrolytes inhibit its use in room temperature batteries.<sup>[4]</sup> Such a battery is referred to as a room temperature sodium battery and not a sodium-ion battery. The challenge of making a rechargeable, room temperature lithium or sodium

batteries has remained unresolved for over 50 years. In the sodium case, this is made more complicated by the higher reactivity and lower melting point of metallic Na (note that the reactivity increases with the atomic number for the alkali-metal elements). BroadBit is one of the few companies taking up the challenge of a commercial rechargeable sodium battery.<sup>[125]</sup>

Judging by recent successful applications in prototype and near-commercialization cells, HC is the anode material of choice for SIBs.<sup>[126]</sup> Figure 13 illustrates the advantages of this attractive capacity and low voltage as it attains the highest energy density among intercalation-based materials. Furthermore, due to a relative cost advantage and natural abundance of precursors, carbonaceous materials will continually dominate the discussion on anode material for SIBs. Challenges with HC arise from its low potential and an irreversible capacity upon the first cycle. This severely penalizes the practical application of this material in SIB full cells. Since anodic capacity losses cannot be compensated and charging rates must be kept low to avoid sodium plating, the search therefore continues for safer and higher capacity anode materials for SIB applications. Novel perspectives are leaning toward carbonaceous nanomaterials<sup>[49,127–129]</sup> and anatase titanium dioxide nanomaterials<sup>[83,84,130]</sup> in order to match the rate performance of graphite in LIB.

#### 4.4.2. Cycle Life Performance of Anode Materials

Figure 14 compares the number of cycles versus the gravimetric storage capacity of various anode materials. It can be seen that alloy-based electrodes (cyan diamonds) and conversion-based electrodes (red squares) have a relatively poor cycleability while the intercalation-based electrodes (blue circles) have the highest cycleability on average. Although an impressive cycling performance of 8000 cycles can be achieved with graphite, the insertion mechanism involves solvent cointercalation in an ether-based solvent.<sup>[45,55]</sup> This however seriously limits the cell configurations for this electrode.

Cycleability however must be taken in the context of the gravimetric capacity of the materials. The product of the cycle number and gravimetric storage capacity give interesting values for the cumulative electrode capacities, as shown by the 4 contour lines in Figure 14 representing 5, 25, 100, and 500 Ah g<sup>-1</sup>. This benchmarks the performance between electrodes of different specific capacities and cycle performance. For example, although phosphorus has a very high storage capacity, its low cycleability results in a cumulative capacity that is rather modest, around 30 Ah g<sup>-1</sup>. The combination of a high storage capacity with an average number of cycles implies that Sn electrodes, for example, are as competitive as graphite, HC, and Fe<sub>3</sub>O<sub>4</sub> anodes (see the 500 Ah g<sup>-1</sup>line). Based on the data in

Figures 13 and 14, intercalation-based HC and alloy-based Sn emerge as stand-out anode materials based on high cumulative capacity and energy density. Nevertheless, the material abundance of Sn, as illustrated in Figure 1, is even lower than that of Li and this explains the subdued interest in the further development of this anode material.

#### 4.4.3. Cathode Materials

Electrodes with a potential above 2 V versus Na<sup>+</sup>/Na are generally classified as cathode materials in SIBs. Historically, research in cathode materials started in the 1970s when the structural and electrochemical properties of Na insertion in NaCoO<sub>2</sub> were explored and it was found to be a feasible cathode material for SIBs.<sup>[131]</sup> In the early 1980s, studies on other layered oxides of 3d transition metals such as Na<sub>x</sub>CrO<sub>2</sub>,<sup>[132]</sup> Na<sub>x</sub>MnO<sub>2</sub>,<sup>[133]</sup> and Na<sub>x</sub>FeO<sub>2</sub><sup>[134]</sup> were further conducted, credit to the pioneering work of Delmas co-workers. During that time and due to the instability of the electrolyte in the initial cycles, these studies were only limited to 3.5 V versus Na<sup>+</sup>/Na.<sup>[102]</sup> As a consequence of the phenomenal success of LIBs, subsequent investigations accorded to the SIB technology eventually became sparse.

Compared to anodic materials, a larger repertoire of material choices exists for the cathodes, this is true for either SIB or LIB cathode materials. Synthesis methods developed over the past three decades for LIB can be seamlessly adopted and the relatively facile, solid-state method can be applied in the synthesis of SIB cathode materials.

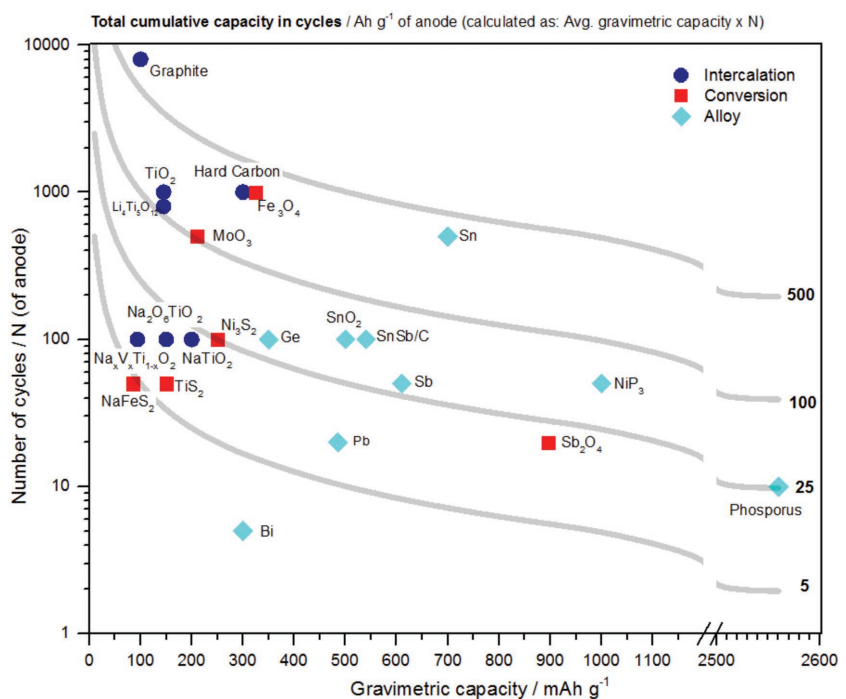


**Figure 14.** Number of cumulated cycles during their cycle life versus the storage capacity of the anode material for SIB. Intercalation materials (blue), conversion materials (red), and alloy materials (cyan). The cumulative capacities are shown in the four contour lines (5, 25, 100, and 500 Ah g<sup>-1</sup>), calculated as the product of the average capacity and number of cycles. Data derived from refs. [45,48,55,58,75,83,84,89,92,96,100,103–106,109,111–123].

#### 4.5. Classification of Cathode Materials

Most cathode materials can be classified into two major groups: either as layered metal oxides (LMeOs) or polyanion compounds. These materials reversibly intercalate  $\text{Na}^+$  during electrochemical charge and discharge and manifest stable phase transformations.

Conforming to the notation proposed by Delmas et al. in 1980,<sup>[135]</sup> most LMeO crystal structures are classified as either P2-type or O3-type. Here, the letters "P" and "O" stand for prismatic and octahedral, respectively, denoting the lattice site occupied by alkali ion, while the numbers "2" and "3" stand for the number of layers or stacks in a repeat unit of the LMeO crystal structure. Where repetitions are not possible, due to in-plane crystal lattice distortions, a prime symbol is added; thus giving O'3-type and P'2-type notation.<sup>[62]</sup> Figure 15 illustrates the lattice configurations in O3, O2, P3, and P2 crystal structures. One advantageous feature of the larger sized sodium ions is that they are able to occupy trigonal prismatic sites and form stable P2-type phases, which do not exist in the case of Li-based LMeOs.<sup>[17,136]</sup>

The other major class of cathode materials is polyanionic compounds, which are generally characterized by attractive properties of good cycleability, attractively high electrode potentials, and robust structural frameworks. In contrast

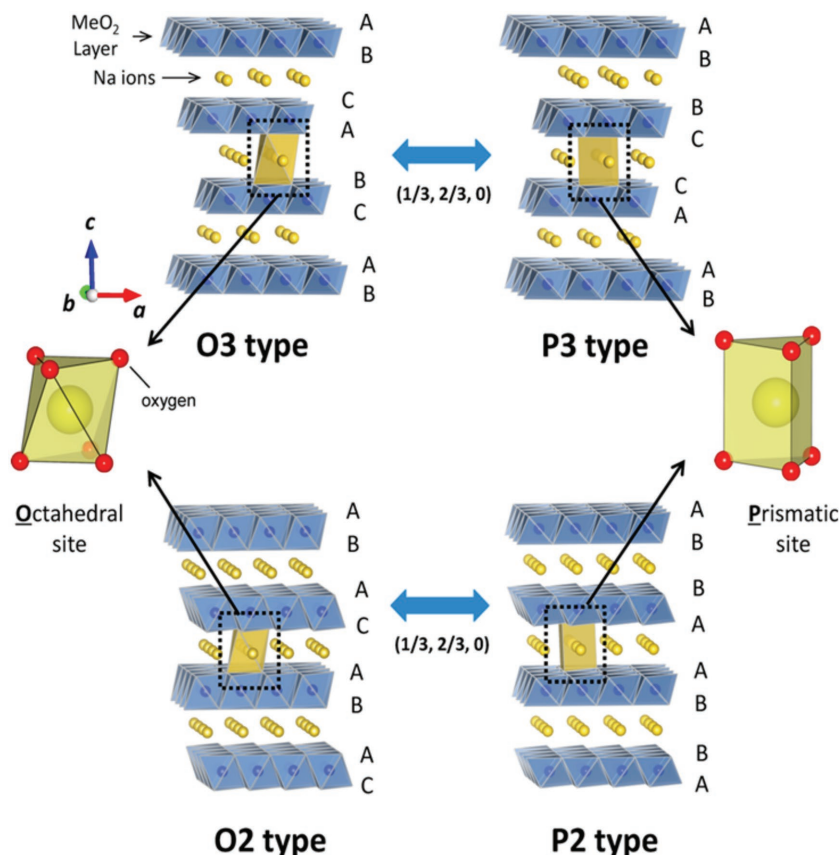


**Figure 15.** Classification of layered materials and illustration of the phase transition processes induced by sodium extraction. Here, the stacking of  $\text{MeO}_2$  ( $\text{Me}$ : transition metal) sheets in layered metal oxide and the O3, O2, P3 and P2 phases are shown. Reproduced with permission.<sup>[17]</sup> Copyright 2014, American Chemical Society.

to LMeO, polyanionic compounds are generally innocuous, show good thermal stability, and exhibit a high tolerance to overcharge and discharge. Representative crystal structures of polyanionic compounds are shown in Figure 16. Phosphates ( $\text{NaMePO}_4$ ), pyrophosphates ( $\text{Na}_2\text{MeP}_2\text{O}_7$ ), and fluorophosphates ( $\text{Na}_2\text{Me}(\text{PO})_4\text{F}$ ), where Me represents a transition metal, are illustrated. Because the electrode potentials of polyanionic compounds are influenced by the inductive effect of oxide, fluoride, and sulfate anions, the potential of the redox couple can be tuned by interchanging  $\text{F}^-$  and  $\text{O}^{2-}$  for example.<sup>[17]</sup> As a result, the electrode potentials between sodium-based and analogous lithium-based polyanionic compounds are comparable. Such attractive features endear polyanionic compounds to researchers and battery manufacturers alike and appropriate them for large-scale EES applications.

#### 4.6. Layered Metal Oxides as Cathode Materials

Taking a cue from the remarkable progress in lithium-based LMeO, sodium-based LMeO ( $\text{Na}_x\text{MeO}_2$ ) have similarly taken prime consideration over recent years as candidate cathode materials for SIBs. As previously mentioned, more variety of stable LMeO structures are possible for SIB cathodes due to the larger size of the sodium ion. The main drawback associated with sodium-based LMeOs, however, is the poor cycle life performance due to instabilities in their crystal structures.<sup>[138]</sup>

Generally, sodium extraction from either the O3-type or the P2-type phase induces irreversible structural and phase transitions in the cathode material thereby affecting their cycleability. For example, layers in the P2-type phase reposition after the removal of sodium ions to form the O2-type phase, while in the P3-type phase sodium extraction results in the O3-type phase. The P2 phase is however more favorable to Na-ion diffusivity due to a lower activation barrier compared to the O2 structure,<sup>[139]</sup> and it is known to exhibit better cycleability and air stability.<sup>[140]</sup> These biphasic occurrences also lead to the characteristic stepwise voltage profiles due to sequential two-phase and solid solution insertion mechanisms.

LMeOs nevertheless remain popular in research. An overview of the number of published literature since 2010 reveals that LMeOs are the most extensively studied materials in relation to cathode materials for SIBs.<sup>[17]</sup> While the general representation of the LMeO formulation is simplified, it is a rarity to find LMeO formulations with a single transition element species in practice. Even though some LMeOs with a single transition element have been reported for SIB application,<sup>[131,134,141–145]</sup> a combination of two or three transition elements has emerged as a popular strategy due to advantages in

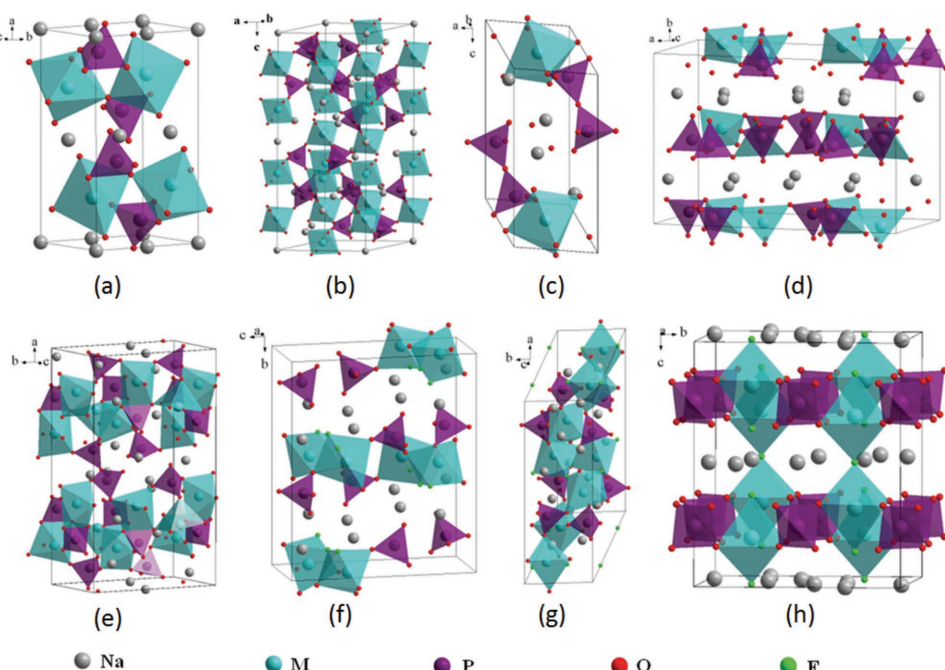


**Figure 16.** Crystal structures of polyanionic compounds: a) olivine  $\text{MePO}_4$ , b) NASICON  $\text{Na}_3\text{V}_2(\text{PO}_4)_3$ , c) triclinic  $\text{Na}_2\text{MeP}_2\text{O}_7$ , d) orthorhombic  $\text{Na}_2\text{MeP}_2\text{O}_7$ , e) orthorhombic  $\text{Na}_4\text{Me}_3(\text{PO}_4)_2\text{P}_2\text{O}_7$ , f) orthorhombic  $\text{Na}_2\text{Me}(\text{PO}_4)_2\text{F}$ , g) monoclinic  $\text{Na}_2\text{Me}(\text{PO}_4)_2\text{F}$ , and h) tetragonal  $\text{Na}_3\text{Me}_2(\text{PO}_4)_2\text{F}_3$ . Symbol Me represents a transition metal. Reproduced with permission.<sup>[137]</sup> Copyright 2015, Wiley-VCH.

material costs and structural stability as elaborated in the following sections.

#### 4.6.1. Layered Metal Oxides with One Transition Element

The oldest type of LMeO cathode insertion material for SIBs is  $\text{NaCoO}_2$ , initially studied in the 1980s.<sup>[131,146,147]</sup> In these pioneering studies, four thermodynamically stable phases, O3, O'3, P3, and P2 types, were readily prepared achieving good cycleability, in particular the P2-type phase.<sup>[146]</sup> The observed cycle life was surprising on account of concomitant phase transitions that can be identified by nonlinearities in the voltage profiles and the relatively large volume changes due to Na intercalation.

P2-type  $\text{Na}_{1-x}\text{CoO}_2$  is currently the most extensively studied polymorph due to its recently discovered thermoelectric properties<sup>[148]</sup> and superconductivity of the hydrate compound  $\text{P}2\text{-Na}_{0.35}\text{CoO}_2 \cdot 1.3\text{H}_2\text{O}$ .<sup>[149]</sup> Several phase diagrams have thus been proposed, based on first-principles calculations, and have been verified experimentally.<sup>[150,151]</sup> Figure 17 illustrates the charge and discharge behavior of P2-type  $\text{NaCoO}_2$ . As many as nine potential drops due to successive phase transitions involving single-phase domains and biphasic domains are evidenced.<sup>[150]</sup> Since such phase transitions are often complicated to analyze and are unique to the sodium-based system, phase diagrams from thermoelectric studies have allowed detailed insights into the nature of successive domains observed upon sodium intercalation.

While previous reports on  $\text{NaCoO}_2$  exhibited a poor cycle life of about 100 cycles,<sup>[152,153]</sup> improved electrochemical properties of 300 cycles with 86% initial capacity retention have

been recently reported by Fang et al.<sup>[154]</sup> in their study of  $\text{P}2\text{-Na}_{0.7}\text{CoO}_2$ . In general,  $\text{NaCoO}_2$  in its various polymorphs has attractive electrochemical properties with regard to high rate capability, high voltage stability, and a wide range of reversible sodium content.<sup>[154,155]</sup> Nevertheless, it shows a sloping voltage profile and has a tendency to react with  $\text{NaPF}_6$  containing electrolytes.<sup>[156]</sup> A more critical deterrent, however, is the high cost of Co that inhibits the large-scale applicability of all Co-based electrode materials. Since reducing the cost of the batteries has become a major issue, LMeOs based on manganese and iron are highly favored for SIB applications.

O3-Type  $\text{NaFeO}_2$ , which similarly debuted in the 1980s, was prepared by Tekeda et al.<sup>[157]</sup> via solid-state reaction at 700 °C. Due to the philosophy of abundant and low-cost electrode materials,  $\text{NaFeO}_2$  has been subject to several electrochemical investigations. Yabuuchi et al.<sup>[158]</sup> in a systematic study of the effect of cutoff voltage on the electrode performance observed that  $\text{Na}_{1-x}\text{FeO}_2$  delivers a low reversible capacity of 80–100 mAh g<sup>-1</sup> ( $0 < x < 0.45$ ) and has a poor rate capability, based on the  $\text{Fe}^{4+}/\text{Fe}^{3+}$  redox reaction.<sup>[159]</sup> Figures 15b and 18a illustrate the effect of cutoff voltage on the cycleability of O3- $\text{NaFeO}_2$ .

On account of the high voltage of 3.3 V and a flat plateau voltage profile concomitant with minimal polarizations, the energy efficiency during (dis)charge cycles is impressive. The electrode however only manages good capacity retention for a cutoff voltage of 3.4 V (vs  $\text{Na}^+/\text{Na}$ ). At higher oxidation states, i.e.,  $x > 0.5$  and cutoff voltages above 3.5 V, irreversible structural changes appear in the material. Partial substitution of Fe with either Co,<sup>[155]</sup> Mn,<sup>[160]</sup> or Ni<sup>[161,162]</sup> has however proved to be an effective strategy to overcome these structural changes and increase the storage capacity while maintaining favorable material costs.

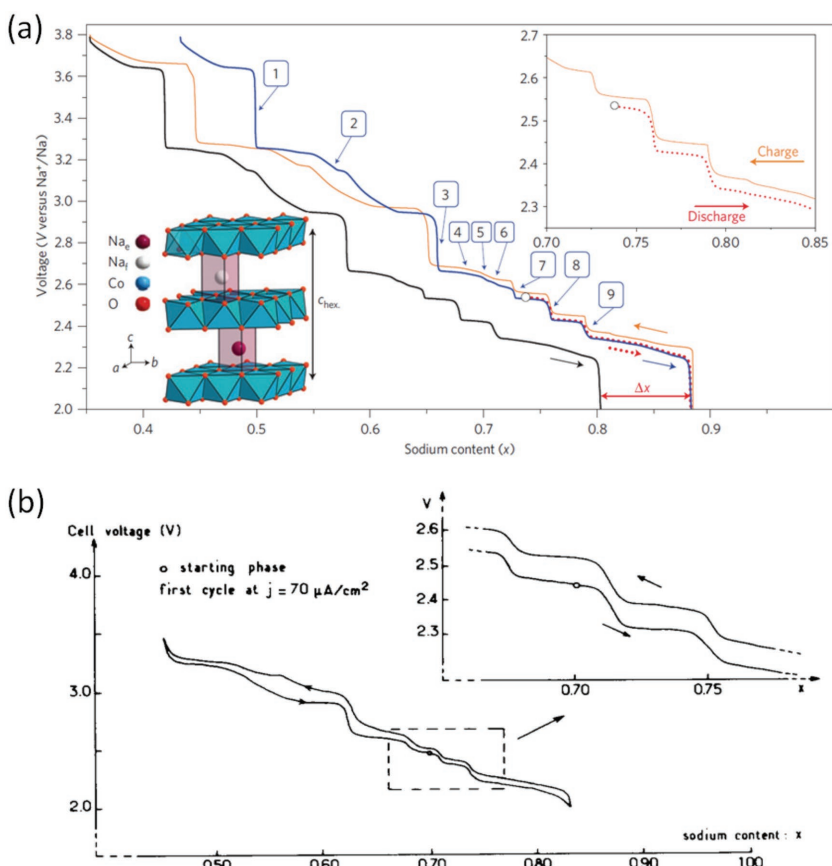


**Figure 17.** Charge and discharge voltage profiles of P2-type  $\text{NaCoO}_2$ . a) The cycling curve showing as many as nine potential plateaux and voltage drops. The first discharge and charge cycles are shown in the main frame and top-right inset by the red dotted lines and orange solid lines, respectively. A lower potential is obtained in the second discharge cycle due to electrolyte oxidation at high potential, and this feature is corrected by shifting the curve by  $\Delta x$  to obtain a perfectly matching discharge profile, exemplified by the blue solid lines. The bottom-left inset shows the P2 layered structure  $\text{NaCoO}_2$ . b) Similar charge and discharge profile in the pioneering publication. The top inset highlights the potential drops as well as their reversibility. a) Reproduced with permission.<sup>[150]</sup> Copyright 2011, Macmillan Publishers Limited. b) Reproduced with permission.<sup>[131]</sup> Copyright 1981, Elsevier.

Several polymorphs of  $\text{NaMnO}_2$ , in particular the O'3-type and P2-type, have been examined as LMeO electrodes for SIB applications.<sup>[133,163,164]</sup> Early electrochemical investigations in 1985 by Mendiboure et al.<sup>[133]</sup> on  $\text{NaMnO}_2$  premised an impractically low reversible capacity of only  $54 \text{ mAh g}^{-1}$  for cathode application. Undeterred by these initial findings, Ma et al.<sup>[165]</sup> nevertheless revised O'3-NaMnO<sub>2</sub> using modified experimental conditions and obtained a larger first cycle capacity of  $200 \text{ mAh g}^{-1}$ . Although issues such as stepwise voltage profiles, low Coulombic efficiency, poor cycle life, and low rate capability persisted, the electrode material showed remarkable robustness to overcharge at 4.2 V. Before the discovery of the O'3-type phase, the P2-type phase had been the preferred  $\text{NaMnO}_2$  phase for SIB applications. Caballero et al.<sup>[163]</sup> synthesized and characterized P2- $\text{Na}_{0.6}\text{MnO}_2$  and obtained a reversible capacity of  $140 \text{ mAh g}^{-1}$  and remarkable thermal stability. Although all  $\text{NaMnO}_2$  LMeOs are remarkably resistant to conversion to the spinel structure,<sup>[140]</sup> rapid structural degradations were however evidenced with complete destruction of the crystalline

framework after only eight cycles. Failure to accommodate the Jahn-Teller distortions in crystal frameworks, following the reduction of  $\text{Mn}^{4+}$  to  $\text{Mn}^{3+}$ , is understood to be the cause of the structural instability in mixed valence manganese oxides.<sup>[166]</sup> Figure 18c-f shows the comparative electrode performances of O'3 and P2 type  $\text{NaMnO}_2$ . Generally, similar “signature” voltage profiles are here evidenced. Besides showing poor cycleability in micrometer-sized samples, an intrinsic demerit of either the O'3 or the P2-type  $\text{NaMnO}_2$  is a rather low average voltage of less than 2.8 V due to the  $\text{Mn}^{4+}/\text{Mn}^{3+}$  redox couple. This restricts the deliverable energy density of full cells made with such cathode materials.

O3-type  $\text{NaCrO}_2$  and O'3-type  $\text{NaNiO}_2$  are also investigated as candidate electrode materials for SIBs. Concurrent electrochemical studies of  $\text{NaCrO}_2$  and  $\text{NaNiO}_2$  first appeared in 1982.<sup>[132]</sup> While very low electrode capacities were reported in these initial studies, with  $x \leq 0.2$  in  $\text{Na}_{1-x}\text{MeO}_2$  ( $\text{Me} = \text{Ni/Cr}$ ), the strong reducing power of the Ni and Cr redox couples allowed attractively high electrode potentials to be obtained. Nearly three decades later in 2010, the electrode properties of  $\text{NaCrO}_2$  were nevertheless revisited by Komaba et al.<sup>[141]</sup> Yet again, an impressive discharge capacity of  $120 \text{ mAh g}^{-1}$  in the first cycle was therein obtained with reasonable capacity retention over 50 cycles. Such findings emphasize the importance of the experimental conditions when drawing conclusions on electrode properties.

Figure 18g,h shows the voltage profiles and cycling tests of O3-type  $\text{NaCrO}_2$ . Electrolyte decomposition was identified as the major cause of the capacity degradation,

therefore carbon coating in subsequent studies proved to be an effective way to enhance capacity retention.<sup>[167]</sup> Further endearing features include a nearly flat and high cell voltage, close to 3 V, an outstanding rate capability (up to 150 C-rate in carbon-coated samples), and superior thermal stability. These exceptional properties make O3- $\text{NaCrO}_2$  an attractive and versatile positive electrode material for SIB applications.<sup>[141,168,169]</sup> Although the electrochemical properties of O'3- $\text{NaNiO}_2$  were similarly revisited by Vassilaras et al.<sup>[143]</sup> and while a reversible capacity of  $120 \text{ mAh g}^{-1}$  was therein reported, complex phase transitions upon charge/discharge cycles, low Coulombic efficiency, and low cycle life meant that no SIB full cells have thus been fabricated with this cathode material. Meanwhile, two SIB full cells with O3- $\text{NaCrO}_2$  as cathode have been reported: a moderate temperature cell, using ionic liquid electrolyte at  $90^\circ\text{C}$ ,<sup>[168]</sup> and a room temperature cell, based on aprotic solvents.<sup>[170]</sup> Both cells show reasonable capacity retention and serve to demonstrate the potential of  $\text{NaCrO}_2$  cathodes for advanced, high-power, SIB applications.

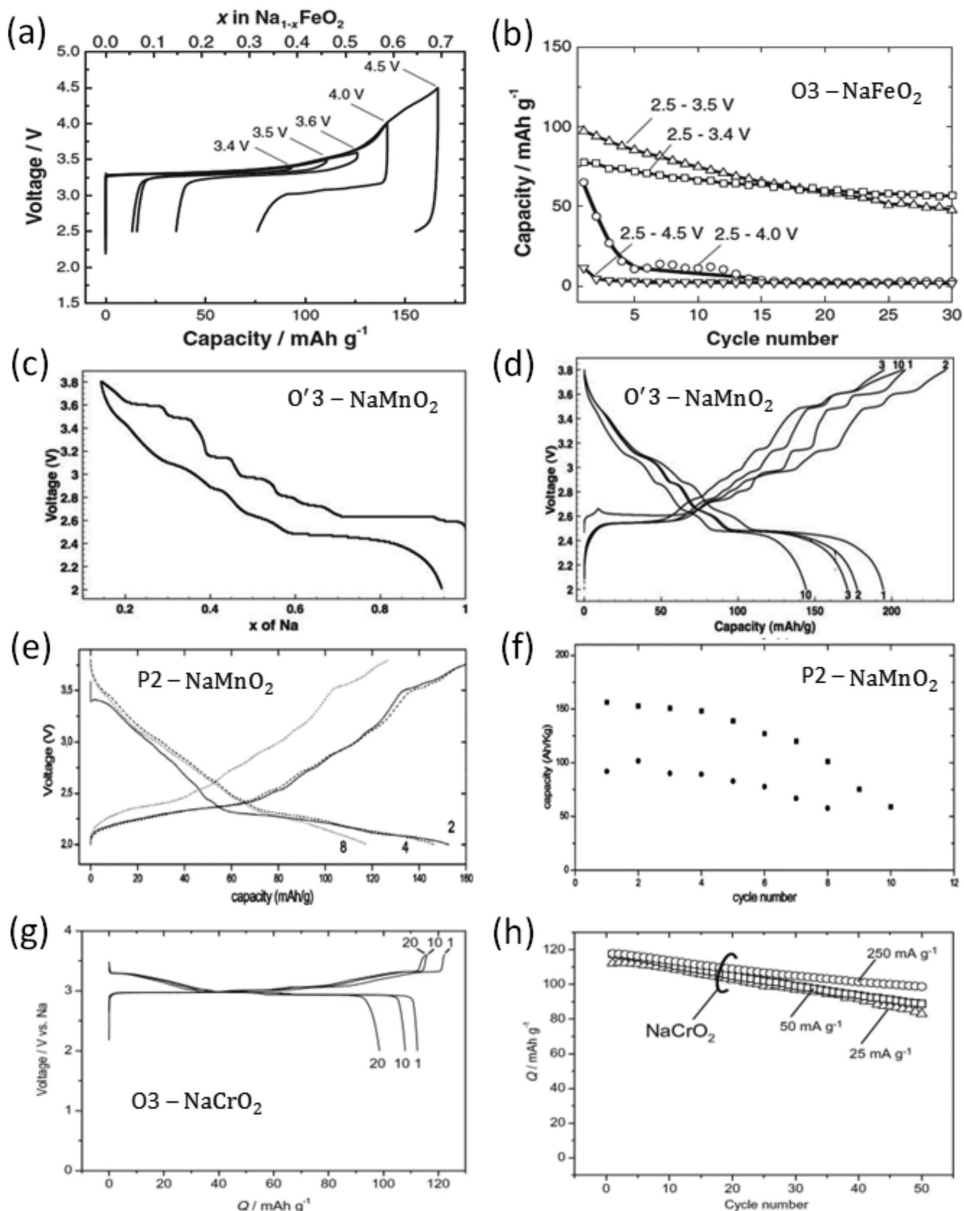


**Figure 18.** Properties of various layered metal oxide cathodes with one transition element. a,b) systematic studies on the effect of cutoff voltage on the performance of O3-Type NaFeO<sub>2</sub>. c,d) Charge and discharge voltage profiles of O'3-type NaMnO<sub>2</sub>. e,f) Charge and discharge voltage profiles of P2-type NaMnO<sub>2</sub>. g) First, second, and twentieth charge and discharge voltage profiles of O3-type NaCrO<sub>2</sub> at 25 mA g<sup>-1</sup>. h) Cycleability test of O3-type NaCrO<sub>2</sub> in 1 M NaClO<sub>4</sub> PC solutions.<sup>[141]</sup> a,b) Reproduced with permission.<sup>[158]</sup> Copyright 2012, The Electrochemical Society of Japan. c,d) Reproduced with permission.<sup>[165]</sup> Copyright 2011, The Electrochemical Society. e,f) Reproduced with permission.<sup>[163]</sup> Copyright 2002, The Royal Society of Chemistry. g,h) Reproduced with permission.<sup>[141]</sup> Copyright 2010, Elsevier.

#### 4.6.2. Layered Metal Oxides with Two or Three Transition Elements

As a general observation, LMeOs based on a single transition element suffer from a poor cycle life. This is probably due to multiple phase transformations and structural instabilities.<sup>[138]</sup> LMeOs with at least two transition elements prepared by partial metal substitution have been effectively used to improve the electrochemical performances of LMeOs. Binary, tertiary, and quaternary LMeOs have thus been prepared with enhanced electrochemical properties compared to single-metal oxides. This, furthermore, reduces the dependence on uneconomical

elements in battery materials thereby reducing the overall cost of battery materials.

A promising binary LMeO is P2-Na<sub>0.66</sub>[Fe<sub>0.5</sub>Mn<sub>0.5</sub>]O<sub>2</sub>. Although the material exhibits a modest capacity of 138 mAh g<sup>-1</sup> in the first cycle, a remarkable capacity increase to nearly 190 mAh g<sup>-1</sup> is reached in the second cycle. This is due to sodium enrichment in the cathode by accommodating extra sodium ions issued from the metallic sodium anode in half-cells.

Only such electrochemically inserted sodium is reversible. For example, chemically synthesized O3-Na[Fe<sub>0.5</sub>Mn<sub>0.5</sub>]O<sub>2</sub>, a sodium rich phase, has a lower reversible capacity of

110 mAh g<sup>-1</sup>. Furthermore, this O3-type phase manifests a larger voltage hysteresis thus making it unattractive as an energy efficient cathode material. However, P2-Na<sub>0.66</sub>[Fe<sub>0.5</sub>Mn<sub>0.5</sub>]O<sub>2</sub> has an attractively high average voltage of about 3 V versus Na<sup>+</sup>/Na and good rate capability of micrometer-sized particles without needing carbon coating.<sup>[160,171]</sup> Such outstanding electrochemical properties are evidently superior to those attained in either NaFeO<sub>2</sub> or NaMnO<sub>2</sub> and gainfully increase the energy density of full cells made with O3-Na[Fe<sub>0.5</sub>Mn<sub>0.5</sub>]O<sub>2</sub> cathode materials.

Before the P2-type phase can be successfully used as cathode material in SIBs; however, several hurdles need to be overcome. The chief hurdle among them is the need to increase the sodium content in the pristine, chemically synthesized material. The reason why the reversible capacity increases beyond the first cycle capacity is because more sodium ions, from the metallic sodium anode in Na//Na<sub>0.66</sub>[Fe<sub>0.5</sub>Mn<sub>0.5</sub>]O<sub>2</sub> cells, compensate for the sodium deficiency in the as-prepared samples. In the absence of a metallic anode, Singh et al.<sup>[171]</sup> proposed NaN<sub>3</sub> as a sacrificial salt to provide the extra sodium content. Therein, composite electrodes containing 5 wt% NaN<sub>3</sub> reported an estimated gain of 32 mAh g<sup>-1</sup> in reversible capacity after the first cycle. NaN<sub>3</sub>, thus decomposes to Na and N<sub>2</sub> after the first charge, thereby compensating the sodium deficiency in the cathode material. A similar strategy has also been used to compensate the initial charge irreversibility in LIB.<sup>[172]</sup> Other issues of practical concern include the hygroscopic nature, arising from possible intercalation of water and a volume expansion of 11.3% upon charge insertion, which is relatively large among intercalation-based materials.<sup>[17,173]</sup>

Another successful Fe-containing binary LMeO is O3-Na[Fe<sub>0.5</sub>Co<sub>0.5</sub>]O<sub>2</sub>, with excellent rate capability (up to 30 C-rate at micrometer-sized), and shows reasonably good capacity retention (85% capacity retention after 50 cycles).<sup>[155]</sup> In contrast to the characteristic, stepwise and sloping voltage profile of NaCoO<sub>2</sub> and the low capacity of NaFeO<sub>2</sub>, O3-Na[Fe<sub>0.5</sub>Co<sub>0.5</sub>]O<sub>2</sub> has a smooth and nearly flat voltage profile. Another merit for this cathode material, for energy efficiency considerations, is a very low polarization between the (dis)charge voltage profiles therein observed. In addition, the material exhibits an attractively high average voltage of 3.1 V and has a comparatively high reversible capacity of 160 mAh g<sup>-1</sup> due to the formation of a sodium-rich phase.<sup>[155]</sup> The presence of Co thus proved effective in enhancing the structural stability of the iron containing LMeO and improved the electrical conductivity of Na[Fe<sub>0.5</sub>Co<sub>0.5</sub>]O<sub>2</sub>. This results in the attractive electrode properties mentioned above.

Because Co is not an abundant element, one approach to reduce Co content has been to formulate ternary LMeOs, such as O3-Type Na[Ni<sub>0.33</sub>Co<sub>0.33</sub>Fe<sub>0.33</sub>].<sup>[162]</sup> Interestingly, most of the attractive electrochemical properties of Na[Fe<sub>0.5</sub>Co<sub>0.5</sub>]O<sub>2</sub>, in terms of excellent rate capability, low-voltage polarization, and high reversible capacity, are herein retained. While this approach highlights the effectiveness of Ni substitution, the use of Co remains a major deterrent for economical large-scale applications.

Co-free, binary, and tertiary LMeOs have also been reported as cathode materials for SIB applications. O3-type Na[Ni<sub>0.5</sub>Mn<sub>0.5</sub>]O<sub>2</sub>, for example, is known to have one of the highest reversible capacities of 185 mAh g<sup>-1</sup> among LMeOs, when cycled in the 2.2–4.5 V range (versus Na<sup>+</sup>/Na).<sup>[174]</sup> However, the cycle life of this material is greatly influenced by the

(dis)charge protocol. For example, improved reversibility is only observed when the upper cutoff voltage is 3.8 V versus Na<sup>+</sup>/Na. Moreover, it exhibits a highly sloping and cascading voltage profile due to the multiple phase transformations in the order O3 → O'3 → P3 → P'3 → P3'' during sodium extraction.

Hasa et al.<sup>[175]</sup> investigated the electrode performance of P2-Na<sub>0.5</sub>[Ni<sub>0.23</sub>Fe<sub>0.13</sub>Mn<sub>0.63</sub>]O<sub>2</sub> and obtained an attractively high reversible capacity of 200 mAh g<sup>-1</sup> with good capacity retention (100 reversible cycles reported) and an excellent rate capability (up to 5 C-rate in micrometer-sized, carbon-coating free samples). Based on the economic benefits of its elemental composition, this material can indeed be considered one of the most promising cathode materials for SIB applications. However, the voltage profile therein obtained was sloping in the 1.5–4.5 V range (vs Na<sup>+</sup>/Na) and a high degree of polarization between the charge and discharge curves was evidenced. Subsequent optimization studies by the same authors on the effect of the Ni-to-Fe ratio and the Na content on the electrochemical performance revealed that the changes in the Ni-to-Fe ratio only lead to minor electrode capacity improvements.<sup>[176]</sup> The presence of Ni however remains crucial to reach higher electrode potentials and to avoid electrode dissolution.

#### 4.7. Polyanionic Compounds as Cathode Materials

The other major class of cathode materials is polyanionic compounds. The most widely studied polyanionic groups contain sulfate (SO<sub>4</sub>)<sup>2-</sup>, phosphate (PO<sub>4</sub>)<sup>3-</sup>, and pyrophosphate (P<sub>2</sub>O<sub>7</sub>)<sup>4-</sup> ions.<sup>[177]</sup> In general, polyanionic compounds are characterized by remarkable structural stability and have an adjustable electrode potential due to the inductive effect.<sup>[178–180]</sup> The most prolific structures within the family of polyanionic compounds are the olivine, maricite, and NASICON-like frameworks.<sup>[177]</sup> Figure 19 illustrates the differences between olivine-type and maricite-type crystal structures<sup>[181]</sup> The olivine-type structure is renowned for its open diffusion pathways and is the most ubiquitous phase for LIB cathode applications. In the SIB case, the maricite-type NaFePO<sub>4</sub> is the thermodynamically stable structure. Regrettably, at temperatures above 450 °C, olivine-type NaFePO<sub>4</sub> transforms into maricite-type NaFePO<sub>4</sub>.

A new series of mixed polyanion systems for SIB applications, analogous to Na<sub>4</sub>Fe<sub>3</sub>(PO<sub>4</sub>)<sub>2</sub>(P<sub>2</sub>O<sub>7</sub>) and carbonophosphates, Na<sub>3</sub>MePO<sub>4</sub>CO<sub>3</sub> (where Me = Fe or Mn), has also been reported.<sup>[182,183]</sup> The Mn compound, in particular, has been unveiled as a promising polyanionic carbonophosphate cathode material. To realize its full potential, however, electrode optimization to reduce a 50% capacity loss in the first cycles (from 200 to 100 mAh g<sup>-1</sup>) is needed. Furthermore the rate performance is not that impressive. Nevertheless, a reasonable capacity retention observed is enough to cause optimism in this material.<sup>[182]</sup>

##### 4.7.1. Phosphates

Three polymorphs of NaFePO<sub>4</sub>, olivine, maricite, and amorphous NaFePO<sub>4</sub>, have thus far been reported to be electrochemically active in SIBs.<sup>[184–191]</sup> Among these, amorphous NaFePO<sub>4</sub> shows the most attractive electrode properties for

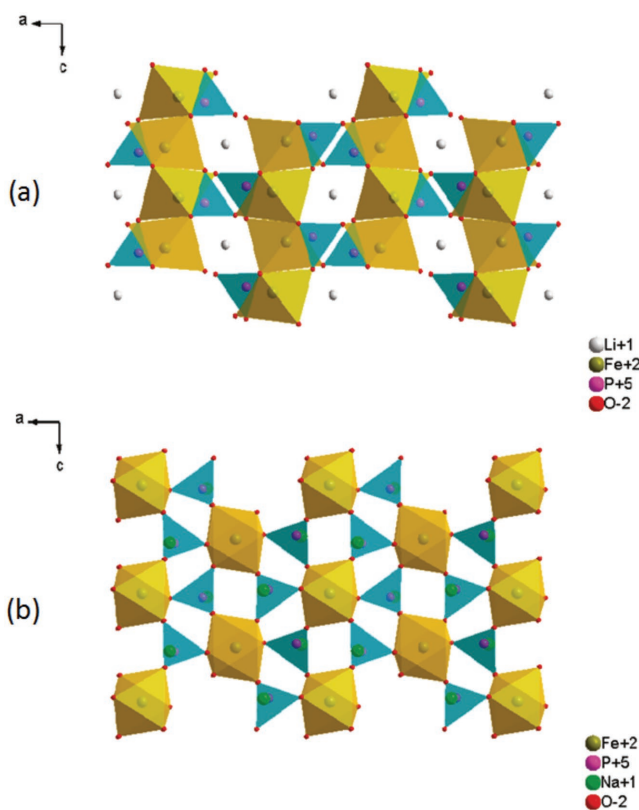


**Figure 19.** Crystal structures of lithium iron phosphate and sodium iron phosphate shown in the 101 plane of a) olivine  $\text{LiFePO}_4$ , and the open structure allows lithium-ion migration; b) maricite  $\text{NaFePO}_4$ ,  $\text{PO}_4^{3-}$  tetrahedra totally isolates the sodium cations and blocks sodium-ion diffusion. Reproduced with permission.<sup>[181]</sup> Copyright 2011, American Chemical Society.

electrode applications. Because of the low cost and abundance of elemental iron, iron-based materials are highly attractive in the quest for robust, scalable, cost effective, and environmentally benign cathode materials.

Because of the success of olivine-type  $\text{LiFePO}_4$  as a cost effective, ultrafast cathode material for LIBs,<sup>[192–194]</sup> similar electrode performances had been anticipated in olivine-type  $\text{NaFePO}_4$ . Oh et al.<sup>[186]</sup> thus investigated the electrode properties of olivine-type  $\text{NaFePO}_4$ , prepared from olivine-type  $\text{LiFePO}_4$  via electrochemical delithiation followed by sodiation. Total delithiation before sodium insertion is crucial because any remaining lithium results in structural defects that inhibit free sodium diffusion.<sup>[189]</sup> A comparative study of the different electrode properties of olivine-type, carbon-coated  $\text{NaFePO}_4$ , and  $\text{LiFePO}_4$  was then carried out by Zhu et al.<sup>[195]</sup> wherein spherical active particles of approximately equal sizes (about 80 nm) were used. Figure 20 illustrates the respective electrochemical properties of the two olivine-type electrode materials. The two equilibrium open-circuit potentials here show relative similarity, characterized by long plateau voltage profiles during (dis)charge and suggestive of a two-phase insertion mechanism. However, the potential plateau observed in  $\text{NaFePO}_4$  at 2.86 V (vs  $\text{Na}^+/\text{Na}$ ) is 540 mV lower compared to that observed in  $\text{LiFePO}_4$  and exhibits ≈4 times more voltage hysteresis. The

rate performance in the carbon coated samples of  $\text{NaFePO}_4$  is also not impressive either. Nearly 80% capacity loss is recorded at 2 C-rate. Figure 20e,f shows the comparative Cycleability of  $\text{NaFePO}_4$  and  $\text{LiFePO}_4$ . Although carbon-coated  $\text{NaFePO}_4$  is able to withstand over 100 cycles with a reasonable capacity retention of nearly 90%, other vital electrode properties as mentioned above do not match those of  $\text{LiFePO}_4$ .

While olivine-type  $\text{NaFePO}_4$  did not yield the desired results, attractive electrochemical performances were nevertheless obtained in amorphous  $\text{NaFePO}_4$  ( $\alpha\text{-NaFePO}_4$ ). Li et al.<sup>[191]</sup> synthesized hollow  $\alpha\text{-NaFePO}_4$  nanospheres via a simple in situ hard template process while Fang et al.<sup>[196]</sup> prepared pomegranate-like  $\alpha\text{-NaFePO}_4$  nanospheres via a chemically induced precipitation method. Although the material shows a relatively low average voltage of 2.4 V, based on the  $\text{Fe}^{3+}/\text{Fe}^{2+}$  redox couple, it exhibits a virtually theoretical gravimetric capacity of 152 mAh g<sup>-1</sup> (99% of the theoretical capacity), an outstanding cycle life (300 cycles with ≈95% capacity retention), and a superior rate capability of up to 10 C-rate in carbon coating-free samples.<sup>[191]</sup> Figure 21a,b illustrates the material properties and electrode performance of nanometer-sized  $\alpha\text{-NaFePO}_4$ . The hollow spherical shape reduces the diffusion length for insertion and enhances surface reactivity. In addition, the structurally robust amorphous phase improves the electronic conductivity and supports multiple (dis)charge cycling in the as-prepared samples. While these synergistic effects have resulted in outstanding electrode properties, a detailed mechanistic understanding is still lacking in order to optimize the electrochemical properties.<sup>[197]</sup> Nevertheless,  $\alpha\text{-NaFePO}_4$  remains a prime candidate for SIB applications.

No reversible redox activity has been reported for maricite-type  $\text{NaFePO}_4$ . In this material, the  $\text{PO}_4^{3-}$  tetrahedra are thought to isolate the sodium cations, resulting in a “closed” framework, devoid of free diffusion pathways.<sup>[186,198,199]</sup> Even though recent discoveries by Kim et al.<sup>[190]</sup> reported that maricite-type  $\text{NaFePO}_4$  reaches a capacity of 142 mAh g<sup>-1</sup> with 95% capacity retention over 200 cycles. It therein appeared that key to this prolonged cycle life was the in situ transformation to amorphous  $\text{FePO}_4$  ( $\alpha\text{-FePO}_4$ ) upon full (de)sodiation. Figure 21c,d illustrates the electrode properties of the maricite-type  $\text{NaFePO}_4$ . The transformation to the amorphous phase after the initial cycles is herein evidenced in the transition electron microscope (TEM) images.

Olivine phosphate  $\text{NaFe}_{0.5}\text{Mn}_{0.5}(\text{PO}_4)_3$  directly synthesized via a molten salt reaction is also reported as a possible cathode material.<sup>[14,181]</sup> This sodium iron/manganese compound likewise exhibits a sloping profile over the entire voltage range, resulting in a low average electrode potential ( $\approx 2.7$  V vs  $\text{Na}^+/\text{Na}$ ). In general, Fe-containing phosphate compounds are ideal electrodes owing to their low cost, stability, and environmentally benign character; however, the  $\text{Fe}(\text{III})/\text{Fe}(\text{II})$  redox potential is too low for cathode materials and too high for anode materials.<sup>[200]</sup> Ultimately, such an intermediate voltage renders them less attractive.<sup>[14]</sup>

NASICON  $\text{Na}_3\text{V}_2(\text{PO}_4)_3$  (NVP) with a flat voltage plateau is yet another highly promising cathode material for SIBs. Electrode properties of NVP were first investigated by Uebou et al.<sup>[201]</sup> in 2002. The highest gravimetric energy compared to cobalt- and nickel-based LMeOs available that time was

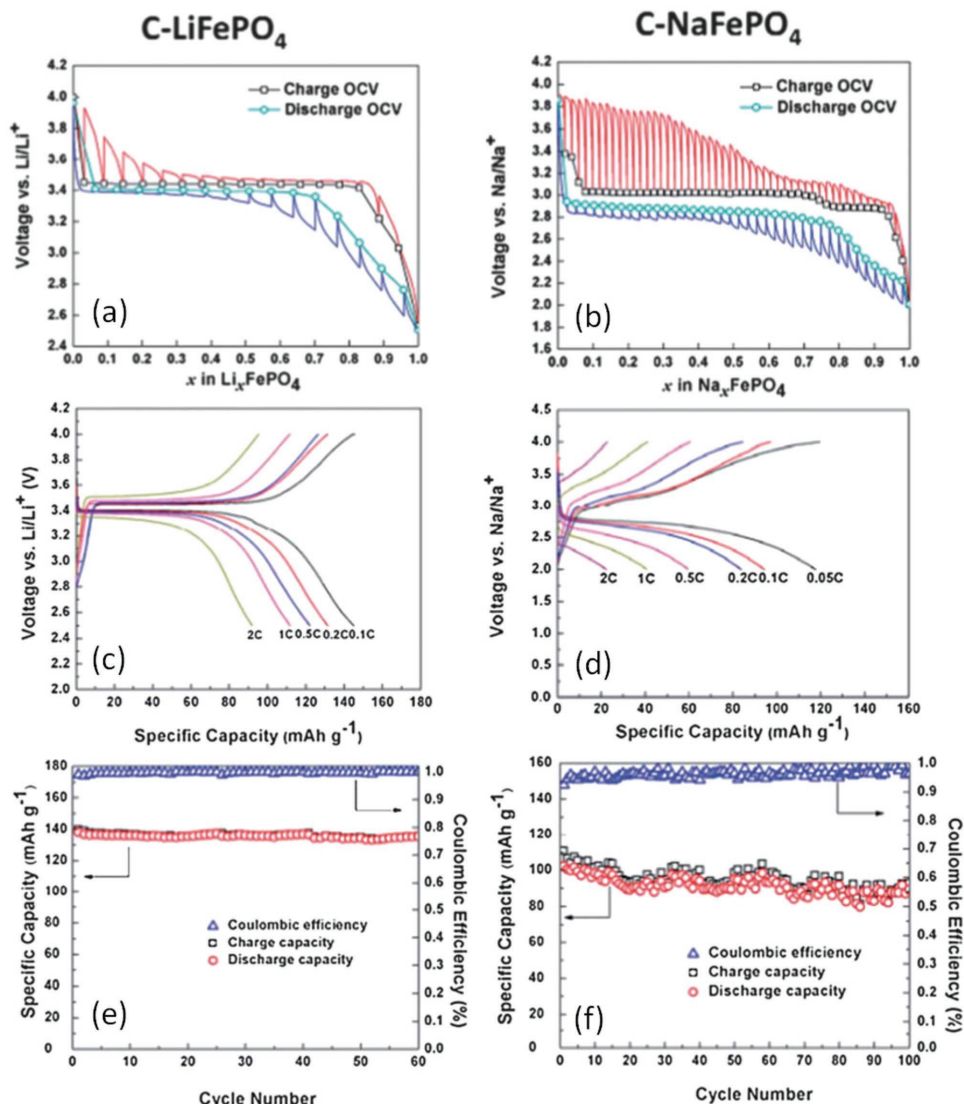


**Figure 20.** Comparative electrode characteristics of carbon-coated, olivine-type  $\text{LiFePO}_4$  (left) and carbon-coated, olivine-type  $\text{NaFePO}_4$  (right). a,b) The (dis)charge open-circuit voltage obtained by galvanostatic intermittent titration technique. c,d) Rate capability tests of  $\text{LiFePO}_4$  and  $\text{NaFePO}_4$ . e,f) Cycleability tests of  $\text{LiFePO}_4$  and  $\text{NaFePO}_4$ . a–f) Reproduced with permission.<sup>[195]</sup> Copyright 2013, The Royal Society of Chemistry.

reported.<sup>[201]</sup> Cyclic voltammograms of carbon-coated NVP/C are shown in Figure 22a. Two characteristic peaks, one at  $\approx 3.4$  V, attributed to the  $\text{V}^{4+}/\text{V}^{3+}$  redox couple, and the other, at a lower redox potential of 1.6 V (vs  $\text{Na}^+/\text{Na}$ ), based on the  $\text{V}^{3+}/\text{V}^{2+}$  redox couple, are evidenced.<sup>[202]</sup> Because of an impressively flat plateau voltage and because 2 moles per formula unit of Na are extracted at the higher electrode potential, corresponding to a theoretical capacity of 118 mAh g<sup>-1</sup>, an optimization practice is to avoid the lower voltage  $\text{V}^{3+}/\text{V}^{2+}$  couple. The different oxidation states of vanadium however permit the use of NVP as both cathode and anode materials in symmetric cells.<sup>[203]</sup> In such cells, the optimal cathode to anode mass quantitative ratio, based on an anode capacity of 36 mAh g<sup>-1</sup>, is 1:3.<sup>[203]</sup>

The crystal structure of NASICON-type NVP is shown in Figure 22c. The 3D open structure with large interstitial spaces is particularly interesting because it facilitates sodium superconductivity, yet it suffers from poor electronic conductivity.<sup>[204]</sup>

It has thus been proposed that carbon coating<sup>[202,205,206]</sup> and the use of nanomaterials<sup>[207,208]</sup> can further enhance the electronic conductivity of NVP. It is however worth mentioning that bare, micrometer-sized samples nevertheless show encouraging electrode and thermal properties.<sup>[208,209]</sup> Cycling tests performed in the 2–4.6 V versus  $\text{Na}^+/\text{Na}$  range reveal a reversible capacity of 113 mAh g<sup>-1</sup> with 95% capacity retention after 50 cycles, without significant potential hysteresis and a surprisingly good rate capability.<sup>[209,210]</sup>

Micrometer-sized NVP particles, attached to graphene surfaces (NVP/graphene), were investigated by Jung et al.<sup>[212]</sup> Compared to bare NVP, improved cycleability, and rate performance, wherein 300 (dis)charge cycles at 10 C-rate were reported. Enhanced cycleability and rate capability were later revealed in carbon-coated, core–shell nanocomposite electrodes, NVP@C as illustrated in Figure 22d.<sup>[211]</sup> Therein, a superior cycling performance, demonstrated by 700 (dis)charge

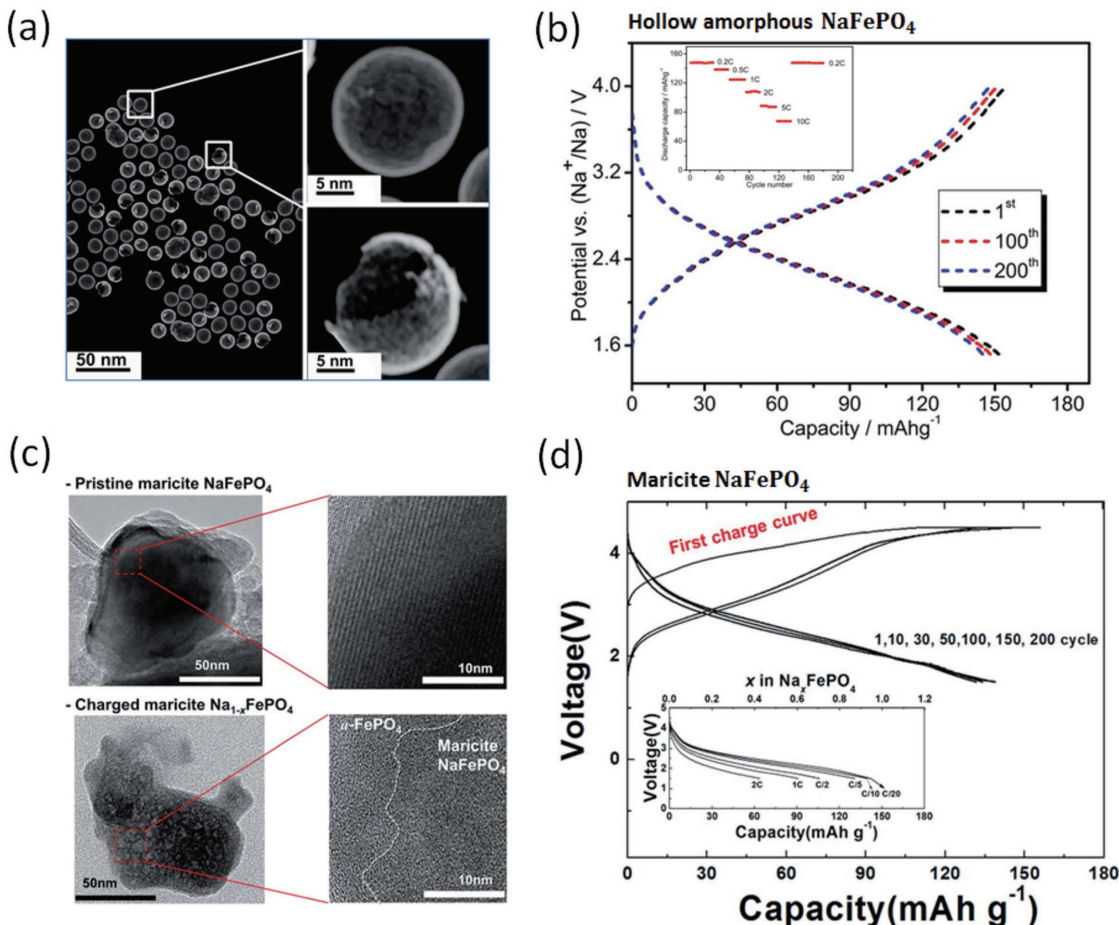


**Figure 21.** Material characteristics and electrochemical performance of maricite and amorphous NaFePO<sub>4</sub>. a) Scanning transition electron microscopy images of single hollow amorphous NaFePO<sub>4</sub> nanospheres. b) Voltage profiles in hollow amorphous NaFePO<sub>4</sub> showing stable cycleability over 200 cycles, and the top inset showing the rate capability tests from 0.2 C-rate to 10 C-rate. c) Transition electron microscopy images showing pristine and partially charged maricite NaFePO<sub>4</sub>. d) Galvanostatic (dis)charge voltage curves of maricite NaFePO<sub>4</sub> cycled over 200 cycles at 0.05 C-rate in a Na cell, and the bottom inset showing rate capability tests of maricite NaFePO<sub>4</sub> from 0.05 up to 2 C-rate. a,b) Reproduced with permission.<sup>[191]</sup> Copyright 2015, The Royal Society of Chemistry. c,d) Reproduced with permission.<sup>[190]</sup> Copyright 2015, The Royal Society of Chemistry.

cycles at 5 C-rate, is evidenced. Later, Jiang et al.<sup>[213]</sup> improved the core-shell nanostructure design by embedding NVP@C in mesoporous carbon CMK-3. A phenomenal cycle life of 2000 (dis)charge cycles at 5 C-rate was achieved in the NVP@C@CMK-3 electrodes. The diffusion length for the sodium during intercalation is thus reduced by the core-shell architecture, while the mesoporous framework enables rapid ion transport and electronic conduction. This “double” carbon-coating design was thereafter improved upon by Rui et al.,<sup>[214]</sup> wherein core-shell NVP@C was embedded in reduced graphene oxide (rGo). The NVP@C@rGo electrode exhibited an ultralong cycle life of 10.000 (dis)charge cycles at an impressive rate capability of 100 C-rate. This design of nanosized, carbon-coated, and carbon-wrapped NVP can indeed be adapted to other materials and cements the prospects of NVP-based electrode materials.<sup>[215]</sup>

Since the first discovery of fast Na<sup>+</sup> diffusion in “skeleton” structures by Goodenough et al.,<sup>[216]</sup> numerous NASICON-type materials, including NaNbFe(PO<sub>4</sub>)<sub>3</sub><sup>[217]</sup> and Na<sub>2</sub>TiMe(PO<sub>4</sub>)<sub>3</sub> (Me = Fe/Cr),<sup>[218]</sup> have been investigated and reported. Phosphate cathode materials are thus expected to accelerate the

practical application of SIBs.<sup>[219]</sup> Despite the weight penalty arising from either the (PO<sub>4</sub>)<sup>3-</sup> or (SO<sub>4</sub>)<sup>2-</sup> anions, they provide structurally robust frameworks that enable high rate capability and extended cycle life, critical requirements for large-scale EES.

#### 4.7.2. Pyrophosphates

Following the success of lithium iron(II) pyrophosphate (Li<sub>2</sub>FeP<sub>2</sub>O<sub>7</sub>) as a positive electrode material for LIBs,<sup>[220,221]</sup> the search of low-cost electrode materials for SIBs soon shifted from the phosphate system to the pyrophosphate system.<sup>[17]</sup> Na<sub>2</sub>FeP<sub>2</sub>O<sub>7</sub>, the analogous Na-based polyanion, forms an open 3D crystal structure that is beneficial for fast sodium diffusion. Although Na<sub>2</sub>FeP<sub>2</sub>O<sub>7</sub> has a low theoretical capacity of 97 mAh g<sup>-1</sup>, based on 1 mole sodium-ion extraction, it shows better rate capability compared to triphylite-NaFePO<sub>4</sub>, due to the open diffusion pathways formed by the pyrophosphate ions.<sup>[17]</sup> Consequently, micrometer-sized Na<sub>2</sub>FeP<sub>2</sub>O<sub>7</sub>, synthesized by solid-state methods, shows good rate capability, even without

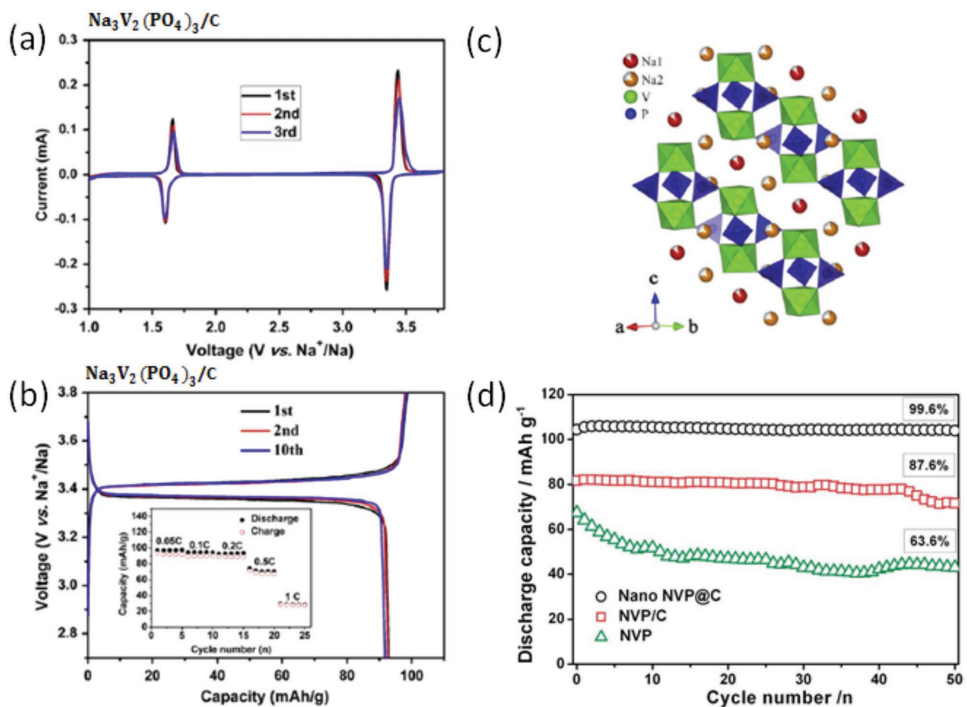


**Figure 22.** Electrode properties of NASICON-type  $\text{Na}_3\text{V}_2(\text{PO}_4)_3$ . a) CV curves for carbon-coated  $\text{Na}_3\text{V}_2(\text{PO}_4)_3/\text{C}$ , showing two redox peaks in a voltage sweep range of 1.0–3.8 V versus  $\text{Na}^+/\text{Na}$ . b) Voltage profiles during 0.05 C-rate (dis)charge cycling of  $\text{Na}_3\text{V}_2(\text{PO}_4)_3/\text{C}$  in a voltage range of 2.7–3.8 V versus  $\text{Na}^+/\text{Na}$ . The inset showing the rate performance. c) Crystal structure of  $\text{Na}_3\text{V}_2(\text{PO}_4)_3$ . d) Comparison of the cycling performance between bare  $\text{Na}_3\text{V}_2(\text{PO}_4)_3$  (NVP), carbon-coated  $\text{Na}_3\text{V}_2(\text{PO}_4)_3$  (NVP/C), and nanostructured, core-shell  $\text{Na}_3\text{V}_2(\text{PO}_4)_3$  (NVP@C). a–c) Reproduced with permission.<sup>[202]</sup> Copyright 2011, Elsevier B.V. d) Reproduced with permission.<sup>[211]</sup> Copyright 2014, The Royal Society of Chemistry.

a carbon coating, and has a negligible volume change of only 3% upon full Na extraction.<sup>[222]</sup> Despite the available energy density, being lower in the pyrophosphate system compared to  $\text{NaFePO}_4$ , its overall electrode properties are promising for large-scale applications.

Pyrophosphate-based electrode materials, containing other transition-metal elements, have also been reported.<sup>[223]</sup> The recently discovered  $\text{Na}_2\text{MnP}_2\text{O}_7$ , which is isostructural to  $\text{Na}_2\text{FeP}_2\text{O}_7$ , also shows good electrode performance.<sup>[224]</sup> Although the available energy density is higher due to the  $\text{Mn}^{3+}/\text{Mn}^{2+}$  redox potential, it also experiences significant voltage hysteresis during cycling, which debilitates the energy efficiency of the electrode.

A polyanion system mixed of phosphate ( $\text{PO}_4$ )<sup>3-</sup> and pyrophosphate ( $\text{P}_2\text{O}_7$ )<sup>4-</sup> has also been prepared.<sup>[225]</sup>  $\text{Na}_4\text{Fe}_3(\text{PO}_4)_2(\text{P}_2\text{O}_7)$  is a mixed polyanion compound with an impressively high average voltage of 3.2 V versus  $\text{Na}^+/\text{Na}$ .<sup>[226]</sup> Compared to  $\text{Na}_2\text{FeP}_2\text{O}_7$ , it exhibits an improved and stable reversible storage capacity of 122 mAh g<sup>-1</sup>, which remains nearly constant over 100 (dis)charge cycles. Quantum leaps toward electrode materials with practical energy density and cycleability were later discovered in vanadium-based *ortho*-diphosphate  $\text{Na}_7\text{V}_4(\text{P}_2\text{O}_7)_4\text{PO}_4$  (VODP).<sup>[227]</sup> VODP exhibits a flat and well-defined voltage plateau at 3.88 V, impressive cycle life of 78% capacity retention after 1000 cycles, excellent rate capability of micrometer-sized powders without carbon coating, and minor volume change of 2.4% upon full cycling. Although the reversible capacity is low (91 mAh g<sup>-1</sup>), its remarkable structural stability makes VODP a prospective cathode material for SIBs.

#### 4.7.3. Fluorophosphates

Fluorophosphates are novel class of high performance cathodes which exploit the inductive effect of the presence of  $\text{PO}_4^{3-}$  and  $\text{F}^-$  anions to achieve high electrode potentials.<sup>[228]</sup> Fluorinated iron phosphate  $\text{Na}_2\text{FePO}_4\text{F}$  with a 2D layered framework is another studied electrode material for SIBs.<sup>[198,229,230]</sup> Although carbon-coated  $\text{Na}_2\text{FePO}_4\text{F}$  has a relatively high electrode potential of 3 V versus  $\text{Na}^+/\text{Na}$  among the Fe-based cathodes, its other electrode properties, such as poor cycleability, high voltage polarization, and moderate capacity of 100 mAh g<sup>-1</sup>, are not so attractive.

Mn substitution results in  $\text{Na}_2\text{Fe}_{0.5}\text{Mn}_{0.5}\text{PO}_4\text{F}$  with a 3D tunnel structure, which favorably facilitates fast sodium diffusion.<sup>[231]</sup>  $\text{Na}_2\text{Fe}_{0.5}\text{Mn}_{0.5}\text{PO}_4\text{F}$  achieves an even higher average electrode potential at 3.5 V versus  $\text{Na}^+/\text{Na}$  because of the  $\text{Mn}^{3+}/\text{Mn}^{2+}$  redox reaction and has a slightly improved reversible capacity of 110 mAh g<sup>-1</sup>. A larger voltage hysteresis, however, upon cycling is therein experienced, which seriously incapacitates the energy efficiency of this electrode.

Carbon-coated  $\text{Na}_2\text{CoPO}_4\text{F}$ , with an impressively high and nearly flat voltage plateau at 4.3 V versus  $\text{Na}^+/\text{Na}$ , is another fluorophosphate.<sup>[232]</sup> Its overall properties, in particular a poor cycle life and a first cycle Coulombic efficiency of only 56%, are however not adequate for practical applications.<sup>[233]</sup> Furthermore, the use of rare-metal Co re-emerges as a major stumbling block. Electrolyte decomposition and side reactions at high potentials are two factors thought to be the main causes of the observed capacity loss.

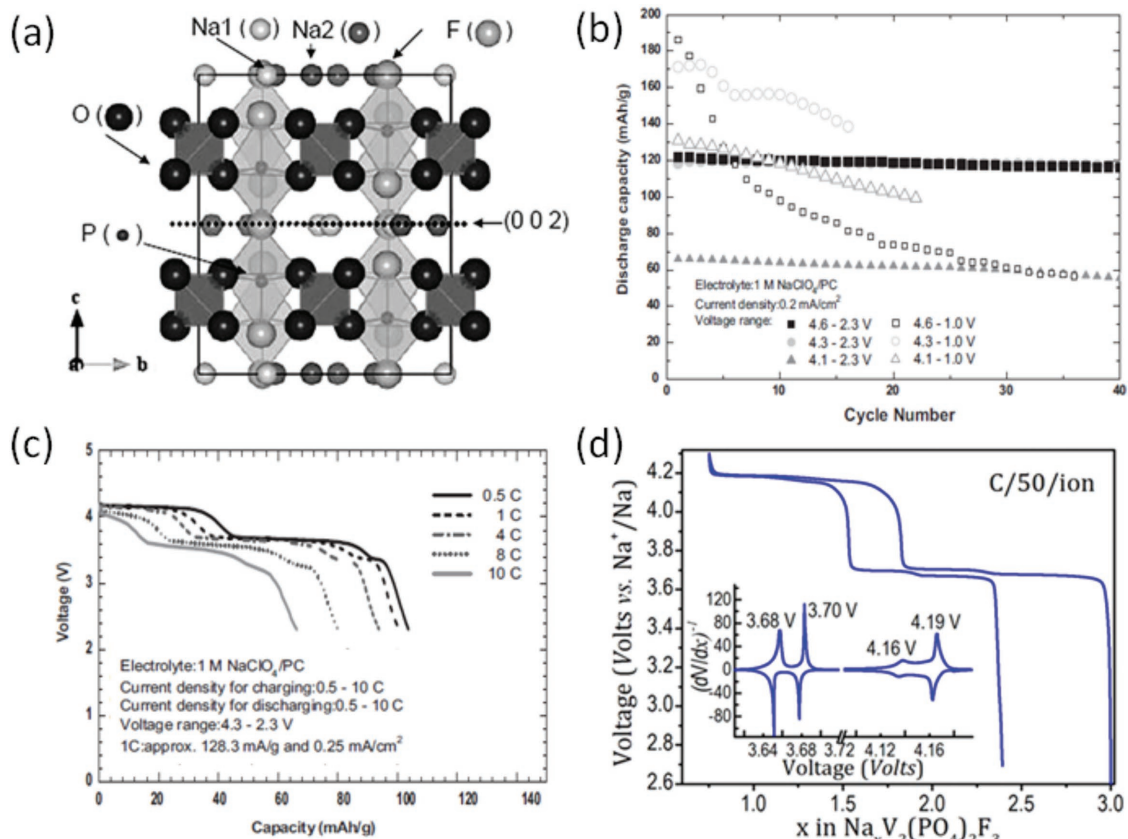


**Figure 23.** Properties of  $\text{Na}_3\text{V}_2(\text{PO}_4)_2\text{F}_3$  cathode material. a) The 3D structure of  $\beta\text{-Na}_3\text{V}_2(\text{PO}_4)_2\text{F}_3$ , viewed along the  $a$ -axis. b) Effect of cutoff voltage on the cycling stability of  $\text{Na}_3\text{V}_2(\text{PO}_4)_2\text{F}_3$ . c) Rate capability tests up to 10 C-rate. d) The (dis)charge voltage profile in  $\text{Na}/[\text{Na}_3\text{V}_2(\text{PO}_4)_2\text{F}_3]$  half-cell at C/50 rate (per exchanged ion), and the inset shows the inverse derivative cyclic voltammetry curve where several redox states can be identified. a–c) Reproduced with permission.<sup>[239]</sup> Copyright 2012, Elsevier. d) Reproduced with permission.<sup>[237]</sup> Copyright 2015, American Chemical Society.

NASICON-type, vanadium-based fluorophosphates, with the general formula  $\text{Na}_3\text{V}_2\text{O}_{2x}(\text{PO}_4)_{2-2x}$ , where  $0 \leq x \leq 1$ , are an appealing family of electrode materials, first introduced by Barker et al.<sup>[126,234,235]</sup> As  $x$  varies, the crystal structure as well as the oxidation state of vanadium (between 3+ and 4+) changes.<sup>[236]</sup> Due to the formation of sodium-rich phases, based on three sodium ions per formula unit and the multiple oxidation states of vanadium, i.e.,  $\text{V}^{3+}$ ,  $\text{V}^{4+}$ , and  $\text{V}^{5+}$ , such compositions were quickly identified as potential solutions to the energy density problems faced by most of the SIB cathode materials.<sup>[237]</sup>

The most prominent forms are the two end members:  $\text{Na}_{1.5}\text{V}^{\text{IV}}\text{OPO}_4\text{F}_{0.5}$ , where  $x = 1$ , and  $\text{Na}_3\text{V}_2^{\text{III}}(\text{PO}_4)_2\text{F}_3$ , where  $x = 0$ . The crystal structure and electrochemical properties of  $\text{Na}_{1.5}\text{V}^{\text{IV}}\text{OPO}_4\text{F}_{0.5}$  were investigated by Sauvage et al.<sup>[238]</sup> The discharge voltage curve exhibited two exceptionally high voltage plateaus nested at about 3.6 and 4.0 V (vs  $\text{Na}^+/\text{Na}$ ). However, a low electrode capacity of 87 mAh g<sup>-1</sup> was recorded with a low capacity retention of 70% after only 50 cycles. The poor electronic conductivity at room temperature ( $1.8 \times 10^{-7}$  S cm<sup>-1</sup>) of the material was thought to be the reason of the poor transport properties. Therefore, carbon coating was expected to enhance the electrode performance. For high energy density considerations,  $\text{Na}_3\text{V}_2^{\text{III}}(\text{PO}_4)_2\text{F}_3$  is the most attractive phase, in which higher voltage plateaus are observed at about 3.7 and 4.2 V (vs  $\text{Na}^+/\text{Na}$ ).<sup>[237]</sup> More impressively, a higher electrode capacity

of 120 mAh g<sup>-1</sup> with exceptional capacity retention (98% after 40 cycles) has been achieved, resulting in a high theoretical energy density of 507 Wh kg<sup>-1</sup> (128 mAh g<sup>-1</sup> × 3.95 V).<sup>[237,239]</sup> This value is close to that of some commercial LIB cathodes,  $\text{LiFePO}_4$  for example has an energy density of 580 Wh kg<sup>-1</sup>. This highlights the potential of this electrode in particular and for the SIB technology in general. Figure 23 illustrates the structure and electrochemical features of  $\text{Na}_3\text{V}_2^{\text{III}}(\text{PO}_4)_2\text{F}_3$  described above.

Shakoor et al.<sup>[240]</sup> in a study of the electrochemical and thermal properties of  $\text{Na}_3\text{V}_2^{\text{III}}(\text{PO}_4)_2\text{F}_3$  reported a very good thermal stability, up to 550 °C, and an attractively small cell volume change of ≈2% during Na-ion (dis)charge. Improved electrochemical performance was however reported by Liu et al.<sup>[241]</sup> in carbon-coated nanosized particles of  $\text{Na}_3\text{V}_2^{\text{III}}(\text{PO}_4)_2\text{F}_3$  embedded in a mesoporous carbon matrix. Therein, ultralong life 3000 (dis)charge cycles were reported with superior rate capability of 30 C-rate. These beneficial characteristics further qualify  $\text{Na}_3\text{V}_2^{\text{III}}(\text{PO}_4)_2\text{F}_3$  as a material of choice for safe, long cycle life, and high energy density SIB.

#### 4.7.4. Sulfates

$\text{Na}_2\text{Fe}_2(\text{SO}_4)_3$  with alluaudite-type sulfate framework is a very promising electrode for SIB applications.<sup>[242]</sup> First, the material

has the highest electrode potential among electrodes based on the  $\text{Fe}^{3+}/\text{Fe}^{2+}$  redox of 3.8 V versus  $\text{Na}^+/\text{Na}$  and the as-prepared  $\text{Na}_2\text{Fe}_2(\text{SO}_4)_3$  electrodes show excellent rate capability of up to 20 C-rate and good cycleability. The charge/discharge cycles exhibit an excellent Coulombic efficiency in the first cycle. Regardless of some structural changes which are evidenced, a homogeneous intercalation mechanism is thought to occur as corroborated by the smooth sloping voltage profile and near-zero volume change of 1.6%. Although the achievable reversible capacity is moderate ( $102 \text{ mAh g}^{-1}$ ) and the hygroscopic nature implies that extra measures must be taken in scaling up production, the ease of processing via low-temperature solid-state methods makes it one of the most attractive cathode materials.

#### 4.8. Other Cathode Materials

Orthorhombic  $\text{Na}_{0.44}\text{MnO}_2$  ( $\text{Na}_4\text{Mn}_9\text{O}_{18}$ ), a member of the family of manganese-based oxides, was first reported by Doeff et al. in the mid-1990s as a cathode for Li and Na batteries.<sup>[243,244]</sup> High capacities in the range of  $160 \text{ mAh g}^{-1}$  were initially reported in Na cells at  $85^\circ\text{C}$ , using solid electrolytes. Although the crystal structure of  $\text{Na}_{0.44}\text{MnO}_2$  was found to have attractively large-sized tunnels, which facilitate sodium storage (see Figure 24c), the pioneering phases, prepared by the solid-state method, were found to contain  $\text{Mn}_2\text{O}_3$  bixbyite impurities.<sup>[245]</sup> Purification, by a hydrochloric acid treatment, inadvertently induced sodium leaching and resulted in isostructural sodium deficient phases.<sup>[243]</sup> Sauvage et al.<sup>[246]</sup> successfully optimized the parameters of the solid-state preparation method and obtained single crystals, while Akimoto et al.<sup>[247]</sup> used the flux method at  $1446^\circ\text{C}$  for the synthesis of pure phases of  $\text{Na}_{0.44}\text{MnO}_2$ .

Electrochemical studies of pure  $\text{Na}_{0.44}\text{MnO}_2$  were then made possible. The complexity of the sodium intercalation phenomena was clearly evidenced by nonsmooth voltage profiles. Multiple distinct phase transitions (up to seven intermediate phases) were then identified, first experimentally<sup>[245,248]</sup> and then by DFT calculations.<sup>[249]</sup> Although an initial capacity of close to  $140 \text{ mAh g}^{-1}$  was observed, cycling tests proceeded with rapid capacity loss and increase in voltage polarization.<sup>[245]</sup> The Jahn–Teller distortion observed in layered manganese oxides is also a concern in such tunnel-type oxides,<sup>[166]</sup> and furthermore, manganese oxides are poor electronic conductors.<sup>[250]</sup> These effects result in a relatively large volume expansion of  $\approx 6\%$ .<sup>[249]</sup> Metal substitution, for example, Cr substitution, to reduce the volume expansion and strategies that increase the conductivity are therefore necessary to minimize the effects of the Jahn–Teller distortion.<sup>[249,251]</sup>

Quantum leaps in electrode performance were however reported in single-crystalline nanowires of  $\text{Na}_{0.44}\text{MnO}_2$ , synthesized by a polymer-pyrolysis method by Cao et al.<sup>[248]</sup> and recently by Zhan et al.<sup>[252]</sup> using the reverse microemulsion method. The pure phase crystallinity and nanowire morphology enabled a high reversible capacity of  $128 \text{ mAh g}^{-1}$  (at 0.1 C-rate), an excellent rate capability ( $80 \text{ mAh g}^{-1}$  at 2 C-rate), and outstanding cycleability, reaching 1000 cycles with 77% capacity retention at 0.5 C-rate. Figure 24 illustrates the electrochemical properties of  $\text{Na}_{0.44}\text{MnO}_2$  nanowires. Although a low

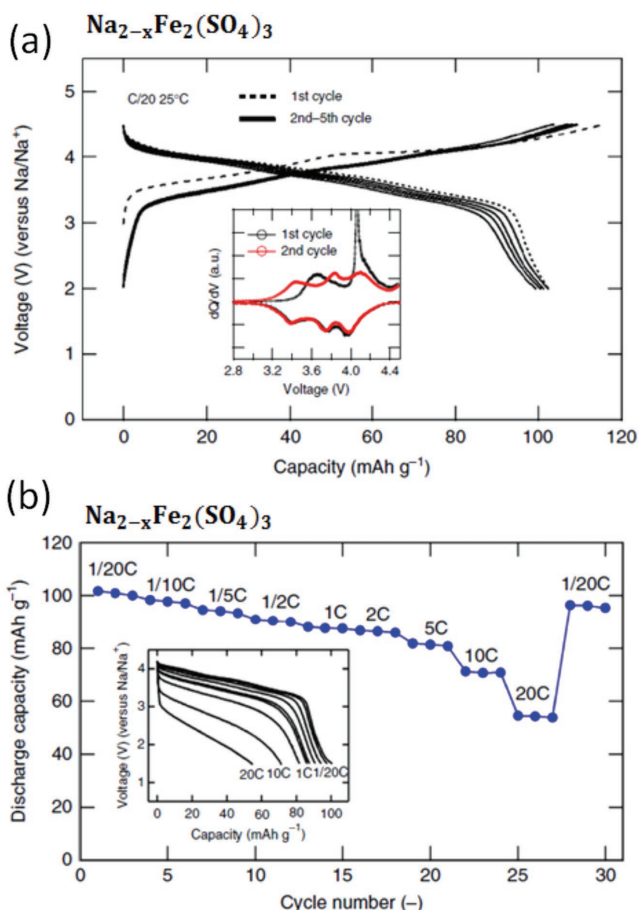


**Figure 24.** Charge and discharge cycles of  $\text{Na}_2\text{Fe}_2(\text{SO}_4)_3$ . a) The voltage profiles in the first five cycles, and the inset showing cyclic voltammetry peaks in the first two sweeps. b) Cycle ability and rate capability of  $\text{Na}_2\text{Fe}_2(\text{SO}_4)_3$ , and the inset shows the voltage curves at various discharge currents. Reproduced with permission.<sup>[242]</sup> Copyright 2014, Macmillan Publishers Limited.

average voltage of  $\approx 2.7 \text{ V}$  and a sloping voltage profile are some unattractive properties of  $\text{Na}_{0.44}\text{MnO}_2$ , its low cost and high storage capacity make it one of the most preeminent cathode materials for large-scale, room temperature SIB.

Metal-organic frameworks (MOFs) have also been unveiled as remarkable structures for charge storage because of their microporous and extensive 3D open channels.<sup>[253,254]</sup> Prussian blue analogs (PBAs), with a general chemical formula  $\text{Na}_{2-x}\text{M}_a[\text{M}_b(\text{CN})_6]_{1-y} \cdot z\text{H}_2\text{O}$ , where  $\text{M}_a$  and  $\text{M}_b$  usually represent Mn, Fe, Co, Ni, Cu, and Zn, constitute one class of sodium-based MOFs.<sup>[255–258]</sup> Due to their large interstitial spaces, PBAs generally contain zeolitic water molecules, which are extremely difficult to remove from their lattices. PBAs however exploit these open sites, to achieve fast charge storage, as seen previously in the NASICON materials, and further rely on their rigid frameworks, to resist structural phase transitions during cycling. Sodium-based PBAs have justifiably received prime attention due to their high theoretical capacity of close to  $170 \text{ mAh g}^{-1}$  (corresponding to two Na ions per formula unit), high rate capability, and extended cycle life. Other endearing features include inexpensive material compositions, low-tem-

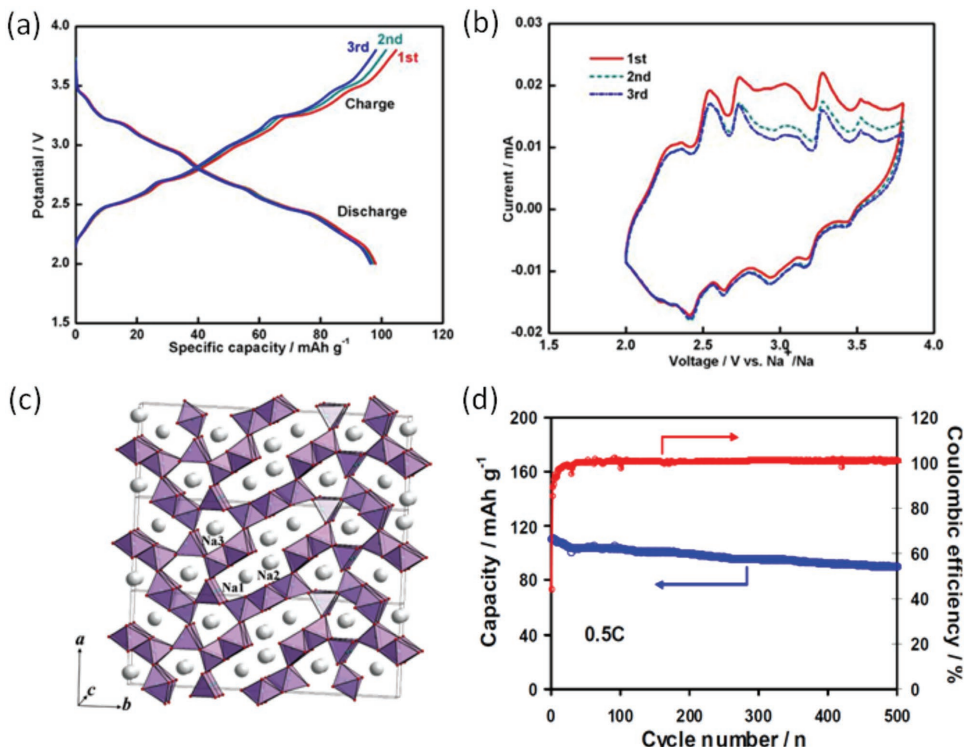


**Figure 25.** Structure and electrochemical properties of  $\text{Na}_{0.44}\text{MnO}_2$  nanowires. a) Voltage profiles during discharge. b) Cyclic voltammetry curves at a scan rate of  $0.1 \text{ mV s}^{-1}$ , showing multiple phase transitions during sodium (dis)charging. c) Illustrative structure of  $\text{Na}_{0.44}\text{MnO}_2$ , perpendicular to the  $ab$  plane, clearly shows the large tunnels that accommodate sodium storage. d) Cycling performance and Coulombic efficiency. a,b,d) Reproduced with permission.<sup>[252]</sup> Copyright 2015, The Electrochemical Society. c) Reproduced with permission.<sup>[245]</sup> Copyright 2007, American Chemical Society.

perature facile synthesis procedures, and a general innocuous nature, which appropriate them for large-scale EES.<sup>[259]</sup>

The original Prussian blue  $\text{KFe}^{\text{II}}\text{Fe}^{\text{III}}(\text{CN})_6$  is a hexacyanide with a cubic crystal structure (see Figure 25a). Isostructural compounds of the Prussian blue family were initially synthesized by replacing  $\text{Fe}^{\text{II}}$  with a transition metal. Wessels et al.<sup>[258]</sup> thus successfully synthesized  $\text{KCuFe}^{\text{III}}(\text{CN})_6$  and reported reversible electrochemical sodium insertion in aqueous electrolytes. Good-enough and co-workers<sup>[260]</sup> inspired by these preceding investigations, and in order to increase the working potential, used aprotic organic electrolytes instead. High-voltage sodium insertion in  $\text{Na}_{2-x}\text{MFe}^{\text{III}}(\text{CN})_6$ , where  $\text{M} = \text{Mn, Fe, Co, Ni, Cu, or Zn}$ , was thus made possible and these results obtained are shown in Figure 25b–g. It can be appreciated that while attractively flat voltage profiles, with an average electrode potential of  $3.3 \text{ V}$  versus  $\text{Na}^+/\text{Na}$  and negligible overpotentials, were obtained in each case, a suitable reversible capacity, close to  $100 \text{ mAh g}^{-1}$ , was only obtained in  $\text{Na}_{2-x}\text{Fe}^{\text{II}}\text{Fe}^{\text{III}}(\text{CN})_6$ . Moreover, an impractical Coulombic efficiency, between  $60$  and  $80\%$ , was recorded in the first  $30$  cycles, a phenomena attributed to zeolitic water decomposition at high potentials, in the as-prepared PBA.

The poor Coulombic efficiency was later revealed to be related to lattice defects and phase transitions in the as-prepared samples.<sup>[256,261]</sup> Sodium insertion in high-quality single crystals of the so-called Berlin green nanoparticles  $\text{FeFe}(\text{CN})_6 \cdot 4\text{H}_2\text{O}$ , without detectable K content, was investigated by Wu et al.<sup>[262]</sup> An enhanced electrode capacity of  $120 \text{ mAh g}^{-1}$  with outstanding Coulombic efficiency and rate capability was

therein reported and thus underlined the importance of phase purity. The lack of sodium content, however, in the as-prepared samples incapacitated the use of this material in full-cell SIBs.

Vacuum-dried and sodium-rich, rhombohedral sodium iron hexacyanoferrate  $\text{Na}_{1.92}\text{FeFe}(\text{CN})_6 \cdot 0.08\text{H}_2\text{O}$ , with negligible water content and remarkable air stability, was then prepared by Wang et al.<sup>[255]</sup> Two high voltage plateaus at  $3.3$  and  $3.0 \text{ V}$  (vs  $\text{Na}^+/\text{Na}$ ) and a high gravimetric capacity of  $160 \text{ mAh g}^{-1}$  were therein reported. Furthermore, an impressive rate capability of up to  $15 \text{ C-rate}$ , a nearly perfect Coulombic efficiency, and remarkable capacity retention of  $\approx 80\%$  after  $1000$  cycles were attained. These phenomenal properties encouraged the fabrication of an SIB full cell using HC anodes, which resulted in a  $3 \text{ V}$  cell with a reversible capacity of  $120 \text{ mAh g}^{-1}$  (based on the mass of active material in the cathode). Due to their low cost, Fe-based PBA are indeed highly promising cathode materials for SIBs. Even though nanosizing and carbon coatings would further enhance their rate capability, full cells fabricated with HC anodes and composite electrodes reveal that rate limitations at the anode are more critical.

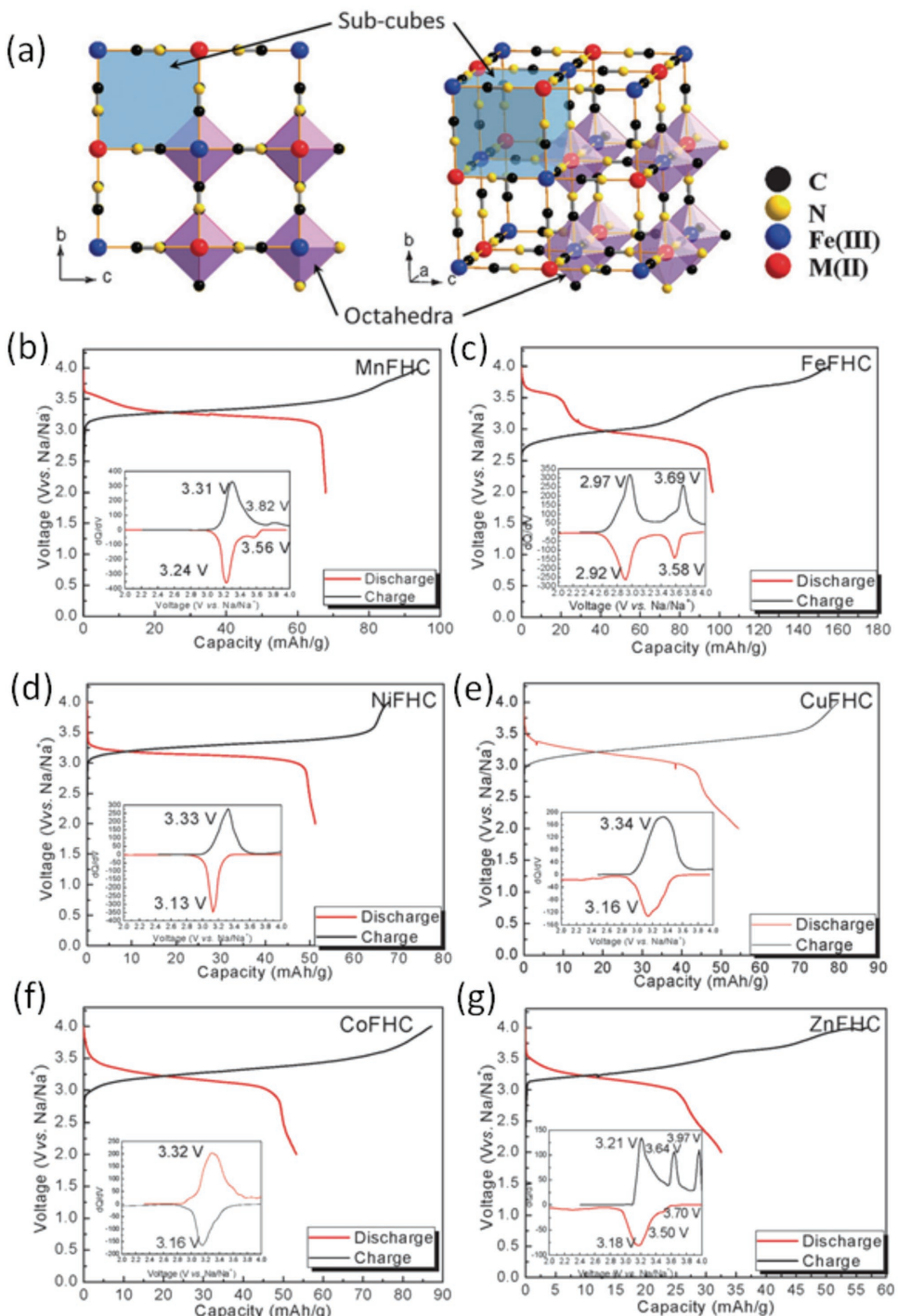
#### 4.9. Comparison of Cathode Materials

The different cathode materials in SIBs are compared in this section, first focusing on the various electrode potentials in relation to the storage capacity and their structures (Section 4.9.1) and then concentrating on their cycleability (Section 4.9.2) using data derived from the referenced papers.

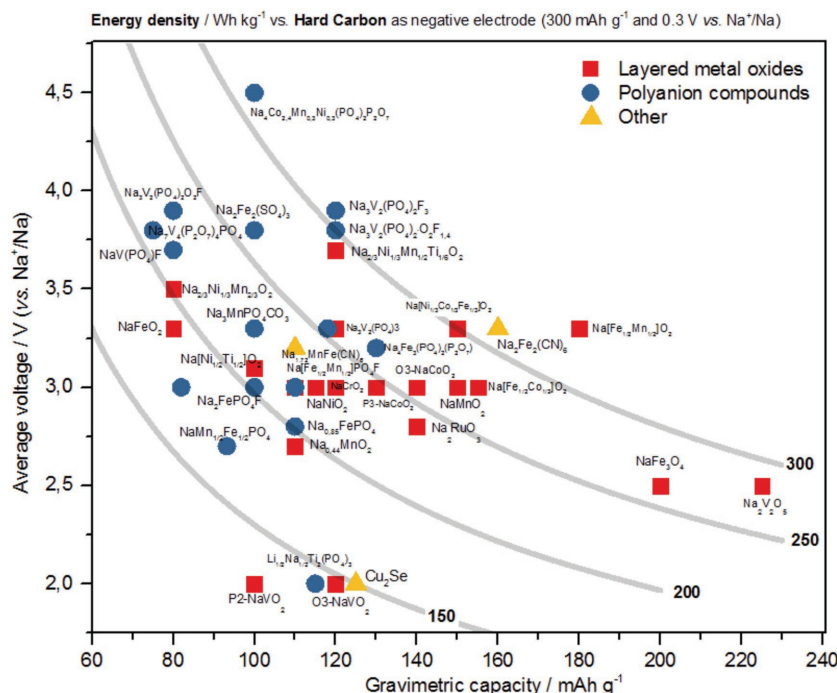
#### 4.9.1. Comparing the Average Voltage and Gravimetric Capacity of Cathode Materials

Figure 26 illustrates the average voltage and specific capacity of the different positive electrodes. Layered metal oxides (red squares), polyanionic compounds (blue circles), as well as other

insertion structures (yellow triangles) such as Prussian blue compounds are here compared. The contour lines are used to represent theoretically calculated energy densities of SIBs fabricated with such cathodes, calculated per kilogram of both the anode and cathode and assuming an HC anode. As discussed in Section 4.1.1, HC has one of the lowest potentials available for the anode.



**Figure 26.** Properties of Prussian blue analogs. a) Prussian blue analog crystal framework. b–g) Third cycle voltage (dis)charge curves at 0.05 C-rate of KMFe(CN)<sub>6</sub> (MFHC) and Prussian blue analogs in SIB half-cells. The insets show the redox activity from cyclic voltammograms. a–g) Reproduced with permission.<sup>[260]</sup> Copyright 2012, The Royal Society of Chemistry.



**Figure 27.** Average cathode voltage during discharge versus the storage capacity of the various cathode materials. Layered metal oxides (red squares), polyanionic compounds (blue circles), as well as other insertion structures (yellow triangles) are shown. The four contour lines (150, 200, 250, and 300 Wh kg<sup>-1</sup>) represent the energy density calculations of SIB fabricated with such cathodes, calculated per kilogram of both the anode and the cathode, and assuming a hard carbon anode. Calculations based on data presented in refs. [3,16,17,21,62,141,143–145,150,155,157,158,161,162,168,174,181,182,187–189,198,204,207,213,225–227,229,230,238,239,241,242,248,263–277].

From Figure 27 it can be seen that the polyanionic compounds can attain a desirably high electrode potential while the electrode potential of the layered metal oxides is mostly moderate, in the range of 2.5 and 3.5 V. Higher gravimetric capacities are however observed in layered oxides because the presence of heavy polyanionic species,  $(XO_4)^3-$ , reduces the energy density of polyanionic compounds. In general, the achievable energy densities among the different cathode materials are encouraging, using an  $\text{LiMn}_2\text{O}_4$ -based LIB as a benchmark whose energy density is  $\approx 300 \text{ Wh kg}^{-1}$ . Several cathode materials are found beyond the  $300 \text{ Wh kg}^{-1}$  contour line range and can thus compete with LIBs.

Another observation is the importance of mastering the chemistry and redox potentials of cobalt, manganese, and vanadium to achieve high energy density storage in SIBs. However, the practical challenges with regard to Mn and Co couples and the toxic nature of vanadium have been discussed in the preceding sections. On the other hand, the properties of the economically attractive Fe-based materials are unappealing as such cathodes rarely attain electrode potentials above 3 V.

#### 4.9.2. Cycle Life Performance of Cathode Materials

Figure 28 illustrates the relative cycleability of the different cathode materials that are reported for SIBs. The red squares represent the layered oxides, the blue circles represent polyanionic

compounds, while the yellow triangles represent other insertion materials. The cumulative capacity values of 1, 5, 20, and 100 Ah g<sup>-1</sup> are here used to compare the different electrode materials which takes into account the gravimetric storage capacity of the material and the reported number of cycles. Compared to the layered oxides, polyanionic compounds are able to achieve higher cycle numbers due to their structural stability. Since metallic Na is used as the anode in these experiments, the resulting cell voltage makes it difficult to overlook the role of the electrolyte and additives used. One thus must bear in mind the influence of the experimental conditions in order to make a conclusive conclusion on the cycleability of a given cathode material.

Nevertheless, some outstanding performers can be identified, based on data shown in Figures 26 and 28. In particular, the polyanion  $\text{Na}_3\text{V}_2(\text{PO}_4)_2\text{F}_3$ , the layered oxide  $\text{Na}_2\text{V}_2\text{O}_5$ , and the Prussian blue  $\text{Na}_2\text{Fe}_2(\text{CN})_6$  electrodes show a good combination of high energy density and good cycle life. These features together with inexpensive material combinations and remarkable rate capability make them prime candidates for large-scale EES applications at room temperature. Because of the number of available interesting materials, compared to the anode materials, the outlook on SIB cathode materials is therefore more promising.

## 5. Electrolytes for Sodium-Ion Batteries

Most electrolytes are liquids at room temperature that consist of electrolytic solutions of salts dissolved in solvents. If the solvent contains labile H<sup>+</sup> (e.g., water or ethanol) it is called a “protic” solvent, conversely the term “aprotic” solvent is used. Although usually conceived as a passive component, the electrolyte constitutes an integral part of any given electrochemical device. Beside the bulk properties of the electrolyte (see the general requirements of an electrolyte below), interfaces formed between the electrolyte and the two electrodes are often decisive to the overall performance of the battery. Therefore, understanding the chemical nature of electrolytes as well as the structure and properties of the electrolyte/electrode interphase is a vital step in the development of SIBs and indeed constitutes the bedrock of modern electrochemistry.<sup>[278]</sup>

In contrast to the LiPF<sub>6</sub> salt dissolved in organic carbonate solvents, which nowadays is the standard electrolyte used in LIB, a generally acceptable electrolyte composition is yet to be identified for SIBs.<sup>[279,280]</sup> This challenge however presents a great opportunity for research because energy density, cycling ability, reversible storage capacity, safety, and rate capability of future SIB greatly depend on the electrolyte. Fortunately, several DFT and experimental optimization approaches have been applied to determine the appropriate aprotic electrolyte composition in SIBs and have become a cornerstone to the current state-of-the-art.<sup>[281–283]</sup>

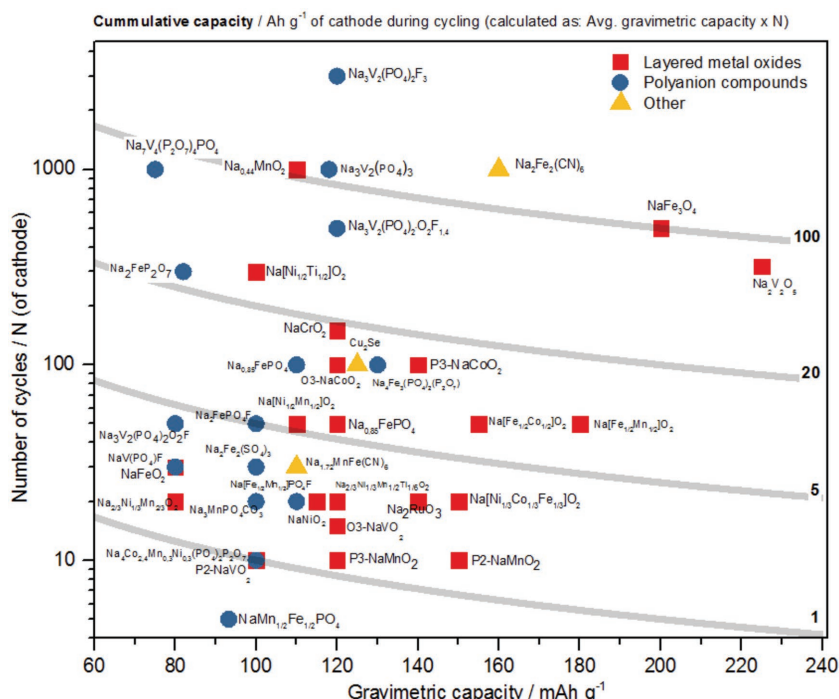


**Figure 28.** Number of cycles reported for SIB versus the storage capacity of the various cathode materials. Layered metal oxides (red squares), polyanionic compounds (blue circles), as well as other insertion structures (yellow triangles) are shown. Cumulative capacity values of 1, 5, 20, and 100 Ah g<sup>-1</sup> are represented by the four contour lines, calculated as the product of the average capacity and number of cycles. Data derived from refs. [3,16,17,21,62,141,143–145,150,155,157,158,161,162,168,174,181,182,187–189,198,204,207,213,225–227,229,230,238,239,241,242,248,263–277].

### **5.1. General Requirements for Electrolytes and Solvents**

In general, an appropriate electrolyte/solvent should satisfy the following criteria:<sup>[284]</sup> a) electrochemical stability, ensuring that it does not react at the surfaces of either electrodes within the operating voltage window. b) Wide operating temperature that allows the solvent to remain in the liquid state at the desired operating temperature range. As will be seen later, nonliquid electrolytes exist, however there are more advantages with using liquid electrolytes. c) A low viscosity that promotes ionic conductivity. d) A high dielectric permittivity to allow the solvent to dissolve a high concentration of solutes. e) The solvent should finally be nontoxic and available at low cost.

Evidently, it is difficult, if not impossible, for a single solvent to satisfy all the above requirements. In the following sections, these features are explored in more detail.

### *5.1.1. Electrochemical and Chemical Stability*

The electrochemical stability of an electrolyte is quantified by the voltage range between the oxidation and reduction reaction limits. This voltage range is referred to as the electrochemical stability window (ESW). Thermodynamically, the ESW corresponds to the energy separation between the lowest unoccupied molecular orbital and the highest occupied molecular orbital of the electrolyte.<sup>[279]</sup> For a stable battery operation, to avoid side

reactions, it is important that the working potentials of both electrode materials fall within this electrochemical window or for the electrolyte to have a wide ESW.

Electrochemical stability is often challenged by the strong oxidizing and reducing power of the cathode and the anode materials used. High-voltage cathodes and low-voltage anodes are constantly being pursued for higher energy density cells. As a result, most of the electrolytes used for SIBs and LIBs are metastable due to formation of passivation layers (SEI at the anode and surface layers (SLs) at the cathode).

On the other hand, the requirement of chemically stability ensures that no chemical reactions occur between the electrolyte and all other cell components such as separators, charged electrode materials, current collectors, and cell packaging materials.

### 5.1.2. Wide Operating Temperature Range

An ideal electrolyte should remain liquid within a wide operating temperature range, this is due to the performance advantages of using liquid electrolytes in batteries. To achieve a high liquid range, the melting point should be considerably lower and the boiling point should be higher than the operation temperature. Furthermore, for safety consid-

erations, a low vapor pressure and a high flash point temperature are desirable to ensure it does not ignite easily. Current organic electrolytes employed in LIBs and SIBs generally have a wide liquid range. However, these electrolytes are also associated with high vapor pressures and are flammable at elevated temperatures (such as would be caused by thermal runaways). On the other hand, ionic liquids, polymers, and gel electrolytes have a low flammability risks although their liquid range is less desirable.

### 5.1.3. Low Viscosity

When solvated ions are transported in an electrolyte, drag forces exerted by surrounding solvent molecules are quantified by the dynamic viscosity. Based on the Stokes–Einstein equation, ionic mobility is inversely proportional to the solvent viscosity, low viscosity therefore facilitates good ionic mobility through the bulk of the electrolyte.<sup>[285]</sup> This also ensures a low Ohmic resistance in the cell. In practice, the ionic conductivity should be at least higher than  $1 \text{ mS cm}^{-1}$  at the operating temperature.<sup>[279]</sup>

Good ionic conductivity ensures that charged species in the electrolyte are responsive to an electric field, the effective charge transfer between the anodic and cathodic electrodes however depends on the mobility of the particular ion of interest, in this case  $\text{Na}^+$ . The fraction of the current due to  $\text{Na}^+$  mobility from

the total current is referred to as the transference number ( $t_{\text{Na}}$ ). The transference number ( $t_i$ ) of a given ion  $i$  is defined as

$$t_i = \frac{|z_i| c_i u_i}{\sum_i^n |z_i| c_i u_i}; 0 \leq t_i \leq 1 \quad (7)$$

where  $z_i$  is the valence state of the ion  $i$ ,  $c_i$  is the molar concentration, and  $u_i$  is the mobility of the ion  $i$  of interest in a total of  $n$  ionic species (cations and anions).  $t_{\text{Na}}$  therefore also depends on the mobility of the other ionic species present in the electrolyte. A common approach in analytical electrochemistry is to add an electrolyte support (an electrochemically inert ion that has a high transference number) so that the transport mechanism for the ion of interest is “effectively” purely diffusive. In a battery, however, it is desirable to have fast ion transport and to reduce concentration polarizations that result from a low transference number for the ion of interest. To achieve this, the electrolyte must therefore favor the transference of the cation. A modeling study of the effect of adding Li-based supporting salts to electrolytes was performed by Danilov and Notten.<sup>[286]</sup>

Unfortunately, because of the formation of a stable solvation shell around the cation, the transference numbers for  $\text{Na}^+$  and  $\text{Li}^+$  are rarely above 0.4, this means organic solvents favor the conductivity of the anions.<sup>[287–291]</sup> Compared to analogous  $\text{Li}^+$  solvent complexes,  $\text{Na}^+$  solvent complexes have a lower binding energy, up to 15–20% less, due to the weaker Lewis acidity.<sup>[292]</sup> Therefore, sodium-based salts should in general have higher conductivity than analogous lithium-based salts. Higher transference numbers, i.e.,  $t_{\text{Na}} = 1$ , are possible if anions are tethered to the polymer matrix, as in the case of ion selective polymer electrolytes.

Another advantage of low viscosity is wettability of the solvent which is often measured by the contact angle made by the solvent on the cell components. Wettability is essential to ensure good contact between the solid phases and the liquid phases in order to facilitate ionic transport across the interphases. For the above reasons, solvents with low viscosity are always considered ideal candidates for electrolytes.

It is also worth highlighting that while the electrolyte must allow high ionic conductivity, when an electric field is applied, it should at the same time be an electrical insulator. Electronic conductivity is detrimental to its proper function and results in short-circuiting and self-discharge in the cell. In general, the separation between the electrodes is large enough to avoid electrical conduction. Although electrical conductivity across the cell in liquid electrolytes is not a major concern, electrical conductivity at the surface layers formed (SEI or SL) results in poor Coulombic efficiencies, electrolyte degradation, and unstable SEI layers.

#### 5.1.4. High Dielectric Permittivity

The dielectric permittivity is a parameter which indicates the effectiveness of the solvent in screening dissolved ionic species. In order to effectively dissolve a salt, the formation of close ion pairings must be prevented. The dielectric permittivity therefore characterizes the effectiveness of the solvent molecules to

separate anion–cation pairings. A high dielectric permittivity in a solvent thus ensures that ion pairings have a low probability of occurring at a given salt concentration and temperature. Comparing sodium-ion and lithium-ion salts, DFT calculations reveal that ion–ion pairings are reduced by ≈80% with  $\text{Na}^+$  as the cation.<sup>[281]</sup> This means the problem of salt solubility is less severe in SIBs than in LIBs and this will open the door for more salt options in SIBs.

No single practical solvent available to date simultaneously possesses a high dielectric permittivity and a low dynamic viscosity.<sup>[280]</sup> The successful strategy that has been employed is to form binary ternary and quaternary mixtures of different solvents in an effort to obtain optimized electrolytes. By mixing a solvent with high dielectric permittivity, usually ethylene carbonate (EC) and another solvent with low viscosity, such as dimethyl carbonate (DMC), suitable formulations have thus been discovered.<sup>[284,293]</sup>

#### 5.1.5. Low Cost and Environmental Friendliness

Finally, the components of the electrolyte need to be environmentally friendly to ensure sustainability. Cost factors have also been decisive in asserting LIB standard electrolytes since the supply chains are well established. This presents an economic challenge to newly emerging battery chemistries, should these electrolytes fail to meet performance standards.

Several liquid, gel, and solid-state electrolytes have been investigated for use in LIBs and recently also in SIBs. The following sections review some of the common electrolytes currently available and their properties for SIB applications.

### 5.2. Organic Liquid-Based Electrolytes

Due to high cathode potentials and the low anode potentials used in LIBs and SIBs, only aprotic polar solvents merit consideration due to their larger ESW. Organic liquid-based liquids have thus emerged as primary solvents. In order to dissolve appreciable amounts of either sodium or lithium salts, carbonyl-, nitrile-, sulfonyl-, and ether-based polar groups have been found to have a large enough permittivity.<sup>[284]</sup>

#### 5.2.1. Propylene Carbonate (PC)-Based Electrolytes

Alkyl carbonate, propylene carbonate, is an attractive electrolyte for battery operation due to its low cost, high dielectric permittivity, and large ESW. Early interest in PC for use in lithium cells arose from its high dielectric constant. However, several problems at the anode soon emerged as PC reacted with freshly deposited Li in PC-based LIBs. The formation of graphite intercalation compounds, via the solvent cointercalation phenomena, is believed to be the cause of the poor cycling.<sup>[294,295]</sup> HC electrodes used in SIBs have also been tested with PC and a similar observation of poor cycling stability has been reported.<sup>[283]</sup> PC, however, remains popular in current electrolyte formulations, statistics show that it forms the base of around 60% of the current SIB electrolytes.<sup>[279]</sup> While its low

cost has undoubtedly been a major driving force, optimized electrolyte properties have also been obtained by mixing PC with other solvents.

### 5.2.2. Ethylene Carbonate-Based Electrolytes

Ethylene carbonate is another successful alkyl carbonate electrolyte for SIBs. Among most common solvents, EC has a low viscosity and a high dielectric permittivity of about 90 (at 40 °C), for comparison, that of water is 79. Despite these remarkable properties, EC is a solid at room temperature and has a relatively high melting point of 36.4 °C, while that of PC is as low as -48.8 °C.

In the late 1970s, it was however discovered that the presence of solutes and a small amount of PC could lower the melting point of EC while maintaining its favorable physical properties.<sup>[296]</sup> An important characteristic of EC is the formation of a highly protective SEI layer at the anode. Half-cell LIB anodes, based on graphite and petroleum coke, were tested in an EC:PC (1:1) electrolyte.<sup>[297]</sup> Stable passivating films were therein formed after the first (dis)charge cycles and this discovery cemented the position of both EC and PC in LIB formulations.

**Figure 29c** illustrates cycling studies performed on Na/Hard Carbon half-cell using either PC alone or EC:PC mixed electrolyte.<sup>[58,283]</sup> The EC:PC mixture emerges as the best solvent formulation regardless of the salt used, i.e., NaClO<sub>4</sub> or NaPF<sub>6</sub>.<sup>[283]</sup> Similar observations in separate studies corroborate these findings.<sup>[225]</sup> The resulting SEI is shown to be more ionically conductive, as indicated by facile charge transfer across the interface layers. This engenders low polarizations and eventually permits the use of the full capacity of HC anodes at the low potentials, as the risks of metallic plating are abridged. The EC:PC mixture is accordingly the most efficient electrolyte for the development of SIBs at the current state-of-the-art.

### 5.2.3. Ether-Based Electrolytes

Following the initial shortcomings of PC, focus soon turned to ethers as alternative electrolytes. The most attractive characteristic of ethers is their low viscosity, which allows for high ionic conductivity. Tetrahydrofuran (THF),<sup>[298]</sup> polymethoxy ether,<sup>[299]</sup> dimethoxy propane,<sup>[300]</sup> diethyl ether,<sup>[301]</sup> diethoxyethane,<sup>[302]</sup> and dimethoxyethane (DME)<sup>[303]</sup> were indeed some of the ether-based solvents tested as electrolytes for LIBs. Despite showing remarkable stability at the anode, ethers however decompose at relatively lower potentials at the cathode, compared to alkyl carbonates. Although THF has been tested in SIB anodes and showed outstanding compatibility with HC electrodes and reduced capacity loss during cycling (see **Figure 30**),<sup>[304]</sup> the aforementioned problems at the cathode limit its practical ESW and eventual use in full cells.

### 5.2.4. Linear Carbonate-Based Electrolytes

Linear carbonates were late entries in the electrolyte family of LIBs. In the mid-1990s dimethyl carbonate became the first successful linear carbonate to be reported in a binary mixture

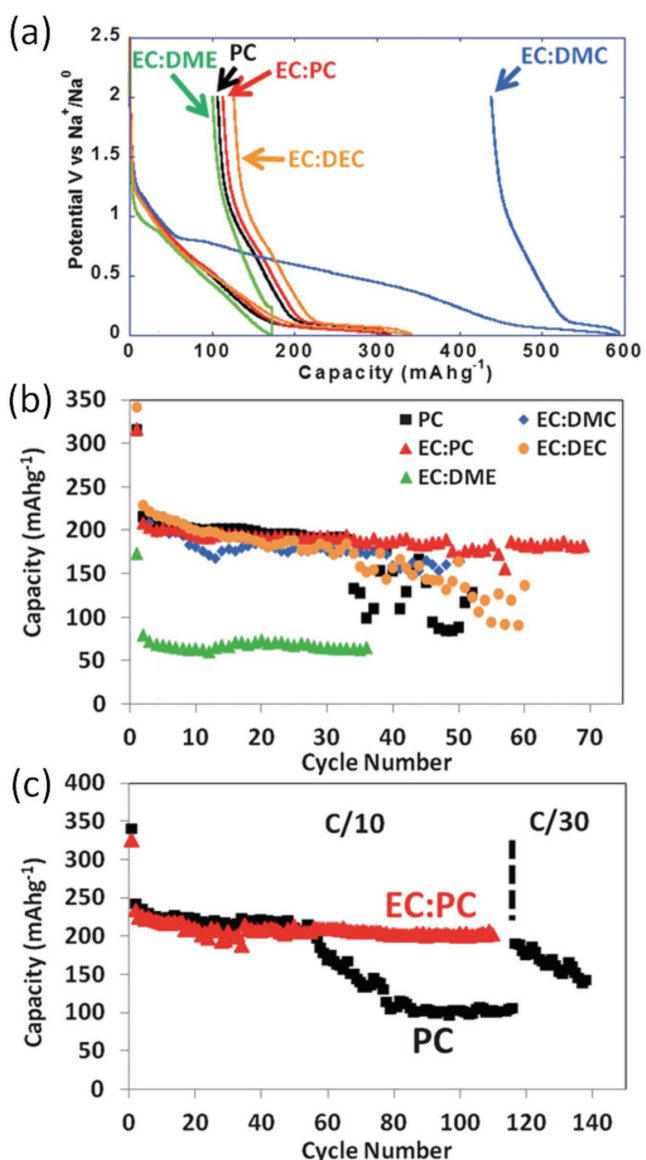


**Figure 29.** a) First cycle voltage versus capacity profiles for hard carbon electrodes cycled in 1 M NaClO<sub>4</sub> in various solvent mixtures recorded at 0.05 C-rate and b) discharge capacity versus cycle number for the corresponding cells. c) Discharge capacity versus cycle number for tape-cast hard carbon electrodes cycled in 1 M NaClO<sub>4</sub> in PC and in EC:PC at a 0.1 C-rate up to 110 cycles and further at 0.033 C-rate. a-c) Reproduced with permission.<sup>[283]</sup> Copyright 2012, The Royal Society of Chemistry.

with EC, as the search for stable electrolytes at high cathode potentials (5 V vs Li<sup>+</sup>/Li) intensified.<sup>[305,306]</sup> Although linear carbonates generally have a desirably low viscosity, which enables good ionic conductivity, their dielectric permittivity is unfortunately low and their safe application as electrolytes is disadvantaged by a low boiling point and low flash point temperatures. As an example, the boiling point and the flash point temperatures for DMC are 91 and 18 °C, respectively.<sup>[284]</sup>

Nevertheless, a trendsetting, serendipitous discovery of mixed formulations involving DMC and EC (a cyclic carbonate), with an attractively wider ESW soon became a standard in LIBs. Other linear carbonates such as diethyl carbonate DEC,<sup>[307]</sup>

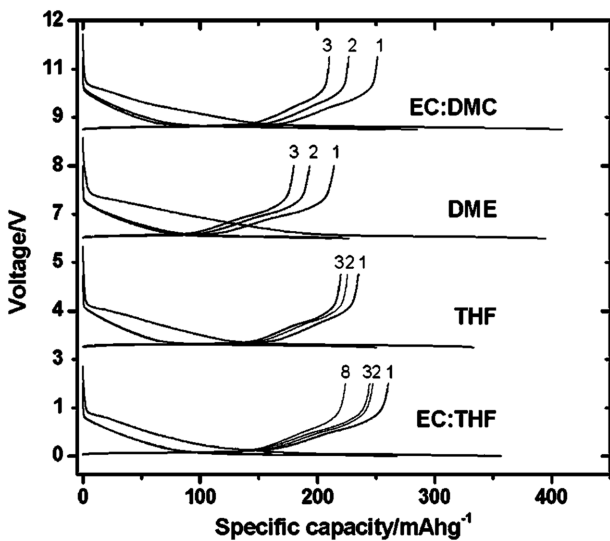


**Figure 30.** Voltage/capacity plots, corresponding to the first discharge/charge cycles of carbon aerogel microspheres in SIB, using 1 M  $\text{NaClO}_4$  dissolved in EC:DMC, DME, THF, and EC:THF as electrolytes. Reproduced with permission.<sup>[304]</sup> Copyright 2005, The Electrochemical Society.

ethylmethyl carbonate (EMC),<sup>[308]</sup> and propylmethyl carbonate<sup>[309]</sup> later emerged, in likewise formulations involving EC. However, compared to EC:DMC mixtures, no significant improvements were obtained.<sup>[284]</sup>

Not surprising, similar formulations have been investigated in SIBs. 1:1 mixtures of EC:DEC, EC:EMC, and EC:DMC electrolytes containing 1 M  $\text{NaClO}_4$  salt were galvanostatically tested in Na/HC half-cells and compared to PC electrolytes.<sup>[283,310]</sup> It soon became apparent that only the EC:DEC formulation had a comparative cycling performance to pure PC electrolyte, reaching 100 reversible cycles while the other formulations were found not to be compatible with metallic sodium. Figure 29a,b illustrates systematic studies to compare the performance of the above-mentioned electrolytes for SIB applications, further cycling tests are also shown in **Figure 31**. The wider ESW of the EC:DEC mixture here enables stable cycling in SIB full cells, thus making it a functional alternative electrolyte.

### 5.3. Ionic Liquid (IL)-Based Electrolytes

Ionic liquids are simply defined as salts in the liquid state. The term has however evolved and is commonly used in reference to room temperature ionic liquids (RTIL), whose melting point or glass transition temperature is arbitrarily set below 100 °C.<sup>[311]</sup> This liquidus temperature demarcation is justified by the myriad possibilities to replace organic liquid applications at low to medium temperatures. Although IL have been known as far back as 1914,<sup>[311–313]</sup> their interest as electrolytes for electrochemical applications, ranging from electrochemical double layer capacitors<sup>[314–317]</sup> to rechargeable batteries,<sup>[318–322]</sup> is a recent phenomenon. IL are excellent solvents and show good thermal, chemical, and electrochemical stability as electrolytes. Perhaps the most intriguing intrinsic property of IL is

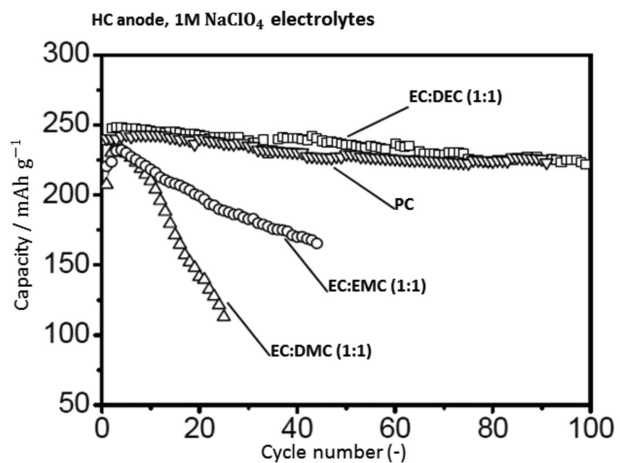


**Figure 31.** EC:EMC and EC:DMC electrolytes containing 1 M  $\text{NaClO}_4$  were galvanostatically tested in Na/HC half-cells and compared to PC electrolytes. Adapted with permission.<sup>[310]</sup> Copyright 2010, The Electrochemical Society.

their ability to have negligible or no detectable vapor pressure and thus earn the reputation of safe, nonflammable electrolytes.<sup>[321]</sup>

Initial IL developed for battery electrolytes focused on aromatic organic cations such as alkyl-substituted imidazolium- and pyrrolidinium-based cations,<sup>[324,325]</sup> instead of lithium cations that are too small and would eventually result in highly viscous and high melting point compounds. IL are therefore composed of large organic cations that form weakly coordinating ligands with inorganic anions. The choice in cation/anion combination inter alia determines the ESW. In relation to battery applications, contemporary RTIL generally contain a cation/anion combination of the following three cations: 1-butyl-3-methylimidazolium (BMIM), bis(trifluoromethanesulfonylimide) (EMIM), and *N,N*-propylmethylpyrrolidinium (P13), and three anions:  $\text{PF}_6^-$ ,  $\text{BF}_4^-$ , and bis(trifluoromethylsulfonyl) imide (TFSI).<sup>[318,323]</sup> **Figure 32** illustrates how the ESW varies with different anion/cation combinations in IL. Here DFT calculations show that BMIM-based IL have narrower ESW and are problematic at low electrode potentials.

Analogous to developments in LIB, IL have been successfully used in SIBs as a new solvent concept. Hagiwara and co-workers<sup>[168,326–329]</sup> investigated ionic liquids based on bis(trifluoromethylsulfonyl)amide and bis(fluorosulfonyl)amide (FSA) anions and reported suitable electrochemical properties such as wide ESW in the range of 5–6 V and good thermal stability although the melting point such ionic liquids was in the intermediate range.

Using an Na/NaFSA – KFSA/NaCrO<sub>2</sub> half-cell at an intermediate temperature range of 90 °C, Chen et al.<sup>[168]</sup> investigated the electrochemical performance of NaCrO<sub>2</sub> in IL and benchmarked the materials properties with respect to previous investigations involving organic electrolytes. Therein, a reversible capacity of 113 mAh g<sup>-1</sup> was obtained which is lower than that obtained in PC solutions.<sup>[141]</sup> Yet, the cycleability was significantly enhanced in IL, reaching 100 cycles with close to 98% initial capacity retention. In addition, a superior rate capability of ≈17 C-rate was also evidenced. **Figure 33a,b** illustrates the

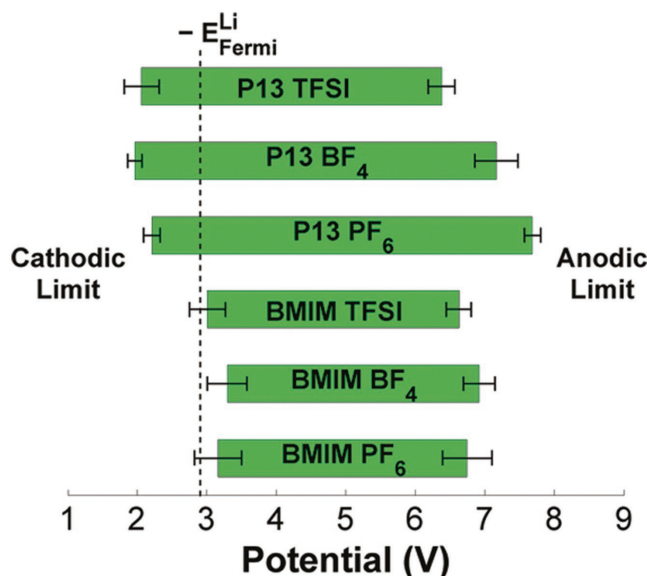


**Figure 32.** The effect of various anion/cation combinations on the electrochemical stability window. The stability windows for ionic liquids are obtained from molecular dynamics and DFT calculations. DFT calculations show a 95% confidence interval. The calculated lithium metal Fermi level ( $-E_{\text{Fermi}}^{\text{Li}}$ ) is also indicated. The potentials are shown relative to the vacuum level. Reproduced with permission.<sup>[323]</sup> Copyright 2011, American Chemical Society.

voltage profiles and cycleability results obtained. Although the rate capability could be an artifact of the elevated temperature, the cycle life improvement can only be attributed to the change to IL electrolytes, which clearly outperform organic liquid systems.<sup>[141,168,169]</sup> Nevertheless, the high melting point of NaFSA-KFSA at 57 °C falls outside the desired practical temperature range of batteries.

The encouraging electrode performance of NaCrO<sub>2</sub> stimulated further investigation in full SIBs. Indeed, Fukunaga et al.<sup>[330]</sup> prepared a 27 Ah, 2.5 V prismatic cell (average cell voltage in the 1.5–3.35 V range) using HC as anode. The NaFSA-KFSA ionic liquid was replaced by the NaFSA-C<sub>3</sub>C<sub>1</sub>pyrrFSA ionic liquid electrolyte, which has a lower melting point and wide operating temperature range of ≈10–90 °C, based on *N*-methyl-*N*-propylpyrrolidinium (C<sub>3</sub>C<sub>1</sub>pyrr) cations. In spite of these changes, the HC/NaFSA – C<sub>3</sub>C<sub>1</sub>pyrrFSA/NaCrO<sub>2</sub> cell showed practical performance at the intermediate temperature of 90 °C. Impressively, however, the cycle life tests revealed nearly 90% capacity retention over 1000 cycles and the cell registered 99.8% and 97.5% in Coulombic efficiency and energy efficiency, respectively, at 90 °C. Such a cell performance thus demonstrates the feasibility of using cathode materials that were previously deemed unpractical and the efficacy of IL based SIB for large-scale EES.

Another investigation by the same authors focused on the electrochemical performance of the economically viable Na<sub>2</sub>FeP<sub>2</sub>O<sub>7</sub> cathode in an Na/NaFSA – C<sub>3</sub>C<sub>1</sub>pyrrFSA/Na<sub>2</sub>FeP<sub>2</sub>O<sub>7</sub> half-cell.<sup>[271]</sup> Therein, a systematic study on the influence of temperature revealed that the electrode performance increased significantly with rises in temperature in the range of –20 to 90 °C. A nearly theoretical electrode capacity

of 90 mAh g<sup>−1</sup> and a superior rate capability of about 41 C-rate were reached at 90 °C. Moreover, the electrode performance at ambient temperature was also encouraging showing only 11% capacity drop when cycled at 25 °C while an average cell voltage of about 3 V is maintained. Figure 33c,d illustrates the voltage profiles and temperature dependence of this half-cell system. Interestingly, when cycled either at 25, 50, and 90 °C, a stable capacity retention of close to 99% after 300 (dis)charge cycles is therein reported regardless of the temperature.

Despite the encouraging results thus obtained, close scrutiny of IL reveals that they are still far from ideal. The purity of IL is a major issue, in general they can contain up to 600 ppm of H<sub>2</sub>O.<sup>[311,331]</sup> Furthermore, several issues with regard to the anions have been identified, for example, doping with PF<sub>6</sub><sup>−</sup> and BF<sub>4</sub><sup>−</sup> anions increases the melting point while TFSI is known to corrode with Al current collectors.<sup>[332]</sup> Compared to organic liquids, the viscosity of IL is significantly higher, about 2 orders of magnitude higher,<sup>[333]</sup> and the situation is further complicated by the formation of stronger ion pairings and the sheer size of the complexes, e.g., [Na(TFSI)<sub>3</sub>]<sup>2−</sup>, formed upon doping.<sup>[333]</sup> The mobility of Na<sup>+</sup> ions in IL therefore becomes an issue. As a word of caution, often high values of ionic conductivity are reported for IL, well above 1 mS cm<sup>−1</sup> yet, only a small fraction of this is due to the mobility of Na<sup>+</sup> ions; the transference number of Na<sup>+</sup> ions is generally low in IL and this problem is exacerbated by the low salt concentrations.<sup>[334,335]</sup>

Although significant progress has been achieved over the past decade in improving the synthesis methods of RTIL, the most crippling setback remaining is their price due to high manufacturing costs and difficulties in purification. The optimization of formulations may eventually lead to breakthroughs in the large scale applications of RTIL, as future generation electrolytes for fire proof SIBs.

#### 5.4. Solid- and Gel-Type Polymer Electrolytes

Polymer electrolytes can be classified into the two major classes: solid polymer electrolytes (SPE) and gel polymer electrolytes (GPE). SPE, also called dry solid polymer electrolytes, are composed of a polymer matrix wherein coordination between the salt ions and the polymer chains dissolves the salt. Although the polymer chains provide much needed mechanical strength, the ionic conductivity is usually poor. By incorporating a high percentage of conventional liquid electrolytes, functioning as both solvent and plasticizer, the ionic conductivity increases. Such polymer electrolytes are then classified as GPE. The tradeoff however for the increase in conductivity in GPE is the loss of mechanical strength and electrochemical stability.<sup>[336]</sup>

Interest in SPE and GPE is mainly driven by their ability to prevent dendritic growth (and hence permit the possible use of metallic anodes) as well as their inherent safety due to generally nonflammable formulations. The use of SPE and GPE therefore promises to usher a new paradigm in cell design and manufacturing, by permitting the fabrication of thin film batteries and high energy density solid-state batteries.

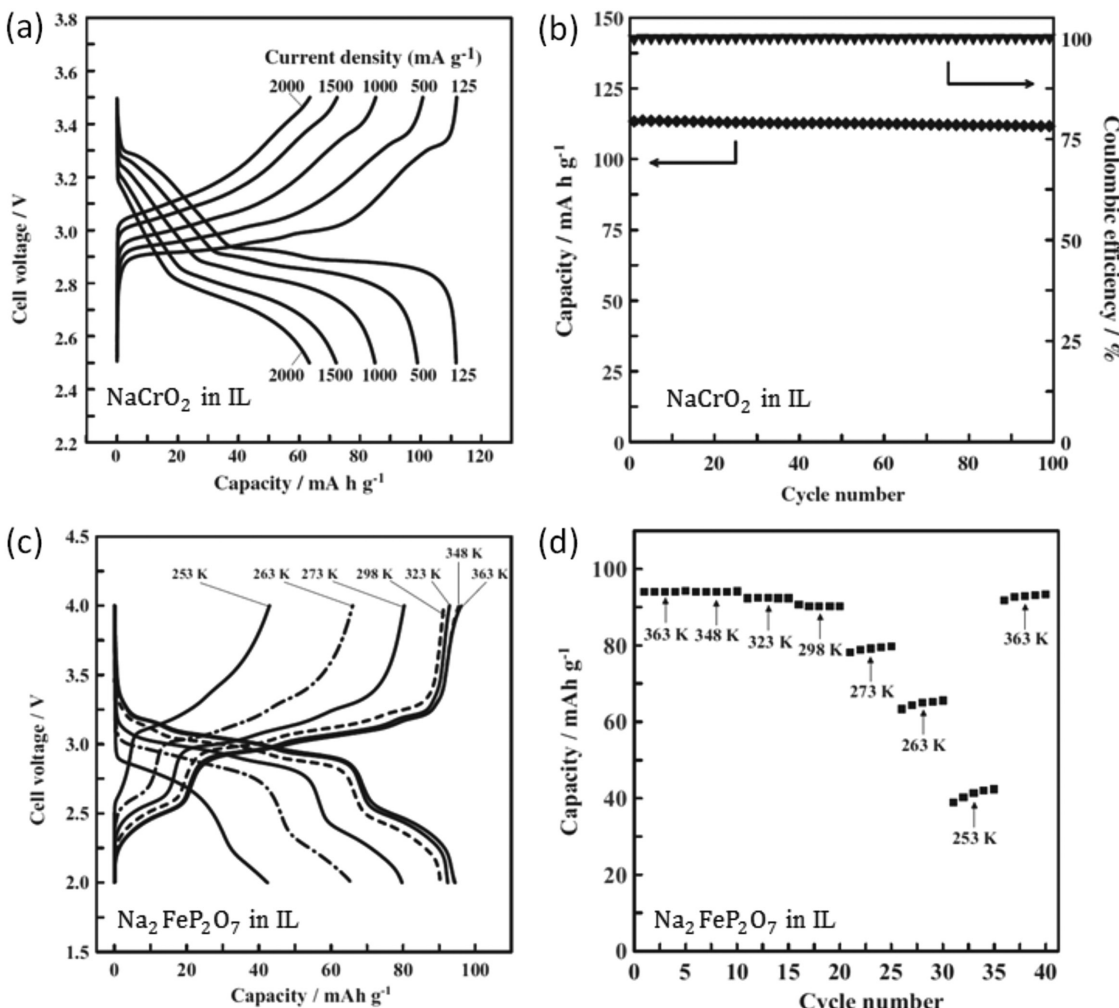


**Figure 33.** Performance of SIB in ionic liquids. a) The voltage profiles at different (dis)charge rates and b) cycling tests of a Na/NaFSA–KFSA/NaCrO<sub>2</sub> half-cell at 90 °C. c) The voltage profiles at different temperatures and d) cycling tests at different temperatures of a Na/NaFSA–C<sub>3</sub>C<sub>6</sub>pyrrFSA/Na<sub>2</sub>FeP<sub>2</sub>O<sub>7</sub> half-cell. a,b) Reproduced with permission.<sup>[168]</sup> Copyright 2013, Elsevier. c,d) Reproduced with permission.<sup>[271]</sup> Copyright 2014, Elsevier.

Traditionally, most of the work performed on SPE focused on poly(ethylene oxide) (PEO). However, an ionic conductivity of 10<sup>-2</sup> to 10<sup>-4</sup> mS cm<sup>-1</sup> in PEO at ambient temperature proved too low for practical usage. Nevertheless, reducing the conduction length with the use of thin film electrolytes appeared to circumvent this shortcoming.<sup>[279]</sup> Recently, discoveries of poly ethylene carbonate (PEC) by Tominaga and Yamazaki<sup>[337]</sup> unveiled SPE with conductivities of the order of 10<sup>-1</sup> mS cm<sup>-1</sup> for LIB. Figure 34 illustrates the remarkable properties of PEC polymer electrolytes with regard to conductivity and glass transition temperature as a function of salt concentration. Additionally, transference numbers were therein estimated to be more than 0.8, at least twice of that reported in liquid electrolytes. SPE therefore hold great promise for practical applications based on such encouraging ion-transport properties.

While not many studies have been devoted to the gel electrolytes for SIB application, SPE based on PEO-NaTFSI have been investigated by Moreno et al.,<sup>[338]</sup> wherein high ionic conductivities on the order of 1 mS cm<sup>-1</sup> at 70 °C were

obtained. A modest of Na<sup>+</sup> transference number, in the range of 0.4–0.5, is however reported and the high temperature needed is particularly discouraging for sodium-metal based rechargeable batteries since sodium has a low melting point of 97.7 °C.

### 5.5. Electrolyte Optimization

As aforementioned, no single “pure” solvent has all the desirable properties of an electrolyte and some solvent mixtures result in favorable synergetic effects for practical electrolytes. The optimization of electrolytes is important and yet not an easy challenge due to the myriad and often antagonistic properties, such as liquid range, ESW, dielectric permittivity, etc., which must be simultaneously ameliorated.

Using differential scanning calorimeter, Ding et al.<sup>[339]</sup> constructed binary phase diagrams of carbonate solvent mixtures, involving EC, PC, DMC, EMC, and DEC. Simple, V-shaped,

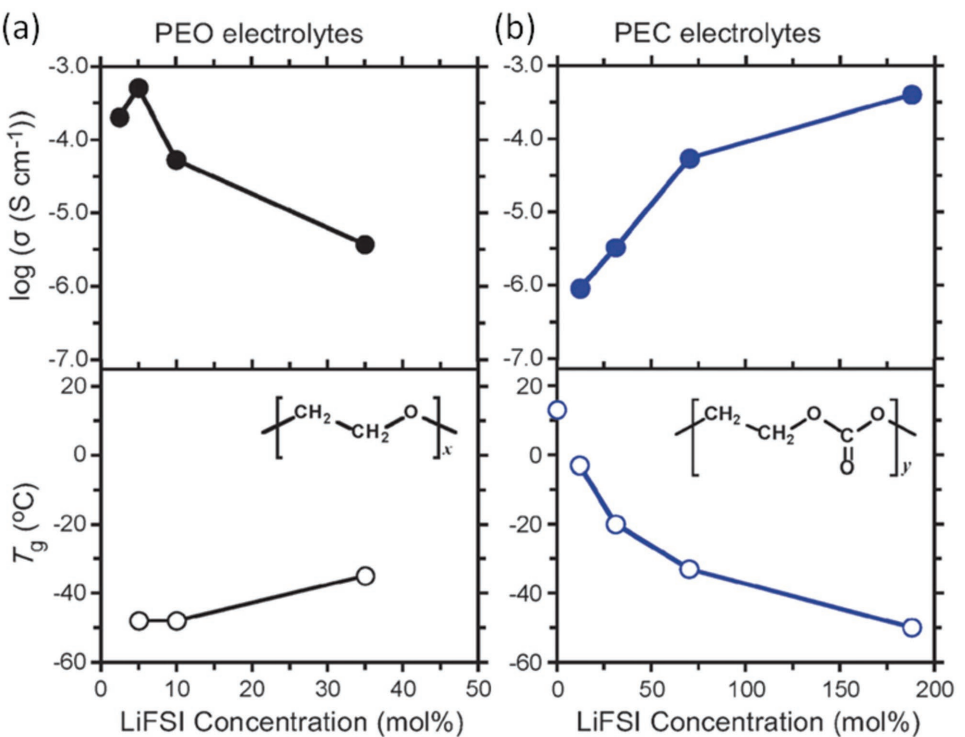


**Figure 34.** Ionic conductivity and the glass transition temperature dependence on concentration at 60 °C in a) PEO-LiFSI and b) PEC-LiFSI electrolyte. Insets show the structure of PEO and PEC. a,b) Reproduced with permission.<sup>[337]</sup> Copyright 2014, The Royal Society of Chemistry.

eutectic phase diagrams were therein obtained as here shown in Figure 35a. Two important observations are that the boiling point in the binary mixtures is affected by the component with the least boiling point and, in order to increase the liquid range, it is important for the two organic solvents to have comparable melting points and molecular structures. This implies that both solvents should be either cyclic or linear. These critical observations largely hold true for tertiary and quaternary mixtures. Nevertheless, on account of other factors, such as ESW, SEI layer stability and ionic conductivity, linear carbonate, and cyclic carbonate combinations remain standard practice.

Realizing the need for similar phase diagrams for higher order mixtures, Liu<sup>[340]</sup> successfully applied computational modeling of a DMC:EC:PC ternary mixture based on thermodynamic interaction parameters and even reproduced experimental results by Ding et al.<sup>[339]</sup> Such a computational approach decreases the number of experiments and provides a basis for rapid screening of multiple combinations and for optimization.

While no “single,” electrochemically stable solvent has been able to simultaneously possess a high dielectric permittivity and a low viscosity, systematic procedures have thus been applied in mixed electrolytes for the optimization of ionic conductivity by lowering the viscosity and increasing the dielectric permittivity.<sup>[284]</sup> Earlier studies on PC:DME binary mixtures by Matsuda et al.<sup>[293,341]</sup> had revealed that while viscosity increased exponentially, the dielectric permittivity increased linearly with partial composition of PC.

Ponrouche et al.,<sup>[282,283]</sup> having already identified the EC:PC mixture to optimally provide stable electrochemical properties

for SIB, carried out further comprehensive studies on formulation optimization in SIB full cells.<sup>[282]</sup> These results are shown in Figure 35b,c. DMC, a low-viscosity cosolvent, was added to the EC:PC solvent in 1 M NaClO<sub>4</sub> and effectively lowered the viscosity of the ternary mixture. The EC:PC:DMC (0.45:0.45:0.1) solvent thus emerged as the optimal composition, with high conductivity and enhanced rate capability. Furthermore, this formulation was found to be compatible with both an HC anode and Na<sub>3</sub>V<sub>2</sub>(PO<sub>4</sub>)<sub>2</sub>F<sub>3</sub> cathode, leading to stable cycling in subsequent SIB full cells. This highlights the relevance of systematic studies in the optimizations of battery performance.

## 6. Outlook on Commercial SIB

### 6.1. Anode Materials

Hard carbon is seemingly set to remain unchallenged as the SIB anode material of choice, for the foreseeable future. Its attractive properties, such as a high electrode capacity of 300 mAh g<sup>-1</sup>, a low plateau voltage between 0.0 and 0.1 V, and relative abundance of precursors, make HC a serious contender for SIB applications.

Nevertheless, Na nucleation on HC has been reported at -0.015 V versus Na<sup>+</sup>/Na.<sup>[64,66]</sup> The low-voltage operation of HC thus conjures safety concerns with regard to Na metal plating during fast charging. This remains the single greatest incentive to replace HC anodes, and other higher voltage alloy-based anodes can leverage their higher capacity to potentially surpass the energy density of HC electrodes. Another concern is

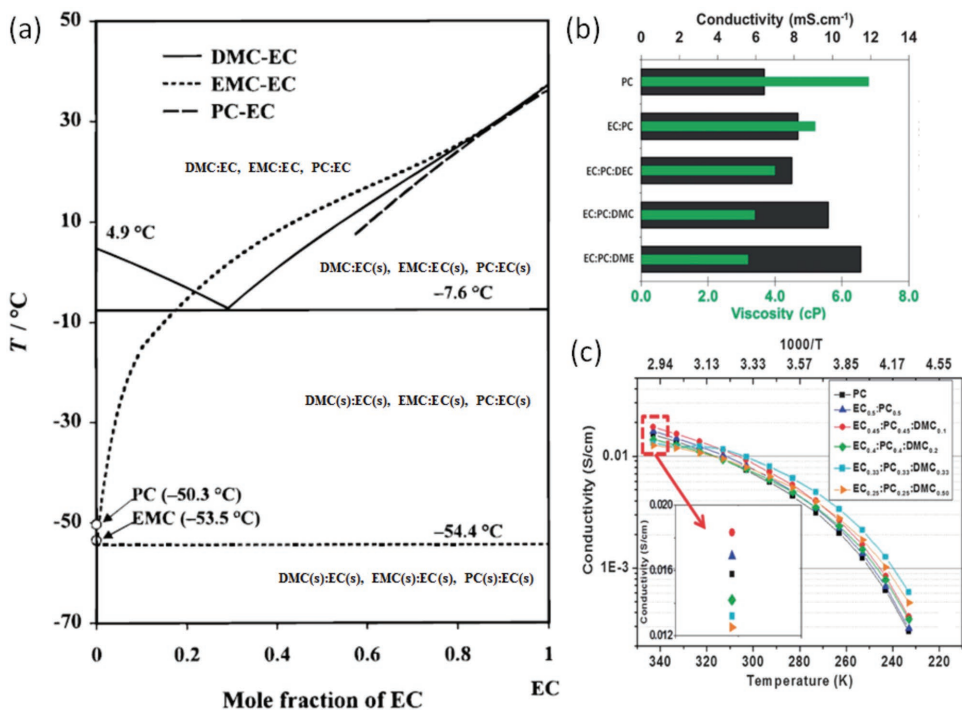


**Figure 35.** Optimization of electrolyte properties. a) Phase diagram of binary mixtures of DMC:EC, EMC:EC, and PC:EC. b) The relationship between conductivity and viscosity in SIB organic electrolytes (PC, EC:PC, EC:PC:DEC, EC:PC:DMC, and EC:PC:DME based on 1 M NaClO<sub>4</sub>), and high viscosity leads to low conductivity and vice versa. c) Electrolyte conductivity variation as a function of temperature. EC:PC:DMC and EC:PC:DME electrolytes based on 1 M NaTFSI. a) Adapted with permission.<sup>[339]</sup> Copyright 2000, The Electrochemical Society. b,c) Reproduced with permission.<sup>[282]</sup> Copyright 2013, The Royal Society of Chemistry.

the large first cycle irreversible capacity of ≈20–30%, which is a great concern for full-cell balancing using HC as the anode.<sup>[342,343]</sup> Current research efforts have thus focused on the contentious mechanistic understanding of Na intercalation in HC,<sup>[63,64,66,344]</sup> modeling,<sup>[66,345]</sup> experimental anode-to-cathode ratio optimizations<sup>[345,346]</sup> and the judicious use of additives such as FEC, NaN<sub>3</sub>, and Na<sub>3</sub>P.<sup>[343,345,346]</sup>

Equally imperative is the development of a highly efficient, low-cost, and ecologically sustainable HC synthesis process. This quest demands i) finding abundant and low-cost precursors, ii) developing a sustainable, generalized industrial processes for high yields, and iii) understanding the relationship between HC microstructural properties and processing conditions such as air flow and carbonization temperature control, for enhanced sodium storage. Recently, a fast, CO<sub>2</sub> laser irradiation technique has been proposed,<sup>[347]</sup> and several biomass derived precursors, such as sucrose,<sup>[56]</sup> banana peels,<sup>[348]</sup> mangosteen shells,<sup>[349]</sup> apple pomace,<sup>[68]</sup> pitch, and lignin,<sup>[350]</sup> have shown great promise. Concerns of low yields in current processes however affect the cost and raise questions on the overall sustainability of HC anode materials.

## 6.2. Cathode Materials

The outlook is however more encouraging with regard to cathode materials, wherein a wide range of interesting options have been identified. Layered transition metal oxides and poly-anionic compounds have established themselves as dominant

material classes while the Prussian blue analogs are gaining increasing attention as low-cost SIB cathode material options. In general, the layered oxides have been able to demonstrate high storage capacity albeit with low cycleability, while the poly-anionic compounds have shown low capacities with attractively stable and fast charge storage capability.

The elimination of the pricey Co and its successful replacement with Ni, V, Mn, and Fe in electrode formulations is a notable achievement in SIB cathode materials. Furthermore, the manipulation of inductive effects of PO<sub>4</sub><sup>3-</sup> and F<sup>-</sup> anions in fluorophosphates has resulted in the 4 V class cathode for SIB. As a result, Na<sub>3</sub>V<sub>2</sub>(PO<sub>4</sub>)<sub>2</sub>F, Na<sub>3</sub>V<sub>2</sub>(PO<sub>4</sub>)<sub>3</sub>, Na<sub>0.44</sub>MnO<sub>2</sub>, and P2-type Na<sub>0.5</sub>[Ni<sub>0.23</sub>Fe<sub>0.13</sub>Mn<sub>0.63</sub>]O<sub>2</sub> have emerged as the most interesting candidate cathode materials for SIB application.

Several environmental, safety, and air stability challenges still persist among cathode materials. For instance, concerns with regard to the use of both Ni and V cannot be overlooked. Ni is classified as a suspect carcinogen<sup>[351,352]</sup> and V<sup>5+</sup> causes soil pollution and poses potential health risks.<sup>[353]</sup> There are therefore no lack of incentives to replace these elements in the future. On the other hand, the use of abundant and environmentally benign Mn- and Fe-based redox couples shows promising signs, in mixed binary, ternary, and quaternary compounds, yet practical issues of concern such as low electrode potential, structural instability and hygroscopic nature in Fe-based and Mn-based compounds have not yet been elucidated. Of late, the use of nanoengineered electrode architectures such as the core-shell design has been heralded as a potential breakthrough, providing phenomenal cycling stability. Nevertheless, the lack

of commercially scalable processing techniques and low active material loading in composite electrodes are some unresolved challenges for the commercialization of nanomaterials.

### 6.3. Electrolytes

A major boost to the commercial prospects of the SIB technology is the successful adoption of standard LIB electrolytes for their use. The EC:PC and EC:DMC mixed electrolyte appear to be the preferred choice due to favorable compatibility with the HC anode. Furthermore, successful, template optimization procedures for the electrolyte have been carried out for SIB cells.

Possibilities of using ether-based electrolytes could usher a new paradigm in the form of graphitic anodes for SIBs; however, these prospects are hindered by the narrow voltage window of such electrolytes. Ionic liquids on the other hand promise a wider voltage window and are also considered safe due to nonflammability. The safety issue may be more severe in the SIB case, compared to LIB case, since metallic Na has a higher chemical activity than Li and poses a higher risk for explosion.<sup>[354]</sup> While such concerns can be managed by using a higher voltage anode, a nonflammable electrolyte is nevertheless highly desired for large-scale EES. Currently, the cost factors for high purity ionic liquids and the poor ionic conductivity at room temperature inhibit their extensive usage.

Finding battery grade salts has also been another critical challenge in the elaboration of SIB cells. Salt purity affects the solubility and electrochemical performance of the cells.<sup>[136]</sup> While in most cases NaPF<sub>6</sub> or NaClO<sub>4</sub> are the salts used in SIB electrolytes, the availability and purity of these salts are currently precarious. For example, the assays of most reagent grade, commercially available salts are about 98% while NaClO<sub>4</sub> has been reported to be potentially explosive and has been discontinued by traditional suppliers.<sup>[136]</sup> This reflects current challenges in the manufacturing and sourcing of salts for SIBs.

Similar to research efforts in solid-state lithium batteries, gel and polymer electrolytes are investigated in the quest for the elusive breakthrough in all solid-state SIBs. The challenges in the room temperature solid-state battery are however more severe in the Na case than in the Li case due to the low melting point and the high chemical activity of Na. Traditional challenges, such as the poor conductivity of solid electrolytes and dendritic growth during cycling, further alienate the prospects of the solid-state SIB.

### 6.4. SIB Technological Trend and Key Challenges

Technological trends usually follow an S-shaped profile. This growth trajectory proceeds in four successive stages of i) pre-development (emerging), ii) take-off (growth), iii) acceleration (maturity), and iv) stabilization (saturation). Figure 36a illustrates the technological trend for an emerging technology. Despite some shortcomings with regard to truly reflecting groundbreaking progress, patent numbers are widely used to benchmark technological trends.<sup>[355]</sup> Most recently, Wagner et al.<sup>[356,357]</sup> performed a patent based analysis to assess research trends and prospects among LIBs, while Golembiewski et al.<sup>[358]</sup>

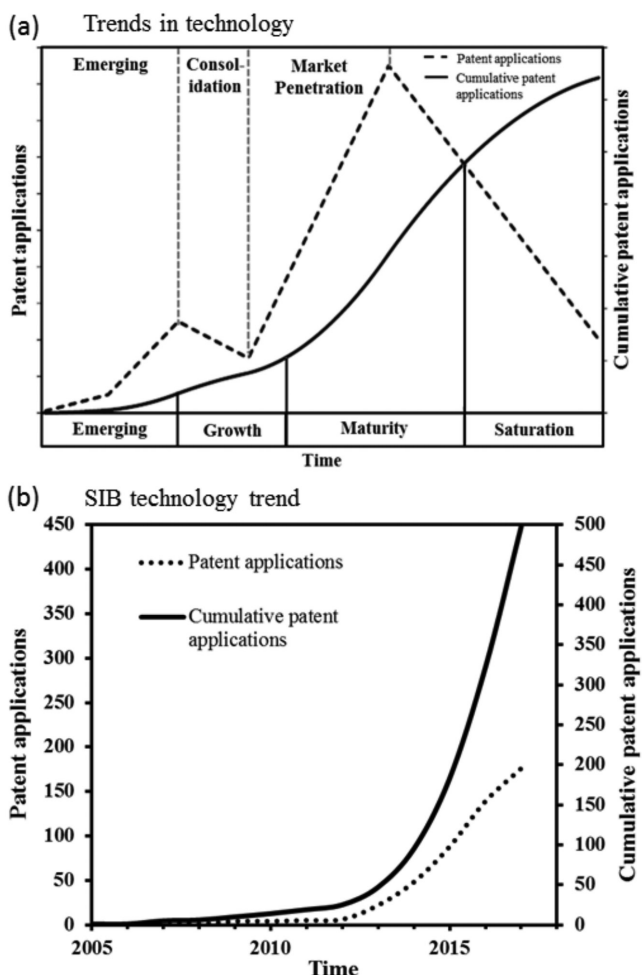


**Figure 36.** Trends in the SIB technology. a) Illustration of the growth patterns based on annual patent applications and cumulative patent filings for an emerging technology. Adapted with permission.<sup>[356]</sup> Copyright 2013, Springer Nature. b) Trends in SIB patents from 2005 to 2017, based on data derived from Espacenet.<sup>[359]</sup>

applied the same analysis to explore trends in electric mobility. In the case of the SIB technology, this analysis is herein performed for the first time.

For this analysis, annual patent application numbers and cumulative growth patterns are used as guiding parameters. Because intensive research efforts usually occur in the emerging stage, a steady yearly growth in patent numbers is realized. This upward trend however subsides once a technology is mature for commercialization. At this stage, prior technological gains are consolidated through commercialization activities. As the technology approaches the maturity stage, the number of patent filings makes a dramatic increase. Here, new companies file patents in the now established technology before finally reaching a saturation stage where radical innovations are no longer possible.<sup>[355]</sup>

The benefits of the patent-based method is that it offers insights into the most recent technological activities while being accessible through dedicated patent search engines.<sup>[356]</sup> For our purpose, we employed the online open services of Espacenet, a multinational patent database, and used smart search features

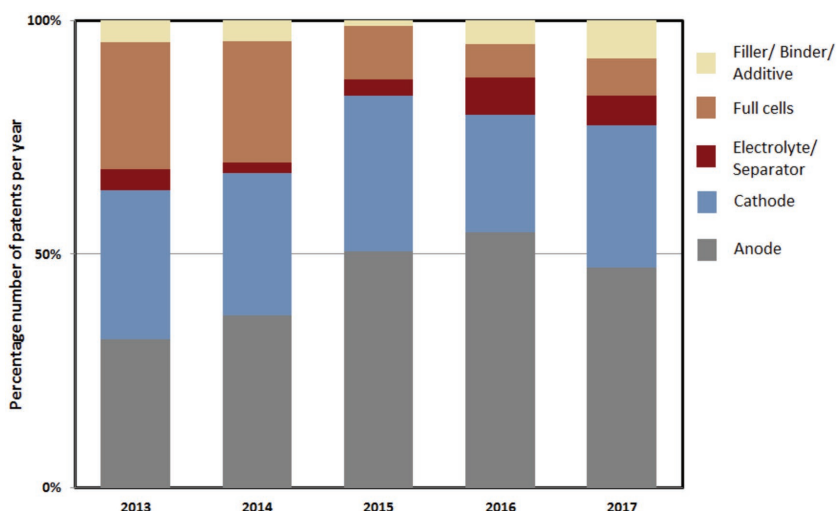


**Figure 37.** Percentage evolution of patents referring full cells and to specific battery components in SIB. Data derived from Espacenet.<sup>[359]</sup>

to specify key words and filling dates.<sup>[359]</sup> Figure 36b shows the trends in SIB technology. A monotonous and sharp increase in patent fillings has been witnessed since 2012 and the cumulative growth pattern shows an exponential upward trend. These encouraging revelations translate to an overall positive appreciation of the SIB technology. Based on these statistics, it can be concluded that the SIB technology is in the emerging stage and will soon enter the growth stage. Huge potential for intellectual property and innovations thus remains to be exploited.

To better understand specific subject areas, the patents filled between the years 2013 and 2017 are further classified according to either SIB full-cell claims or battery components, i.e., anode active, cathode active, electrolyte, separator, conductive filler, binder, and additive. The results obtained are shown in Figure 37 where a percentage scale illustrates the activity distribution per year.

Here, it can be observed that while the total number of full-cell claims has increased, the annual percentage of such claims has decreased over this period. This category has thus experienced slow incremental improvements as opposed to radical changes in terms of cell chemistries and configurations. Several challenges for the full cell have been reported nevertheless. These include industrial scaling procedures, poor cycleability, poor safety characteristics, low energy density, and the optimization of anode and cathode mass ratio for desirable capacity and rate capability. Moreover, during the initial (activation) charge cycles of the SIB, rapid capacity losses and gas evolutions have been reported.<sup>[360–363]</sup> Anodic voltage control charging and passive voltage control are some notable strategies being pursued at cell level,<sup>[364,365]</sup> while advances on specific SIB components in order to address these challenges are herein discussed.

From the data in Figure 37, a large fraction of the patenting activities (above 50% in some years) is targeted toward anode materials. This is an encouraging revelation since the challenges in HC and the needs for more anodic material choices are well documented. Not so impressive however is the fact that most of these claims do not relate to new materials, rather they elaborate new manufacturing methods,<sup>[366–368]</sup> new precursors,<sup>[369–371]</sup>

and Na supplementing to compensate anodic capacity losses.<sup>[372]</sup> Incentives to replace HC are based on improving safety characteristics and suppressing Na electroplating, which is reported to occur on the inner surface of the anodic current collector.<sup>[373]</sup> At the industrial manufacturing scale, a slurry viscosity problem has arisen.<sup>[374]</sup> The HC-based aqueous dispersion is found to have a high viscosity after mixing with other composite electrode components, making it impractical for electrode coating. This unfortunately forces manufacturers to select HC materials based on suitable physical properties, such as pore size, pore volume, and water absorption rate.

The second most patented category, which accounts for approximately a third of yearly claims, is that of cathode materials. While several interesting choices for the cathode have emerged, efforts to increase the capacity and voltage among the existing material classes are underway.<sup>[375–377]</sup> At large scale, the manufacture of a consistent positive electrode coating is similarly affected by gelation issues of the positive electrode paste.<sup>[378,379]</sup> This problem manifests when the pH of the mixture becomes highly basic and cannot be simply remediated by the addition of a neutralizing acid. Finding a viscosity regulating additive is therefore anticipated to provide the needed breakthrough.

Research efforts toward electrolytes and separators is also thriving and constitutes a significant portion of 2016 and 2017 activities. Although classical organic liquid electrolytes continue to dominate, there is a strong case for the flame-retardant ionic liquid electrolytes as well as gel, polymer, and solid electrolytes for all solid-state SIBs.<sup>[380,381]</sup> With the introduction of new electrolytes, new challenges are foreseen, for example, fluorine-containing separators and insulating components show instability issues in ionic liquid electrolytes.<sup>[382]</sup> This certainly will require a replacement of all F-containing insulating components.

Finally, the last category under this trend review is that of conductive fillers, composite electrode binders, and additives. The remarkable growth in this area in recently years has been propelled by the need to address issues of cycleability and capacity fade. Additives are traditionally employed to increase the stability of the SEI, reduce irreversible capacity losses, improve cycleability, and act as fire retardants. In the SIB, additives have further proven useful in controlling the pH of the electrolyte since the NaPF<sub>6</sub> salt is reported to induce the formation of HF which then corrodes the cathode material.<sup>[383]</sup> Notable advances have also emerged in binder research. In particular, there are significant efforts to replace N-methyl-pyrrolidone, an oil-based binder solvent, with an aqueous-based solvent for a homogeneous cathode electrode coating.<sup>[384]</sup> This is expected to significantly reduce manufacturing costs and provide environmentally benign industrial processes.

The overall trend in the SIB technology therefore points toward ample opportunities for investment and intellectual property. While this is encouraging, most of the patent applicants have however emerged from either universities or

research institutes. There is hence a need to forge strategic collaborations with industry if this knowhow is to be valorized. Encouragingly, a gradual recognition by household industrial manufactures such as Panasonic, Nissan, and Toyota is taking place and this is expected to carry the SIB technology into the growth phase.

### 6.5. Benchmarking of SIB Full Cells

According to widely accepted press reports, several prototype and near-commercialization SIB cells, such as HC//Na<sub>3</sub>V<sub>2</sub>(PO<sub>4</sub>)<sub>2</sub>F (NVPF),<sup>[385]</sup> HC//Na<sub>3</sub>V<sub>2</sub>(PO<sub>4</sub>)<sub>3</sub> (NVP),<sup>[386]</sup> HC//Na<sub>0.44</sub>MnO<sub>2</sub> (NMO),<sup>[386]</sup> and HC//NaNi<sub>1-x-y-z</sub>M<sub>x</sub><sup>1</sup>M<sub>y</sub><sup>2</sup>M<sub>z</sub><sup>3</sup>O<sub>2</sub> (NMMMO),<sup>[20]</sup> where M can either be a transition element or Ca, Sb, Bi, Te, Se, etc., and HC//NaFe<sub>0.4</sub>Mn<sub>0.3</sub>Ni<sub>0.3</sub>O<sub>2</sub> (NNFM)<sup>[21,22]</sup> are near commercialization, all based on HC anodes. The French network on electrochemical energy storage (RS2E), comprising mostly of CEA- and CNRS-affiliated researchers, developed the NVPF-based SIB. UK-based FARADION has pursued a doped nickelate, NMMMO-based SIB concept.<sup>[20,387]</sup> The Sumitomo group in Japan has announced plans for NNFM-based SIB and the Pacific Northwest National Laboratory (PNNL) has worked on both NVP-based and nanosized NMO-based SIBs.

In order to anticipate the possible application areas of the different SIB chemistries, the gravimetric and volumetric energy density of these materials is herein calculated and compared to that of the LiFePO<sub>4</sub> (LFP), being one of the cost effective LIBs. While gravimetric storage capacities of the active materials are readily available from various published literature, the active material densities, needed for this calculation, are hardly obtainable. As an alternative, an open-source software, based on supercomputing and thermodynamic analysis functionalities of the "Materials Project," is herein used for the estimation of unknown parameters.<sup>[388]</sup> This enabled an extensive set of material properties to be deduced, allowing cell balancing calculations to be performed, based on model guidelines as reported by Berg et al.<sup>[389]</sup>

Table 2 shows a list of the parameters used in the calculation of the gravimetric and energy density in SIB full cells. For the unavailable data of active material density, an estimate in the range of other SIB cathode materials was made. The gravimetric and volumetric capacities were then calculated by considering the materials that constitute the composite electrode and did not consider the mass and volume of current collectors, separators, and casings.

Figure 38 shows the results thus obtained. LFP has the highest gravimetric and volumetric energy density compared to all calculated SIBs. Another observation is that the gravimetric energy density scales linearly with volumetric energy density, and therefore, low gravimetric energy densities lead to lower volumetric energy densities among the

**Table 2.** Parameters used for the calculation of volumetric and gravimetric energy density.

Cathode material	Cell voltage [V] <sup>a)</sup>	Cathode capacity [mAh g <sup>-1</sup> ]	Porosity [-] <sup>b)</sup>	Density [g cm <sup>-3</sup> ] <sup>d)</sup>
LFP	3.3	160	0.3	3.65 <sup>[389]</sup>
NVPF	3.5	120	0.3	3.01
NMMMO	2.7	145	0.3	3.20 <sup>e)</sup>
NNFM	2.9	125	0.3	3.20 <sup>e)</sup>
NVP	3	92	0.4 <sup>c)</sup>	2.98
MNO	2.4	115	0.4 <sup>c)</sup>	3.20 <sup>e)</sup>

<sup>a)</sup>Average cell voltage versus graphite for LFP and versus hard carbon for SIBs;

<sup>b)</sup>Porosity in composite electrodes, including a binder and conductive filler; <sup>c)</sup>Higher porosity is assumed for electrodes with nanosized active particles; <sup>d)</sup>Density values are taken from the Materials Project database unless a reference is given; <sup>e)</sup>Estimated values due to unavailable data.

SIB herein studied. Comparatively close values in energy density are however obtained in NVPF-, NMMMO-, and NNFM-based SIBs. These encouraging results give a good indication of the ability of SIBs to match the LIB performance. Meanwhile, NMO- and NVP-based SIB suffer from low energy densities resulting from a combination of low cell voltage and low gravimetric capacity. In addition, the low active material loading in NMO and NVP due to nanosized active materials further aggravates their energy delivery and this highlights the need to have micrometer-sized, high voltage, and high-capacity cathode materials for SIBs. Therefore, should HC remain the anode for SIBs, a combination of high cathodic potentials and gravimetric capacity is needed to match both the gravimetric and volumetric energy density of LIBs.

Based on these results, SIBs can be successfully integrated in most stationary applications since these are in general insensitive to both the mass and volume. In addition, the overall

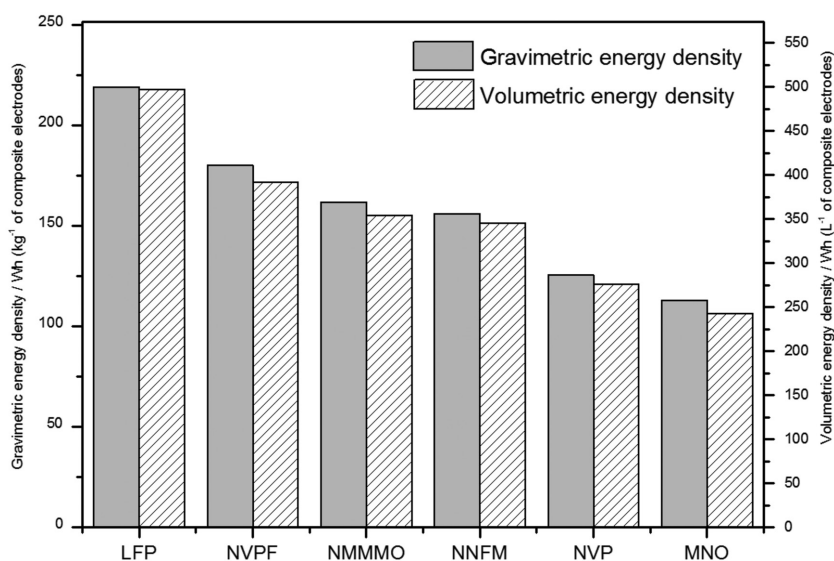


**Figure 38.** Comparison of the gravimetric and volumetric energy density in SIBs and LIBs based on the mass of the composite anode and cathodes. Here, the mass of the current collectors and other auxiliary battery components are not taken into consideration.

commercial prospects of the SIB technology are encouraging, based on the promise of lower battery costs, longer cycle life, and higher power delivery, compared to state-of-the-art LIBs. The raw material aspect is expected to play a major role as LIBs enter the mass market of battery electric vehicles, while the large-scale EES demands will likewise increase with the proliferation of distributed generation technologies.

Since sodium does not alloy with aluminum at the anode, the use of aluminum as the current collector for both the anode and cathode is possible in SIBs, instead of the more expensive copper used in LIB anodes. This not only lowers SIB costs but also allays the risks associated with complete discharge to zero volts in SIB cells. This important characteristic is beneficial for risk-free transportation of shorted SIBs. FARADION has already demonstrated that at zero volts the temperature and pressure in the cells remain constant and the performance of the cell is unaffected.<sup>[390]</sup> It is therefore anticipated that less stringent provisions would be required for the transportation of SIBs while the cost effects on battery management systems is still being assessed.

Frequently, new battery concepts fail commercially because identifying potential niche markets and setting up novel processing platforms is an extremely complex and capital intensive exercise. SIBs however strongly benefit from the conceptual similitude to the LIB technology and current manufacturers can seamlessly adapt existing infrastructure for SIB processing.<sup>[391]</sup> The SIB technology has thus been described as a “drop-in” technology for LIBs.<sup>[343]</sup> Although incremental improvements on material chemistries and on manufacturing processes are expedient, and may eventually lead to second and third generation cells, the performance of current SIB prototype cells goes beyond a proof of concept. Their characteristics, in terms of cycle life, energy density, and rate capability, are outstanding and comparative to those of LIBs. Because of faster sodium-ion conductivity in electrolytes and solid phases, the rate capability of SIBs may actually surpass that in LIBs. Target markets for SIBs therefore include i) frequency regulation, voltage control, and power back-up in grid-scale ESS; ii) start, lighting, and ignition applications for automotive applications; iii) traction motor propulsion; and iv) electronic power tools.

## 7. Conclusions

Progress toward the commercialization of room temperature SIBs continues to gain traction since the discovery of HC as functional anode material. Among the limited number of anode material options available, HC remains the material of choice at the moment. At the cathode side, more attractive options have been unveiled, largely due to similarities in material synthesis methods from LIBs. NASICON structures, layered oxides, and recently introduced Prussian blue analogs have thus emerged as the most stable structures, able to reversibly accommodate sodium in their lattices. The choice of elemental compositions has emerged as a strategy to tune the redox potentials while nanosizing and carbon coating improve the materials rate capability and cycleability. In order to identify the most appropriate electrode material, it is important to consider

the storage capacity and voltage characteristics, as well as the cycling ability. The roadmap toward the development of superior cathode materials for SIB applications is thus guided by resource constraints and the mastering of crystallography and elemental compositions. Electrolyte development through systematic studies has been able to identify the EC:PC mixed electrolyte as the optimum choice in the voltage window of SIBs while ionic liquids and polymer electrolytes promise safer batteries. These promising trends are also reflected in the patent-based analyses. Research among anode and cathode materials is indeed thriving and the SIB technology is soon expected to cross from the emerging stage to the growth stage. In terms of gravimetric and volumetric energy density, SIBs can compete with some of the most successful LIBs, such as the LiFePO<sub>4</sub> and LiMn<sub>2</sub>O<sub>4</sub> batteries. Given the above characteristics, the endeavor toward commercialization and the goals of a cheap, scalable, large-scale EES systems depends on more industrial adoptions of this groundbreaking SIB technology.

## Acknowledgements

The Authors acknowledge Jerry Barker for some helpful discussions. D.L.D. appreciates support from DEMOBASE project financed by EU HORIZON 2020-CV-2017 program. This article was published as part of the *Advanced Energy Materials* Excellence in Energy special series.

## Conflict of Interest

The authors declare no conflict of interest.

## Keywords

anodes, cathodes, electrolytes, patents, sodium-ion batteries

Received: January 8, 2018

Revised: March 6, 2018

Published online: April 30, 2018

- [1] A. Manthiram, in *Lithium Batteries: Science and Technology* (Eds.: G. A. Nazri, G. Pistoia), Springer, New York **2009**, Ch. 1.
- [2] J. M. Tarascon, M. Armand, *Nature* **2001**, 414, 359.
- [3] L. Wang, Y. Lu, J. Liu, M. Xu, J. Cheng, D. Zhang, G. John, *Angew. Chem., Int. Ed.* **2013**, 52, 7.
- [4] M. D. Slater, D. Kim, E. Lee, C. S. Johnson, *Adv. Funct. Mater.* **2013**, 23, 26.
- [5] C. J. Yang, R. B. Jackson, *Renewable Sustainable Energy Rev.* **2011**, 15, 1.
- [6] US Department of Energy, Global Energy Storage Database, <http://www.energystorageexchange.org> (accessed: December 2017).
- [7] H. Chen, T. N. Cong, W. Yang, C. Tan, Y. Li, Y. Ding, *Prog. Nat. Sci.* **2009**, 19, 3.
- [8] J. Kondoh, I. Ishii, H. Yamaguchi, A. Murata, K. Otani, K. Sakuta, N. Higuchi, S. Sekine, M. Kamimoto, *Energy Convers. Manage.* **2000**, 41, 17.
- [9] R. J. Bones, D. A. Teagle, S. D. Brooker, F. L. Cullen, *J. Electrochem. Soc.* **1989**, 136, 5.
- [10] T. Oshima, M. Kajita, A. Okuno, *Int. J. Appl. Ceram. Technol.* **2004**, 1, 3.
- [11] C. H. Dustmann, *J. Power Sources* **2004**, 127, 2.

- [12] D. Kundu, E. Talaie, V. Duffort, L. F. Nazar, *Angew. Chem., Int. Ed.* **2015**, *54*, 11.
- [13] L. Marcoux, E. Seo, in *New Uses Sulfur* (Ed: J. R. West), American Chemical Society, Washington, DC **1975**.
- [14] B. L. Ellis, L. F. Nazar, *Curr. Opin. Solid State Mater. Sci.* **2012**, *16*, 4.
- [15] K. West, B. Zachau-Christiansen, T. Jacobsen, S. Skarup, *Solid State Ionics* **1989**, *26*, 4.
- [16] J. M. Tarascon, G. W. Hull, *Solid State Ionics* **1986**, *22*, 1.
- [17] N. Yabuuchi, K. Kubota, M. Dahbi, S. Komaba, *Chem. Rev.* **2014**, *114*, 23.
- [18] D. A. Stevens, J. R. Dahn, *J. Electrochem. Soc.* **2000**, *147*, 4.
- [19] Faradion, Sodium-Ion Technology, <http://www.faradion.co.uk> (accessed: December 2017).
- [20] J. Barker, R. Heap, N. Roche, C. Tan, R. Sayers, Y. Liu, Presented at the 17th International Meeting on Lithium Batteries, IMLB, Como, Italy, **2014**.
- [21] S. Kuze, J. Kageura, S. Matsumoto, T. Nakayama, M. Makidera, M. Saka, T. Yamaguchi, T. Yamamoto, K. Nakane, *Sumitomo Kagaku* **2013**, 1.
- [22] Nikkei Asian Review, Sumitomo Electric to Start Supplying Sodium-Ion Batteries, <https://asia.nikkei.com/Business/Companies/Sumitomo-Electric-to-start-supplying-sodium-ion-batteries> (accessed: December 2017).
- [23] B. Nykvist, M. Nilsson, *Nat. Clim. Change* **2015**, *5*, 4.
- [24] P. K. Nayak, L. Yang, W. Brehm, P. Adelhelm, *Angew. Chem., Int. Ed.* **2017**, *57*, 1.
- [25] J. Y. Hwang, S. T. Myung, Y. K. Sun, *Chem. Soc. Rev.* **2017**, *46*, 12.
- [26] Y. Mido, S. A. Iqbal, M. Satake, M. S. Sethi, *Chemistry of S Block Elements*, Discovery Publishing House, New Delhi, India **1994**.
- [27] H. Kang, Y. Liu, K. Cao, Y. Zhao, L. Jiao, Y. Wang, H. Yuan, *J. Mater. Chem. A* **2015**, *3*, 35.
- [28] M. Rosa Palacín, *Chem. Soc. Rev.* **2009**, *38*, 9.
- [29] C. Poinsignon, M. Armand, *Europhys. News* **1993**, *24*, 1.
- [30] J. B. Clarke, J. W. Hastie, L. H. E. Kihlborg, R. Metselaar, M. M. Thackeray, *Pure Appl. Chem.* **2009**, *66*, 3.
- [31] M. Winter, J. O. Besenhard, M. E. Spahr, P. Novák, *Adv. Mater.* **1998**, *10*, 10.
- [32] A. Anani, R. A. Huggins, *J. Power Sources* **1992**, *38*, 3.
- [33] W. J. Zhang, *J. Power Sources* **2011**, *196*, 1.
- [34] C. K. Chan, H. Peng, G. Liu, K. McIlwrath, X. F. Zhang, R. A. Huggins, Y. Cui, *Nat. Nanotechnol.* **2008**, *3*, 1.
- [35] M. T. McDowell, I. Ryu, S. W. Lee, C. Wang, W. D. Nix, Y. Cui, *Adv. Mater.* **2012**, *24*, 45.
- [36] H. Wu, G. Chan, J. W. Choi, I. Ryu, Y. Yao, M. T. McDowell, S. W. Lee, A. Jackson, Y. Yang, L. Hu, Y. Cui, *Nat. Nanotechnol.* **2012**, *7*, 5.
- [37] N. Liu, Z. Lu, J. Zhao, M. T. McDowell, H.-W. Lee, W. Zhao, Y. Cui, *Nat. Nanotechnol.* **2014**, *9*, 3.
- [38] Y. Li, K. Yan, H.-W. Lee, Z. Lu, N. Liu, Y. Cui, *Nat. Energy* **2016**, *1*, 2.
- [39] F. Klein, B. Jache, A. Bhide, P. Adelhelm, *Phys. Chem. Chem. Phys.* **2013**, *15*, 38.
- [40] G. G. Amatucci, N. Pereira, *J. Fluorine Chem.* **2007**, *128*, 4.
- [41] M. Armand, J. Tarascon, *Nature* **2008**, *415*, 7179.
- [42] B. Scrosati, J. Hassoun, Y. K. Sun, *Energy Environ. Sci.* **2011**, *4*, 9.
- [43] C. Julien, A. Mauger, A. Vijh, K. Zaghib, *Lithium Batteries*, Springer International Publishing, Switzerland, **2016**.
- [44] Y. Li, W. Zhou, X. Chen, X. Lü, Z. Cui, S. Xin, L. Xue, Q. Jia, J. B. Goodenough, *Proc. Natl. Acad. Sci. USA* **2016**, *113*, 47.
- [45] B. Jache, P. Adelhelm, *Angew. Chem., Int. Ed.* **2014**, *53*, 38.
- [46] D. A. Stevens, J. R. Dahn, *J. Electrochem. Soc.* **2001**, *148*, 8.
- [47] P. Ge, M. Fouletier, *Solid State Ionics* **1988**, *28*, 2.
- [48] Y. Wen, K. He, Y. Zhu, F. Han, Y. Xu, I. Matsuda, Y. Ishii, J. Cumings, W. Chunsheng, *Nat. Commun.* **2014**, *5*, 4033.
- [49] Y. Cao, L. Xiao, M. L. Sushko, W. Wang, B. Schwenzer, J. Xiao, Z. Nie, L. V. Saraf, Z. Yang, J. Liu, *Nano Lett.* **2012**, *12*, 7.
- [50] Y. Liu, B. V. Merinov, W. A. Goddard, *Proc. Natl. Acad. Sci. USA* **2016**, *113*, 14.
- [51] J. Sangster, *J. Phase Equilib. Diffus.* **2007**, *28*, 6.
- [52] K. Nobuhara, H. Nakayama, M. Nose, S. Nakanishi, H. Iba, *J. Power Sources* **2013**, *243*, 1.
- [53] J. Gole, *Mater. Sci. Eng.* **1977**, *31*, 309.
- [54] H. Kim, J. Hong, Y. U. Park, J. Kim, I. Hwang, K. Kang, *Adv. Funct. Mater.* **2015**, *25*, 4.
- [55] A. P. Cohn, K. Share, R. Carter, L. Oakes, C. L. Pint, *Nano Lett.* **2016**, *16*, 1.
- [56] Y. Li, S. Xu, X. Wu, J. Yu, Y. Wang, Y. S. Hu, H. Li, L. Chen, X. Huang, *J. Mater. Chem. A* **2015**, *3*, 1.
- [57] V. Simone, A. Boulineau, A. de Geyer, D. Rouchon, L. Simonin, S. Martinet, *J. Energy Chem.* **2016**, *25*, 5.
- [58] A. Ponrouch, A. R. Goñi, M. R. Palacín, *Electrochim. Commun.* **2013**, *27*.
- [59] B. Jin, F. Gao, Y.-F. Zhu, X.-Y. Lang, G.-F. Han, W. Gao, Z. Wen, M. Zhao, J. C. Li, Q. Jiang, *Sci. Rep.* **2016**, *6*, 19317.
- [60] E. Irisarri, A. Ponrouch, M. R. Palacín, *J. Electrochem. Soc.* **2015**, *162*, 14.
- [61] R. Alcántara, J. M. Jiménez-Mateos, P. Lavela, J. L. Tirado, *Electrochim. Commun.* **2001**, *3*, 11.
- [62] S. Komaba, W. Murata, T. Ishikawa, N. Yabuuchi, T. Ozeki, T. Nakayama, A. Ogata, K. Gotoh, K. Fujiwara, *Adv. Funct. Mater.* **2011**, *21*, 20.
- [63] S. Qiu, L. Xiao, M. L. Sushko, K. S. Han, Y. Shao, M. Yan, X. Liang, L. Mai, J. Feng, Y. Cao, X. Ai, H. Yang, J. Liu, *Adv. Energy Mater.* **2017**, *7*, 17.
- [64] B. Zhang, C. M. Ghimebeu, C. Laberty, C. Vix-Guterl, J. M. Tarascon, *Adv. Energy Mater.* **2016**, *6*, 1.
- [65] P. Tsai, S. C. Chung, S. Lin, A. Yamada, *J. Mater. Chem. A* **2015**, *3*, 18.
- [66] C. Bommier, T. W. Surta, M. Dolgos, X. Ji, *Nano Lett.* **2015**, *15*, 9.
- [67] Y. Chen, L. Shi, S. Guo, Q. Yuan, X. Chen, J. Zhou, H. Song, *J. Mater. Chem. A* **2017**, *5*, 37.
- [68] X. Dou, C. Geng, D. Buchholz, S. Passerini, *APL Mater.* **2018**, *6*, 4.
- [69] S. Huang, Z. Li, B. Wang, J. Zhang, Z. Peng, R. Qi, J. Wang, Y. Zhao, *Adv. Funct. Mater.* **2018**, *28*, 10.
- [70] J. S. Chen, D. Luan, C. M. Li, F. Y. C. Boey, S. Qiao, X. W. Lou, *Chem. Commun.* **2010**, *46*, 43.
- [71] Z. Chen, I. Belharouak, Y. K. Sun, K. Amine, *Adv. Funct. Mater.* **2013**, *23*, 8.
- [72] S. T. Myung, N. Takahashi, S. Komaba, C. S. Yoon, Y. K. Sun, K. Amine, H. Yashiro, *Adv. Funct. Mater.* **2011**, *21*, 7.
- [73] N. D. Trinh, O. Crosnier, S. B. Schougaard, T. Brousse, *ECS Trans.* **2011**, *35*, 32.
- [74] Z. Yang, D. Choi, S. Kerisit, K. M. Rosso, D. Wang, J. Zhang, G. Graff, J. Liu, *J. Power Sources* **2009**, *192*, 2.
- [75] G. H. Newman, L. P. Klemann, *J. Electrochem. Soc.* **1980**, *127*, 10.
- [76] M. Zanini, J. L. Shaw, G. J. Tennenhouse, *J. Electrochem. Soc.* **1981**, *128*, 8.
- [77] C. Delmas, F. Cherkaoui, A. Nadiri, P. Hagenmuller, *Mater. Res. Bull.* **1987**, *22*, 5.
- [78] C. Delmas, A. Nadiri, J. L. Soubeyroux, *Solid State Ionics* **1988**, *28*.
- [79] Mineral Commodity Summaries 2015, U.S. Geological Survey, <https://minerals.usgs.gov/minerals/pubs/mcs/2015/mcs2015.pdf> (accessed: January 2015).
- [80] T. Ohzuku, T. Kodama, T. Hirai, *J. Power Sources* **1985**, *14*.
- [81] M. S. Mattsson, M. Veszelei, G. A. Niklasson, C. G. Granqvist, A. Stashans, S. Lunell, in *Proc III Symp Electrochromic Materials and Their Applications*, **1996**.
- [82] S. Lunell, A. Stashans, L. Ojamäe, H. Lindström, A. Hagfeldt, *J. Am. Chem. Soc.* **1997**, *119*, 31.
- [83] Y. Xu, E. M. Lotfabad, H. Wang, B. Farbod, Z. Xu, A. Kohandehghan, D. Mitlin, *Chem. Commun.* **2013**, *49*, 79.

- [84] L. Wu, D. Buchholz, D. Bresser, L. Gomes Chagas, S. Passerini, *J. Power Sources* **2014**, 251.
- [85] P. Senguttuvan, G. Rousse, V. Seznec, J. M. Tarascon, M. R. Palacín, *Chem. Mater.* **2011**, 23, 18.
- [86] H. Song, H. Jiang, T. Liu, X. Liu, G. Meng, *Mater. Res. Bull.* **2007**, 42, 2.
- [87] D. Yang, Z. Zheng, H. Liu, H. Zhu, X. Ke, Y. Xu, D. Wu, Y. Sun, *J. Phys. Chem. C* **2008**, 112, 42.
- [88] K. Chiba, N. Kijima, Y. Takahashi, Y. Idemoto, J. Akimoto, *Solid State Ionics* **2008**, 178, 33.
- [89] A. Rudola, K. Saravanan, C. W. Mason, P. Balaya, *J. Mater. Chem. A* **2013**, 1, 7.
- [90] J. Xu, C. Ma, M. Balasubramanian, Y. Shirley Meng, *Chem. Commun.* **2014**, 50, 83.
- [91] M. Shirpour, J. Cabana, M. Doeff, *Energy Environ. Sci.* **2013**, 6, 8.
- [92] A. Rudola, K. Saravanan, S. Devaraj, H. Gong, P. Balaya, *Chem. Commun.* **2013**, 49, 67.
- [93] T. Ohzuku, A. Ueda, N. Yamamoto, *J. Electrochem. Soc.* **1995**, 142, 5.
- [94] Z. Liang, P. Hui-Lin, H. Yong-Sheng, L. Hong, C. Li-Quan, *Chin. Phys. B* **2012**, 21, 2.
- [95] Y. Sun, L. Zhao, H. Pan, X. Lu, L. Gu, Y. S. Hu, H. Li, M. Armand, Y. Ikuhara, L. Chen, X. Huang, *Nat. Commun.* **2013**, 4, 1870.
- [96] F. Zhao, P. Xue, H. Ge, L. Li, B. Wang, *J. Electrochem. Soc.* **2016**, 163, 5.
- [97] L. Gao, L. Wang, S. Dai, M. Cao, Z. Zhong, Y. Shen, M. Wang, *J. Power Sources* **2017**, 344, 223.
- [98] G. Xu, Y. Tian, X. Wei, L. Yang, P. K. Chu, *J. Power Sources* **2017**, 337, 180.
- [99] S. Komaba, Y. Matsuura, T. Ishikawa, N. Yabuuchi, W. Murata, S. Kuze, *Electrochem. Commun.* **2012**, 21, 65.
- [100] L. D. Ellis, B. N. Wilkes, T. D. Hatchard, M. N. Obrovac, *J. Electrochem. Soc.* **2014**, 161, 3.
- [101] U. Arrieta, N. A. Katcho, O. Arcelus, J. Carrasco, *Sci. Rep.* **2017**, 7, 1.
- [102] J. Xu, J. Xu, *Designing and Diagnosing Novel Electrode Materials for Na-Ion Batteries: Potential Alternatives to Current Li-Ion Batteries*, University of California, San Diego, CA **2014**.
- [103] Y. Liu, N. Zhang, L. Jiao, Z. Tao, J. Chen, *Adv. Funct. Mater.* **2015**, 25, 2.
- [104] L. Baggetto, J. K. Keum, J. F. Browning, G. M. Veith, *Electrochem. Commun.* **2013**, 34, 41.
- [105] N. Yabuuchi, Y. Matsuura, T. Ishikawa, S. Kuze, J.-Y. Son, Y.-T. Cui, H. Oji, S. Komaba, *ChemElectroChem* **2014**, 1, 3.
- [106] J. Qian, Y. Chen, L. Wu, Y. Cao, X. Ai, H. Yang, *Chem. Commun.* **2012**, 48, 56.
- [107] J. Song, Z. Yu, M. L. Gordin, S. Hu, R. Yi, D. Tang, T. Walter, M. Regula, D. Choi, X. Li, A. Manivannan, D. Wang, *Nano Lett.* **2014**, 14, 11.
- [108] R. F. Service, *Science* **2016**, 352, 6289.
- [109] T. B. Kim, J. W. Choi, H. S. Ryu, G. B. Cho, K. W. Kim, J. H. Ahn, K. K. Cho, H. J. Ahn, *J. Power Sources* **2007**, 174, 2.
- [110] Z. Hu, Z. Zhu, F. Cheng, K. Zhang, J. Wang, C. Chen, J. Chen, *Energy Environ. Sci.* **2015**, 8, 4.
- [111] Q. Sun, Q. Q. Ren, H. Li, Z. W. Fu, *Electrochem. Commun.* **2011**, 13, 12.
- [112] S. Hariharan, K. Saravanan, P. Balaya, *Electrochem. Commun.* **2013**, 31, 5.
- [113] M. Keller, C. Vaalma, D. Buchholz, S. Passerini, *ChemElectroChem* **2016**, 3, 7.
- [114] P. Senguttuvan, G. Rousse, M. E. Arroyo y de Dompablo, H. Vezin, J. M. Tarascon, M. R. Palacín, *J. Am. Chem. Soc.* **2013**, 135, 10.
- [115] H. Pan, X. Lu, X. Yu, Y. S. Hu, H. Li, X. Q. Yang, L. Chen, *Adv. Energy Mater.* **2013**, 3, 9.
- [116] Y. Wang, X. Yu, S. Xu, J. Bai, R. Xiao, Y.-S. Hu, H. Li, X.-Q. Yang, L. Chen, X. Huang, *Nat. Commun.* **2013**, 4, 2365.
- [117] L. Xiao, Y. Cao, J. Xiao, W. Wang, L. Kovarik, Z. Nie, J. Liu, *Chem. Commun.* **2012**, 48, 27.
- [118] J. Fullenwarth, A. Darwiche, A. Soares, B. Donnadieu, L. Monconduit, *J. Mater. Chem. A* **2014**, 2, 7.
- [119] J. Park, J. S. Kim, J.-W. Park, T. H. Nam, K. W. Kim, J. H. Ahn, G. Wang, H. J. Ahn, *Electrochim. Acta* **2013**, 92, 427.
- [120] Y. Wang, J. Liu, B. Lee, R. Qiao, Z. Yang, S. Xu, X. Yu, L. Gu, Y. S. Hu, W. Yang, K. Kang, H. Li, X. Q. Yang, L. Chen, X. Huang, *Nat. Commun.* **2015**, 6, 6401.
- [121] D. Su, C. Wang, H. Ahn, G. Wang, *Phys. Chem. Chem. Phys.* **2013**, 15, 30.
- [122] H. S. Ryu, J. S. Kim, J. Park, J. Y. Park, G. B. Cho, X. Liu, I. S. Ahn, K. W. Kim, J. H. Ahn, J. P. Ahn, S. W. Martin, G. Wang, H. J. Ahn, *J. Power Sources* **2013**, 244, 764.
- [123] R. Fielden, L. Cole, M. N. Obrovac, *J. Electrochem. Soc.* **2017**, 164, 2.
- [124] X. Wu, Y. Cao, X. Ai, J. Qian, H. Yang, *Electrochem. Commun.* **2013**, 31, 145.
- [125] Broadbit Batteries, Green Battery Technology, <http://www.broadbit.com/#menu-home> (accessed: December 2017).
- [126] J. Barker, M. Y. Saidi, J. L. Swoyer (Faradion Ltd.), *US6872492 B2*, 2005.
- [127] K. Tang, L. Fu, R. J. White, L. Yu, M.-M. Titirici, M. Antonietti, J. Maier, *Adv. Energy Mater.* **2012**, 2, 7.
- [128] Z. Wang, L. Qie, L. Yuan, W. Zhang, X. Hu, Y. Huang, *Carbon* **2013**, 55, 328.
- [129] Y. Liu, F. Fan, J. Wang, Y. Liu, H. Chen, K. L. Jungjohann, Y. Xu, Y. Zhu, D. Bigio, T. Zhu, C. Wang, *Nano Lett.* **2014**, 14, 6.
- [130] K. T. Kim, G. Ali, K. Y. Chung, C. S. Yoon, H. Yashiro, Y. K. Sun, J. Lu, K. Amine, S. T. Myung, *Nano Lett.* **2014**, 14, 2.
- [131] C. Delmas, J.-J. Braconnier, C. Fouassier, P. Hagenmuller, *Solid State Ionics* **1981**, 3, 165.
- [132] J. J. Braconnier, C. Delmas, P. Hagenmuller, *Mater. Res. Bull.* **1982**, 17, 1.
- [133] A. Mendiboure, C. Delmas, P. Hagenmuller, *J. Solid State Chem.* **1985**, 57, 3.
- [134] Y. Takeda, K. Nakahara, M. Nishijima, N. Imanishi, O. Yamamoto, M. Takano, R. Kanno, *Mater. Res. Bull.* **1994**, 29, 6.
- [135] C. Delmas, C. Fouassier, P. Hagenmuller, *Physica B+C* **1980**, 99, 81.
- [136] K. Kubota, S. Kornaba, *J. Electrochem. Soc.* **2015**, 162, 14.
- [137] X. Xiang, K. Zhang, J. Chen, *Adv. Mater.* **2015**, 27, 36.
- [138] D. Yuan, W. He, F. Pei, F. Wu, Y. Wu, J. Qian, Y. Cao, X. Ai, H. Yang, *J. Mater. Chem. A* **2013**, 1, 12.
- [139] D. H. Lee, J. Xu, Y. S. Meng, *Phys. Chem. Chem. Phys.* **2013**, 15, 9.
- [140] Z. Dai, U. Mani, H. T. Tan, Q. Yan, *Small Methods* **2017**, 1, 5.
- [141] S. Komaba, C. Takei, T. Nakayama, A. Ogata, N. Yabuuchi, *Electrochem. Commun.* **2010**, 12, 3.
- [142] S. Komaba, T. Nakayama, A. Ogata, T. Shimizu, C. Takei, S. Takada, A. Hokura, I. Nakai, *ECS Trans.* **2009**, 16, 42.
- [143] P. Vassilaras, X. Ma, X. Li, G. Ceder, *J. Electrochem. Soc.* **2013**, 160, 2.
- [144] C. Didier, M. Guignard, C. Denage, O. Szajwaj, S. Ito, I. Saadoune, J. Darriet, C. Delmas, *Electrochim. Solid-State Lett.* **2011**, 14, 5.
- [145] D. Hamani, M. Ati, J. M. Tarascon, P. Rozier, *Electrochim. Commun.* **2011**, 13, 9.
- [146] L. W. Shacklette, T. R. Jow, L. Townsend, *J. Electrochim. Soc.* **1988**, 135, 11.
- [147] C. Fouassier, G. Matejka, J. M. Reau, P. Hagenmuller, *J. Solid State Chem.* **1973**, 6, 4.
- [148] I. Terasaki, Y. Sasago, K. Uchinokura, *Phys. Rev. B* **1997**, 56, 20.
- [149] K. Takada, H. Sakurai, E. Takayama-Muromachi, F. Izumi, R. A. Dilanian, T. Sasaki, *Nature* **2003**, 422, 6927.
- [150] R. Berthelot, D. Carlier, C. Delmas, *Nat. Mater.* **2011**, 10, 1.
- [151] Y. Hinuma, Y. S. Meng, G. Ceder, *Phys. Rev. B* **2008**, 77, 22.
- [152] J. J. Ding, Y. N. Zhou, Q. Sun, X. Q. Yu, X. Q. Yang, Z. W. Fu, *Electrochim. Acta* **2013**, 87, 388.
- [153] A. K. Rai, L. T. Anh, J. Gim, V. Mathew, J. Kim, *Ceram. Int.* **2014**, 40, 1.
- [154] Y. Fang, X. Y. Yu, X. W. D. Lou, *Angew. Chem., Int. Ed.* **2017**, 56, 21.

- [155] H. Yoshida, N. Yabuuchi, S. Komaba, *Electrochim. Commun.* **2013**, 34, 60.
- [156] X. Xia, J. R. Dahn, *J. Electrochem. Soc.* **2012**, 159, 5.
- [157] Y. Takeda, J. Akagi, A. Edagawa, M. Inagaki, S. Naka, *Mater. Res. Bull.* **1980**, 15, 8.
- [158] N. Yabuuchi, H. Yoshida, S. Komaba, *Electrochemistry* **2012**, 80, 10.
- [159] J. Zhao, L. Zhao, N. Dimov, S. Okada, T. Nishida, *J. Electrochem. Soc.* **2013**, 160, 5.
- [160] N. Yabuuchi, M. Kajiyama, J. Iwatate, H. Nishikawa, S. Hitomi, R. Okuyama, R. Usui, Y. Yamada, S. Komaba, *Nat. Mater.* **2012**, 11, 6.
- [161] N. Yabuuchi, M. Yano, H. Yoshida, S. Kuze, S. Komaba, *J. Electrochem. Soc.* **2013**, 160, 5.
- [162] P. Vassilaras, A. J. Toumar, G. Ceder, *Electrochim. Commun.* **2014**, 38, 79.
- [163] A. Caballero, L. Hernán, J. Morales, L. Sánchez, J. S. Peña, M. A. G. Aranda, *J. Mater. Chem.* **2002**, 12, 4.
- [164] J. P. Parant, R. Olazcuaga, M. Devalette, C. Fouassier, P. Hagenmuller, *J. Solid State Chem.* **1971**, 3, 1.
- [165] X. Ma, H. Chen, G. Ceder, *J. Electrochem. Soc.* **2011**, 158, 12.
- [166] M. M. Doeff, A. Anapolsky, L. Edman, T. J. Richardson, L. C. D. Jonghe, *J. Electrochem. Soc.* **2001**, 148, 3.
- [167] J. J. Ding, Y. N. Zhou, Q. Sun, Z. W. Fu, *Electrochim. Commun.* **2012**, 22, 85.
- [168] C. Y. Chen, K. Matsumoto, T. Nohira, R. Hagiwara, A. Fukunaga, S. Sakai, K. Nitta, S. Inazawa, *J. Power Sources* **2013**, 237, 52.
- [169] X. Xia, J. R. Dahn, *Electrochim. Solid-State Lett.* **2011**, 15, 1.
- [170] C. Y. Yu, J. S. Park, H. G. Jung, K. Y. Chung, D. Aurbach, Y. K. Sun, S. T. Myung, *Energy Environ. Sci.* **2015**, 8, 7.
- [171] G. Singh, B. Acebedo, M. C. Cabanas, D. Shanmukaraj, M. Armand, T. Rojo, *Electrochim. Commun.* **2013**, 37, 61.
- [172] D. Shanmukaraj, S. Grignon, S. Laruelle, G. Douglade, J. M. Tarascon, M. Armand, *Electrochim. Commun.* **2010**, 12, 10.
- [173] Z. Lu, J. R. Dahn, *Chem. Mater.* **2001**, 13, 4.
- [174] S. Komaba, N. Yabuuchi, T. Nakayama, A. Ogata, T. Ishikawa, I. Nakai, *Inorg. Chem.* **2012**, 51, 11.
- [175] I. Hasa, D. Buchholz, S. Passerini, B. Scrosati, J. Hassoun, *Adv. Energy Mater.* **2014**, 4, 15.
- [176] I. Hasa, D. Buchholz, S. Passerini, J. Hassoun, *ACS Appl. Mater. Interfaces* **2015**, 7, 9.
- [177] P. Barpanda, J. M. Tarascon, in *Lithium Batteries: Advanced Technologies and Applications* (Eds: B. Scrosati, K. M. Abraham, W. V. Schalkwijk, J. Hassoun), John Wiley & Sons, Inc., Hoboken, NJ **2013**.
- [178] A. Manthiram, J. B. Goodenough, *J. Solid State Chem.* **1987**, 71, 2.
- [179] A. Manthiram, J. B. Goodenough, *J. Power Sources* **1989**, 26, 3.
- [180] C. Masquelier, L. Croguennec, *Chem. Rev.* **2013**, 113, 8.
- [181] K. T. Lee, T. N. Ramesh, F. Nan, G. Botton, L. F. Nazar, *Chem. Mater.* **2011**, 23, 16.
- [182] H. Chen, Q. Hao, O. Zivkovic, G. Hautier, L.-S. Du, Y. Tang, Y.-Y. Hu, X. Ma, C. P. Grey, G. Ceder, *Chem. Mater.* **2013**, 25, 14.
- [183] H. Chen, G. Hautier, G. Ceder, *J. Am. Chem. Soc.* **2012**, 134, 48.
- [184] M. Casas-Cabanas, V. V. Roddatis, D. Saurel, P. Kubiak, J. Carretero-González, V. Palomares, P. Serras, T. Rojo, *J. Mater. Chem.* **2012**, 22, 34.
- [185] M. Galceran, D. Saurel, B. Acebedo, V. V. Roddatis, E. Martin, T. Rojo, M. Casas-Cabanas, *Phys. Chem. Chem. Phys.* **2014**, 16, 19.
- [186] S. M. Oh, S. T. Myung, J. Hassoun, B. Scrosati, Y. K. Sun, *Electrochim. Commun.* **2012**, 22, 149.
- [187] P. Moreau, D. Guyomard, J. Gaubicher, F. Boucher, *Chem. Mater.* **2010**, 22, 14.
- [188] Y. Fang, Q. Liu, L. Xiao, X. Ai, H. Yang, Y. Cao, *ACS Appl. Mater. Interfaces* **2015**, 7, 32.
- [189] K. Zaghib, J. Trottier, P. Hovington, F. Brochu, A. Guerfi, A. Mauger, C. M. Julien, *J. Power Sources* **2011**, 196, 22.
- [190] J. Kim, D. H. Seo, H. Kim, I. Park, J. K. Yoo, S. K. Jung, Y. U. Park, W. A. G. Iii, K. Kang, *Energy Environ. Sci.* **2015**, 8, 2.
- [191] C. Li, X. Miao, W. Chu, P. Wu, D. Ge Tong, *J. Mater. Chem. A* **2015**, 3, 16.
- [192] B. Kang, G. Ceder, *Nature* **2009**, 458, 7235.
- [193] A. K. Padhi, K. S. Nanjundaswamy, J. B. Goodenough, *J. Electrochem. Soc.* **1997**, 144, 4.
- [194] S. Y. Chung, J. T. Bloking, Y. M. Chiang, *Nat. Mater.* **2002**, 1, 2.
- [195] Y. Zhu, Y. Xu, Y. Liu, C. Luo, C. Wang, *Nanoscale* **2013**, 5, 2.
- [196] Y. Fang, L. Xiao, J. Qian, X. Ai, H. Yang, Y. Cao, *Nano Lett.* **2014**, 14, 6.
- [197] Y. Fang, Z. Chen, L. Xiao, X. Ai, Y. Cao, H. Yang, *Small* **2018**, 14, 9.
- [198] B. L. Ellis, W. R. M. Makahnouk, Y. Makimura, K. Toghill, L. F. Nazar, *Nat. Mater.* **2007**, 6, 10.
- [199] S. Ping Ong, V. L. Chevrier, G. Hautier, A. Jain, C. Moore, S. Kim, X. Ma, G. Ceder, *Energy Environ. Sci.* **2011**, 4, 9.
- [200] A. K. Padhi, K. S. Nanjundaswamy, C. Masquelier, S. Okada, J. B. Goodenough, *J. Electrochem. Soc.* **1997**, 144, 4.
- [201] Y. Uebou, T. Kiyabu, S. Okada, J. I. Yamaki, *Rep. Inst. Adv. Mater. Study* **2002**, 16, 1.
- [202] Z. Jian, L. Zhao, H. Pan, Y.-S. Hu, H. Li, W. Chen, L. Chen, *Electrochim. Commun.* **2012**, 14, 1.
- [203] L. S. Plashnitsa, E. Kobayashi, Y. Noguchi, S. Okada, J. Yamaki, *J. Electrochim. Soc.* **2010**, 157, 4.
- [204] J. Mao, C. Luo, T. Gao, X. Fan, C. Wang, *J. Mater. Chem. A* **2015**, 3, 19.
- [205] J. Kang, S. Baek, V. Mathew, J. Gim, J. Song, H. Park, E. Chae, A. Kumar Rai, J. Kim, *J. Mater. Chem.* **2012**, 22, 39.
- [206] L. Si, Z. Yuan, L. Hu, Y. Zhu, Y. Qian, *J. Power Sources* **2014**, 272, 880.
- [207] S. Tepavcevic, H. Xiong, V. R. Stamenkovic, X. Zuo, M. Balasubramanian, V. B. Prakapenka, C. S. Johnson, T. Rajh, *ACS Nano* **2012**, 6, 1.
- [208] S. Y. Lim, H. Kim, R. A. Shakoor, Y. Jung, J. W. Choi, *J. Electrochim. Soc.* **2012**, 159, 9.
- [209] W. Song, X. Ji, Z. Wu, Y. Zhu, Y. Yang, J. Chen, M. Jing, F. Li, C. E. Banks, *J. Mater. Chem. A* **2014**, 2, 15.
- [210] W. Shen, C. Wang, H. Liu, W. Yang, *Chem. – Eur. J.* **2013**, 19, 43.
- [211] W. Duan, Z. Zhu, H. Li, Z. Hu, K. Zhang, F. Cheng, J. Chen, *J. Mater. Chem. A* **2014**, 2, 23.
- [212] Y. Hwa Jung, C. Hai Lim, D. Kyung Kim, *J. Mater. Chem. A* **2013**, 1, 37.
- [213] Y. Jiang, Z. Yang, W. Li, L. Zeng, F. Pan, M. Wang, X. Wei, G. Hu, L. Gu, Y. Yu, *Adv. Energy Mater.* **2015**, 5, 10.
- [214] X. Rui, W. Sun, C. Wu, Y. Yu, Q. Yan, *Adv. Mater.* **2015**, 27, 42.
- [215] K. Saravanan, C. W. Mason, A. Rudola, K. H. Wong, P. Balaya, *Adv. Energy Mater.* **2013**, 3, 4.
- [216] J. B. Goodenough, H. Y. P. Hong, J. A. Kafalas, *Mater. Res. Bull.* **1976**, 11, 2.
- [217] O. Tillement, J. Angenault, J. C. Couturier, M. Quarton, *Solid State Ionics* **1992**, 53, 391.
- [218] S. Patoux, G. Rousse, J.-B. Leriche, C. Masquelier, *Chem. Mater.* **2003**, 15, 10.
- [219] Y. Fang, J. Zhang, L. Xiao, X. Ai, Y. Cao, H. Yang, *Adv. Sci.* **2017**, 4, 5.
- [220] S. Nishimura, M. Nakamura, R. Natsui, A. Yamada, *J. Am. Chem. Soc.* **2010**, 132, 39.
- [221] H. Zhou, S. Upadhyay, N. A. Chernova, G. Hautier, G. Ceder, M. S. Whittingham, *Chem. Mater.* **2011**, 23, 2.
- [222] P. Barpanda, G. Liu, C. D. Ling, M. Tamaru, M. Avdeev, S.-C. Chung, Y. Yamada, A. Yamada, *Chem. Mater.* **2013**, 25, 17.
- [223] P. Barpanda, S. Nishimura, A. Yamada, *Adv. Energy Mater.* **2012**, 2, 7.
- [224] P. Barpanda, T. Ye, M. Avdeev, S.-C. Chung, A. Yamada, *J. Mater. Chem. A* **2013**, 1, 13.
- [225] J. Y. Jang, H. Kim, Y. Lee, K. T. Lee, K. Kang, N.-S. Choi, *Electrochim. Commun.* **2014**, 44, 74.

- [226] H. Kim, I. Park, D. H. Seo, S. Lee, S.-W. Kim, W. J. Kwon, Y. U. Park, C. S. Kim, S. Jeon, K. Kang, *J. Am. Chem. Soc.* **2012**, *134*, 25.
- [227] S. Y. Lim, H. Kim, J. Chung, J. H. Lee, B. G. Kim, J. J. Choi, K. Y. Chung, W. Cho, S.-J. Kim, W. A. Goddard, Y. Jung, J. W. Choi, *Proc. Natl. Acad. Sci. USA* **2014**, *111*, 2.
- [228] A. Yamada, S. C. Chung, K. Hinokuma, *J. Electrochem. Soc.* **2001**, *148*, 3.
- [229] N. Recham, J. N. Chotard, L. Dupont, K. Djellab, M. Armand, J. M. Tarascon, *J. Electrochem. Soc.* **2009**, *156*, 12.
- [230] Y. Kawabe, N. Yabuuchi, M. Kajiyama, N. Fukuhara, T. Inamasu, R. Okuyama, I. Nakai, S. Komaba, *Electrochemistry* **2012**, *80*, 2.
- [231] O. V. Yakubovich, O. V. Karimova, O. K. Mel'nikov, *Acta Crystallogr. C* **1997**, *53*, 4.
- [232] K. Kubota, K. Yokoh, N. Yabuuchi, S. Komaba, *Electrochemistry* **2014**, *82*, 10.
- [233] H. Zou, S. Li, X. Wu, M. J. McDonald, Y. Yang, *ECS Electrochem. Lett.* **2015**, *4*, 6.
- [234] J. Barker, M. Y. Saidi, J. L. Swoyer (Faradion Ltd.), *US6777132 B2*, **2004**.
- [235] J. Barker, M. Y. Saidi, J. L. Swoyer, *J. Electrochem. Soc.* **2004**, *151*, 10.
- [236] M. Bianchini, N. Brisset, F. Fauth, F. Weill, E. Elkaim, E. Suard, C. Masquelier, L. Croguennec, *Chem. Mater.* **2014**, *26*, 14.
- [237] M. Bianchini, F. Fauth, N. Brisset, F. Weill, E. Suard, C. Masquelier, L. Croguennec, *Chem. Mater.* **2015**, *27*, 8.
- [238] F. Sauvage, E. Quarez, J. M. Tarascon, E. Baudrin, *Solid State Sci.* **2006**, *8*, 10.
- [239] K. Chihera, A. Kitajou, I. D. Gocheva, S. Okada, J. Yamaki, *J. Power Sources* **2013**, *227*, 80.
- [240] R. A. Shakoor, D. H. Seo, H. Kim, Y. U. Park, J. Kim, S.-W. Kim, H. Gwon, S. Lee, K. Kang, *J. Mater. Chem.* **2012**, *22*, 38.
- [241] Q. Liu, D. Wang, X. Yang, N. Chen, C. Wang, X. Bie, Y. Wei, G. Chen, F. Du, *J. Mater. Chem. A* **2015**, *3*, 43.
- [242] P. Barpanda, G. Oyama, S. Nishimura, S. C. Chung, A. Yamada, *Nat. Commun.* **2014**, *5*, 4358.
- [243] M. M. Doeff, M. Y. Peng, Y. Ma, L. C. D. Jonghe, *J. Electrochem. Soc.* **1994**, *141*, 11.
- [244] M. M. Doeff, T. J. Richardson, L. Kepley, *J. Electrochem. Soc.* **1996**, *143*, 8.
- [245] F. Sauvage, L. Laffont, J.-M. Tarascon, E. Baudrin, *Inorg. Chem.* **2007**, *46*, 8.
- [246] F. Sauvage, E. Baudrin, J. M. Tarascon, *Sens. Actuators, B* **2007**, *120*, 2.
- [247] J. Akimoto, H. Hayakawa, N. Kijima, J. Awaka, F. Funabiki, *Solid State Phenom.* **2011**, *170*, 198.
- [248] Y. Cao, L. Xiao, W. Wang, D. Choi, Z. Nie, J. Yu, L. V. Saraf, Z. Yang, J. Liu, *Adv. Mater.* **2011**, *23*, 28.
- [249] H. Kim, D. J. Kim, D.-H. Seo, M. S. Yeom, K. Kang, D. K. Kim, Y. Jung, *Chem. Mater.* **2012**, *24*, 6.
- [250] P. K. Sharma, G. J. Moore, F. Zhang, P. Zavalij, M. S. Whittingham, *Electrochem. Solid-State Lett.* **1999**, *2*, 10.
- [251] M. M. Thackeray, J. O. Thomas, M. S. Whittingham, *MRS Bull.* **2000**, *25*, 3.
- [252] P. Zhan, S. Wang, Y. Yuan, K. Jiao, S. Jiao, *J. Electrochem. Soc.* **2015**, *162*, 6.
- [253] N. L. Rosi, J. Eckert, M. Eddaoudi, D. T. Vodak, J. Kim, M. O'Keeffe, O. M. Yaghi, *Science* **2003**, *300*, 5622.
- [254] M. Dinc, A. Dally, Y. Liu, C. M. Brown, D. A. Neumann, J. R. Long, *J. Am. Chem. Soc.* **2006**, *128*, 51.
- [255] L. Wang, J. Song, R. Qiao, L. A. Wray, M. A. Hossain, Y.-D. Chuang, W. Yang, Y. Lu, D. Evans, J. J. Lee, S. Vail, X. Zhao, M. Nishijima, S. Kakimoto, J. B. Goodenough, *J. Am. Chem. Soc.* **2015**, *137*, 7.
- [256] T. Matsuda, M. Takachi, Y. Moritomo, *Chem. Commun.* **2013**, *49*, 27.
- [257] H. Lee, Y. I. Kim, J. K. Park, J. Wook Choi, *Chem. Commun.* **2012**, *48*, 67.
- [258] C. D. Wessells, R. A. Huggins, Y. Cui, *Nat. Commun.* **2011**, *2*, 550.
- [259] Y. You, X. L. Wu, Y. X. Yin, Y.-G. Guo, *Energy Environ. Sci.* **2014**, *7*, 5.
- [260] Y. Lu, L. Wang, J. Cheng, J. B. Goodenough, *Chem. Commun.* **2012**, *48*, 52.
- [261] D. Asakura, M. Okubo, Y. Mizuno, T. Kudo, H. Zhou, K. Ikeda, T. Mizokawa, A. Okazawa, N. Kojima, *J. Phys. Chem. C* **2012**, *116*, 15.
- [262] X. Wu, W. Deng, J. Qian, Y. Cao, X. Ai, H. Yang, *J. Mater. Chem. A* **2013**, *1*, 35.
- [263] M. J. Aragón, C. Vidal-Abarca, P. Lavela, J. L. Tirado, *J. Mater. Chem. A* **2013**, *1*, 44.
- [264] J. L. Yue, Q. Sun, Z. W. Fu, *Chem. Commun.* **2013**, *49*, 52.
- [265] K. Kubota, H. Yoshida, N. Yabuuchi, I. Ikeuchi, A. Garsuch, M. Schulz-Dobrick, S. Komaba, Presented at the 17th International Meeting on Lithium Batteries - IMLB, Como, Italy **2014**.
- [266] H. Yu, S. Guo, Y. Zhu, M. Ishida, H. Zhou, *Chem. Commun.* **2014**, *50*, 4.
- [267] B. Koo, S. Chattopadhyay, T. Shibata, V. B. Prakapenka, C. S. Johnson, T. Rajh, E. V. Shevchenko, *Chem. Mater.* **2013**, *25*, 2.
- [268] M. Tamaru, X. Wang, M. Okubo, A. Yamada, *Electrochem. Commun.* **2013**, *33*, 23.
- [269] P. Barpanda, T. Ye, S. Nishimura, S.-C. Chung, Y. Yamada, M. Okubo, H. Zhou, A. Yamada, *Electrochem. Commun.* **2012**, *24*, 116.
- [270] H. Kim, R. A. Shakoor, C. Park, S. Y. Lim, J.-S. Kim, Y. N. Jo, W. Cho, K. Miyasaka, R. Kahraman, Y. Jung, J. W. Choi, *Adv. Funct. Mater.* **2013**, *23*, 9.
- [271] C. Y. Chen, K. Matsumoto, T. Nohira, C. Ding, T. Yamamoto, R. Hagiwara, *Electrochim. Acta* **2014**, *133*, 583.
- [272] T. Liu, B. Wang, X. Gu, L. Wang, M. Ling, G. Liu, D. Wang, S. Zhang, *Nano Energy* **2016**, *30*, 756.
- [273] Z. Liu, X. Wang, W. Ying, A. Tang, S. Yang, L. He, *Trans. Nonferrous Met. Soc. China* **2008**, *18*, 2.
- [274] J. Barker, M. Y. Saidi, J. L. Swoyer, *Electrochem. Solid-State Lett.* **2003**, *6*, 1.
- [275] Y. U. Park, D. H. Seo, H. S. Kwon, B. Kim, J. Kim, H. Kim, I. Kim, H. I. Yoo, K. Kang, *J. Am. Chem. Soc.* **2013**, *135*, 37.
- [276] M. Nose, S. Shiotani, H. Nakayama, K. Nobuhara, S. Nakanishi, H. Iba, *Electrochem. Commun.* **2013**, *34*, 266.
- [277] G. Venkatesh, B. Kishore, R. Viswanatha, D. Aurbach, N. Munichandriaiah, *J. Electrochem. Soc.* **2017**, *164*, A2176.
- [278] J. Böckris, A. Reddy, M. Gamboa-Aldeco, *Modern Electrochemistry*, Vol. 2A: *Fundamentals of Electrodics*, Plenum Press, New York **2000**.
- [279] A. Ponrouch, D. Monti, A. Boschin, B. Steen, P. Johansson, M. R. Palacín, *J. Mater. Chem. A* **2015**, *3*, 22.
- [280] K. Xu, *Chem. Rev.* **2014**, *114*, 11503.
- [281] E. Jónsson, P. Johansson, *Phys. Chem. Chem. Phys.* **2012**, *14*, 10774.
- [282] A. Ponrouch, R. Dedryvère, D. Monti, A. E. Demet, J. M. A. Mba, L. Croguennec, C. Masquelier, P. Johansson, M. Rosa Palacín, *Energy Environ. Sci.* **2013**, *6*, 2361.
- [283] A. Ponrouch, E. Marchante, M. County, J.-M. Tarascon, M. Rosa Palacín, *Energy Environ. Sci.* **2012**, *5*, 8572.
- [284] K. Xu, *Chem. Rev.* **2004**, *104*, 4303.
- [285] J. T. Edward, *J. Chem. Educ.* **1970**, *47*, 261.
- [286] D. Danilov, P. H. L. Notten, *J. Power Sources* **2009**, *189*, 303.
- [287] M. Ue, S. Mori, *J. Electrochem. Soc.* **1995**, *142*, 2577.
- [288] M. Ue, *J. Electrochem. Soc.* **1994**, *141*, 3336.
- [289] F. Croce, A. D'Aprano, C. Nanjundiah, V. R. Koch, C. W. Walker, M. Salomon, *J. Electrochem. Soc.* **1996**, *143*, 154.
- [290] S. Tobishima, T. Okada, *Electrochim. Acta* **1985**, *30*, 1715.
- [291] E. Endo, M. Ata, K. Tanaka, K. Sekai, *J. Electrochem. Soc.* **1998**, *145*, 3757.
- [292] M. Okoshi, Y. Yamada, A. Yamada, H. Nakai, *J. Electrochem. Soc.* **2013**, *160*, A2160.
- [293] Y. Matsuda, H. Satake, *J. Electrochem. Soc.* **1980**, *127*, 877.
- [294] R. Selim, P. Bro, *J. Electrochem. Soc.* **1974**, *121*, 1457.
- [295] Y. Takada, R. Fujii, K. Matsuo, *Tanso* **1983**, *1983*, 120.

- [296] G. Pistoia, M. D. Rossi, B. Scrosati, *J. Electrochem. Soc.* **1970**, *117*, 500.
- [297] R. Fong, U. von Sacken, J. R. Dahn, *J. Electrochem. Soc.* **1990**, *137*, 2009.
- [298] V. R. Koch, J. H. Young, *J. Electrochem. Soc.* **1978**, *125*, 1371.
- [299] J. S. Foos, J. McVeigh, *J. Electrochem. Soc.* **1982**, *130*, 1.
- [300] J. S. Foos, T. J. Stolki, *J. Electrochem. Soc.* **1988**, *135*, 2769.
- [301] K. M. Abraham, J. L. Goldman, D. L. Natwig, *J. Electrochem. Soc.* **1982**, *129*, 2404.
- [302] D. Guyomard, J. M. Tarascon, *J. Electrochem. Soc.* **1992**, *139*, 937.
- [303] W. Ebner, D. Fouchard, L. Xie, *Solid State Ionics* **1994**, *69*, 238.
- [304] R. Alcántara, P. Lavela, G. F. Ortiz, J. L. Tirado, *Electrochim. Solid-State Lett.* **2005**, *8*, A222.
- [305] D. Guyomard, J. M. Tarascon, *J. Electrochem. Soc.* **1993**, *140*, 3071.
- [306] J. M. Tarascon, D. Guyomard, *Solid State Ionics* **1994**, *69*, 293.
- [307] D. Aurbach, Y. Ein-Eli, B. Markovsky, A. Zaban, S. Luski, Y. Carmeli, H. Yamin, *J. Electrochem. Soc.* **1995**, *142*, 2882.
- [308] Y. Ein-Eli, S. R. Thomas, V. Koch, D. Aurbach, B. Markovsky, A. Schechter, *J. Electrochem. Soc.* **1996**, *143*, L273.
- [309] Y. Ein-Eli, S. F. McDevitt, D. Aurbach, B. Markovsky, A. Schechter, *J. Electrochem. Soc.* **1997**, *144*, L180.
- [310] S. Komaba, T. Ishikawa, W. Murata, N. Yabuuchi, T. Ozeki, Presented at The 15th International Meeting on Lithium Batteries - IMLB, Montreal, Quebec, Canada **2010**.
- [311] P. Wasserscheid, W. Keim, *Angew. Chem., Int. Ed.* **2000**, *39*, 21.
- [312] S. Sugden, H. Wilkins, *J. Chem. Soc.* **1929**, *0*, 1291.
- [313] P. Walden, *Bull. Acad. Imp. Sci. St.-Petersbourg* **1914**, *1800*, 405.
- [314] A. B. McEwen, S. F. McDevitt, V. R. Koch, *J. Electrochem. Soc.* **1997**, *144*, 4.
- [315] A. B. McEwen, H. L. Ngo, K. LeCompte, J. L. Goldman, *J. Electrochem. Soc.* **1999**, *146*, 5.
- [316] T. Devarajan, S. Higashiya, C. Dangler, M. Rane-Fondacaro, J. Snyder, P. Halder, *Electrochim. Commun.* **2009**, *11*, 3.
- [317] A. Lewandowski, M. Galirski, *J. Phys. Chem. Solids* **2004**, *65*, 2.
- [318] B. Garcia, S. Lavallée, G. Perron, C. Michot, M. Armand, *Electrochim. Acta* **2004**, *49*, 26.
- [319] T. Sugimoto, Y. Atsumi, M. Kikuta, E. Ishiko, M. Kono, M. Ishikawa, *J. Power Sources* **2009**, *189*, 1.
- [320] H. Matsumoto, T. Matsuda, Y. Miyazaki, *Chem. Lett.* **2000**, *29*, 12.
- [321] H. Nakagawa, S. Izuchi, K. Kuwana, T. Nukuda, Y. Aihara, *J. Electrochem. Soc.* **2003**, *150*, 6.
- [322] H. Sakabe, H. Matsumoto, K. Tatsumi, *Electrochim. Acta* **2007**, *53*, 3.
- [323] S. P. Ong, O. Andreussi, Y. Wu, N. Marzari, G. Ceder, *Chem. Mater.* **2011**, *23*, 11.
- [324] J. S. Wilkes, J. A. Levisky, R. A. Wilson, C. L. Hussey, *Inorg. Chem.* **1982**, *21*, 3.
- [325] H. L. Chum, V. R. Koch, L. L. Miller, R. A. Osteryoung, *J. Am. Chem. Soc.* **1975**, *97*, 11.
- [326] K. Kubota, K. Tamaki, T. Nohira, T. Goto, R. Hagiwara, *Electrochim. Acta* **2010**, *55*, 3.
- [327] R. Hagiwara, K. Tamaki, K. Kubota, T. Goto, T. Nohira, *J. Chem. Eng. Data* **2008**, *53*, 2.
- [328] K. Kubota, T. Nohira, T. Goto, R. Hagiwara, *Electrochim. Commun.* **2008**, *10*, 12.
- [329] K. Kubota, T. Nohira, R. Hagiwara, *J. Chem. Eng. Data* **2010**, *55*, 9.
- [330] A. Fukunaga, T. Nohira, R. Hagiwara, K. Numata, E. Itani, S. Sakai, K. Nitta, *J. Appl. Electrochem.* **2016**, *46*, 4.
- [331] I. M. Herfort, H. Schneider, *Liebigs Ann. Chem.* **1991**, *1991*, 1.
- [332] K. Matsumoto, K. Inoue, K. Nakahara, R. Yuge, T. Noguchi, K. Utsugi, *J. Power Sources* **2013**, *231*, 234.
- [333] D. Monti, E. Jónsson, M. R. Palacín, P. Johansson, *J. Power Sources* **2014**, *245*, 630.
- [334] N. Serizawa, S. Seki, S. Tsuzuki, K. Hayamizu, Y. Urabayashi, K. Takei, H. Miyashiro, *J. Electrochem. Soc.* **2011**, *158*, 9.
- [335] M. Forsyth, H. Yoon, F. Chen, H. Zhu, D. R. MacFarlane, M. Armand, P. C. Howlett, *J. Phys. Chem. C* **2016**, *120*, 8.
- [336] L. Long, S. Wang, M. Xiao, Y. Meng, *J. Mater. Chem. A* **2016**, *4*, 26.
- [337] Y. Tominaga, K. Yamazaki, *Chem. Commun.* **2014**, *50*, 34.
- [338] J. Serra Moreno, M. Armand, M. B. Berman, S. G. Greenbaum, B. Scrosati, S. Panero, *J. Power Sources* **2014**, *248*, 695.
- [339] M. S. Ding, K. Xu, T. R. Jow, *J. Electrochem. Soc.* **2000**, *147*, 5.
- [340] Z. K. Liu, *J. Electrochem. Soc.* **2003**, *150*, 3.
- [341] Y. Matsuda, M. Morita, K. Kosaka, *J. Electrochem. Soc.* **1983**, *130*, 1.
- [342] H. Hou, X. Qiu, W. Wei, Y. Zhang, X. Ji, *Adv. Energy Mater.* **2017**, *7*, 24.
- [343] K. Smith, J. Treacher, D. Ledwoch, P. Adamson, E. Kendrick, *ECS Trans.* **2017**, *75*, 22.
- [344] C. Matei Ghimbeu, J. Górká, V. Simone, L. Simonin, S. Martinet, C. Vix-Guterl, *Nano Energy* **2018**, *44*, 327.
- [345] R. Dugas, B. Zhang, P. Rozier, J. M. Tarascon, *J. Electrochem. Soc.* **2016**, *163*, 6.
- [346] J. M. de llarduya, L. Otaegui, J. M. L. del Amo, M. Armand, G. Singh, Presented at the 231st ECS Meeting, New Orleans, LA **2017**.
- [347] B. Zhang, M. Deschamps, M.-R. Ammar, E. Raymundo-Piñero, L. Hennet, D. Batuk, J.-M. Tarascon, *Adv. Mater. Technol.* **2017**, *2*, 3.
- [348] E. M. Lotfabad, J. Ding, K. Cui, A. Kohandehghan, W. P. Kalisvaart, M. Hazelton, D. Mitlin, *ACS Nano* **2014**, *8*, 7.
- [349] K. Wang, Y. Jin, S. Sun, Y. Huang, J. Peng, J. Luo, Q. Zhang, Y. Qiu, C. Fang, J. Han, *ACS Omega* **2017**, *2*, 4.
- [350] Y. Li, Y. S. Hu, H. Li, L. Chen, X. Huang, *J. Mater. Chem. A* **2016**, *4*, 1.
- [351] UNECE, *Globally Harmonized System of Classification and Labelling of Chemicals (GHS)*, Geneva **2015**.
- [352] D. Schaumlöffel, *J. Trace Elem. Med. Biol.* **2012**, *26*, 1.
- [353] A. Aihamaiti, J. Jiang, D. Li, T. Li, W. Zhang, X. Ding, *Environ. Sci. Pollut. Res.* **2017**, *24*, 34.
- [354] Z. Zeng, X. Jiang, R. Li, D. Yuan, X. Ai, H. Yang, Y. Cao, *Adv. Sci.* **2016**, *3*, 9.
- [355] H. Ernst, *Small Bus. Econ.* **1997**, *9*, 361.
- [356] R. Wagner, N. Preschitschek, S. Passerini, J. Leker, M. Winter, *J. Appl. Electrochem.* **2013**, *43*, 5.
- [357] R. Wagner, N. Preschitschek, S. Passerini, J. Leker, M. Winter, Presented at the 225th ECS Meeting, Orlando, FL **2014**.
- [358] B. Golembiewski, N. vorn Stein, N. Sick, H. D. Wiemhöfer, *J. Cleaner Prod.* **2015**, *87*, 800.
- [359] European Patent Office, Online Patent Database, <http://www.epo.org/> (accessed: March 2018).
- [360] E. Kendrick, K. L. Smith, J. C. Treacher (Sharp Kabushiki Kaisha, Faradion Limited), *WO2017073066 (A1)*, **2017**.
- [361] J. C. Treacher, K. L. Smith, E. Kendrick (Sharp Kabushiki Kaisha, Faradion Limited), *WO2017073056 (A1)*, **2017**.
- [362] Q. Zhou, Q. Meng, J. Yu, J. Ma, S. Qiu (China Electronic New Energy (Wuhan) Research Institute Co., Ltd.), *CN107171021 (A)*, **2017**.
- [363] Q. Zhou, Q. Meng, S. Qiu, J. Ma, W. Kong (China Electronic New Energy (Wuhan) Research Institute Co., Ltd.), *CN107171020 (A)*, **2017**.
- [364] K. Nitta, S. Sakai, A. Fukunaga, E. Imazaki, K. Numata, *US2017110756 (A1)*, **2017**.
- [365] H. Nakayama (Toyota Motor Corp.), *JP2014078351 (A)*, **2014**.
- [366] N. Wang, Z. Bai, Z. Lu, B. Tang (Univ. Taiyuan Technology), *CN106654268 (A)*, **2017**.
- [367] H. Wang (Dongguan Jiaqian New Mat. Tech. Co. Ltd.) *CN106602066 (A)*, **2017**.
- [368] Y. Hu, Y. Li, L. Chen (Institute of Physics, the Chinese Academy of Sciences), *WO2017070988 (A1)*, **2017**.
- [369] Y. Wang, F. Wang (Xinyi Zhongnuo New Material Tech Co. Ltd.), *CN107204430 (A)*, **2017**.
- [370] R. Mi, Z. Fu, C. Wang, L. Yuan, M. Liu, M. Zhong, X. Yang, H. Zhao, F. Yang (Laser Fusion Res. CT China Academy Engineering Physics), *CN106744800 (A)*, **2017**.

- [371] Y. Chen, H. Deng (Bsst Tianjin Power Battery Technology Development Co., Ltd), *CN105261785 (A)*, **2016**.
- [372] G. Li, C. Chu, Y. Xu, Y. Zhang, M. Wang, R. Liang, (Sunwoda Electronics Co. Ltd.), *CN106876781 (A)*, **2017**.
- [373] Q. Wang, *CN104009252 (A)*, **2014**.
- [374] Y. Sumiyama, N. Sakai (Sumitomo Bakelite Co.), *JP2016136452 (A)*, **2016**.
- [375] L. Mai, X. Yao, Z. Zhu (Univ. Wuhan Tech.), *CN107123809 (A)*, **2017**.
- [376] Z. Liu, J. Feng (Univ. Jinan), *CN106800312 (A)*, **2017**.
- [377] F. Li, *CN107039639 (A)*, **2017**.
- [378] S. Sakai, A. Fukunaga, K. Nitta (Sumitomo Electric Industries), *JP2017107713 (A)*, **2017**.
- [379] Q. Zhou, J. Yu, W. Kong, Q. Meng, J. Ma, W. Zhang, S. Ren (China Electronic New Energy (Wuhan) Research Institute Co., Ltd.), *CN106602071 (A)*, **2017**.
- [380] B. Li, Q. Lu, Q. Yu, Y. He, Q. Yang, F. Kang (Graduate School Shenzhen Tsinghua Univ.), *CN107154513 (A)*, **2017**.
- [381] S. Sakai, A. Fukunaga, K. Numata, E. Imazaki, K. Senoo, K. Nitta (Sumitomo Electric Industries), *JP2015215968 (A)*, **2015**.
- [382] S. Sakai, A. Fukunaga, K. Numata, E. Imazaki, K. Nitta (Sumitomo Electric Industries), *US2017047614 (A1)*, **2016**.
- [383] S. Nakanishi (Toyota Motor Corp.), *JP2016085890 (A)*, **2016**.
- [384] Q. Zhou, Q. Meng, W. Kong, S. Qiu, J. Ma (China Electronic New Energy (Wuhan) Research Institute Co., Ltd.), *CN107134563 (A)*, **2017**.
- [385] CNRS, A Promising New Prototype of Battery, <http://www2.cnrs.fr/en/2659.htm> (accessed: January 2018).
- [386] X. Li, J. Liu, Y. Shao, H. Pan, P. Yan, C. Wang, W. Wang, V. Sprenkle, *Room Temperature Na-ion Battery Development*, The Pacific Northwest National Laboratory – PNNL, Richland, Washington **2014**.
- [387] J. Barker, R. Heap (Faradion Ltd.), *US9761863 B2*, **2017**.
- [388] A. Jain, S. P. Ong, G. Hautier, W. Chen, W. D. Richards, S. Dacek, S. Cholia, D. Gunter, D. Skinner, G. Ceder, K. A. Persson, *APL Mater.* **2013**, 1, 011002.
- [389] E. Berg, C. Villevieille, D. Streich, S. Trabesinger, P. Novak, *J. Electrochem. Soc.* **2015**, 162, A2468.
- [390] UN/SCETDG/50/INF.13, Committee of Experts on the Transport of Dangerous Goods and on the Globally Harmonized System of Classification and Labelling of Chemicals, Geneva **2016**.
- [391] J. Barker, presented at 3rd Int. Conf. on Na-Ion Batteries, Geelong, Australia, December **2016**.